1-1-2017

Folate Receptor Alpha Targeted Delivery And Characterization Of Polyethyleneimine-Graft-Polycaprolactone-Block-Poly(ethylene Glycol) Containing Sirna Micelleplexes

Steven Jones
Wayne State University,

FOLATE RECEPTOR ALPHA TARGETED DELIVERY AND CHARACTERIZATION OF POLYETHYLENEIMINE-GRAFT-POLYCAPROLACTONE-BLOCK-POLY(ETHYLENE GLYCOL) CONTAINING SIRNA MICELLEPLEXES

by

STEVEN KEVIN JONES

DISSERTATION

Submitted to the Graduate School

of Wayne State University,

Detroit, Michigan

in partial fulfillment of the requirements

for the degree of

DOCTOR OF PHILOSOPHY

2017

MAJOR: CANCER BIOLOGY

Approved By:

_____

Advisor Date

_____

_____

_____

_____

DEDICATION

This dissertation is dedicated to my family, who has given me unwavering support and unconditional love throughout my life and career.

To my mother, Linda, you have been the most tremendous support for me. You gave me passion for science, support to continue my education, and always an ear to hear my frustrations. Your excitement for my work was worth more than I can put into words.

To my father, Robert, you have been a great pillar of support. Every life needs balance and you helped me ground myself so I did not get too lost within in my career. Additionally, offering a great retreat place to unwind.

To my siblings, Robbie, Katie, and William, you three have provided me with support and love. Each of you have provided a unique piece to keep me going throughout my academic career. I would not be here if it weren't for you three.

To my undergraduate advisor, Matthew Mio, you were inspirational and helped me discover my passion for research. You were instrumental in giving me an opportunity to discover my passion.

And last but certainly not least, to my loving fiancé Jazz Mitchell Goodchild. You have been the other half of my life since we met. Thank you for your love, support, and understanding during my long nights, crazy hours, and general frustration. Your presence made many of those long nights in lab tolerable.

ACKNOWLEDGEMENTS

Advisor:

I would like to thank my advisor and mentor, Dr. Olivia Merkel, without whom my project would not have been possible. Dr. Merkel, you have given me the opportunity to take a project and call it my own. I appreciate the freedom you have allowed me within the lab but at the same time being available to help brainstorm. This allowed me to grow and mature as a scientist; to find out where my strengths and weaknesses are, and what I want to do after graduation. You have given me the vital tools in order to which build my career from. I want to extend my warmest heartfelt thank you. I am appreciative of your guidance more than words can show.

Committee Members:

Dr. Larry Matherly: Thank you for providing your insight and expertise towards my project. Your knowledge was invaluable and it helped shape my project to be the most technically sound it could be. Additionally, thank you for giving me the opportunities to present my work at a variety of conferences which were vital for me to develop professionally.

Dr. Manohar Ratnam: Thank you for all of your technical support and folate receptor expertise you have endowed me with to put towards my project. I would like to thank you for supplying SKOV-3 cells when we needed them.

Dr. Joshua Reineke: Thank you for your help and support during my graduate school, even as you started at your new position. I was always appreciative of your insights towards my project from a pharmaceutical sciences view point from my committee.

Lab Members:

Daniel Feldmann: I cannot thank you enough for your support and friendship while at Wayne State. From lab work to house work, it was great to have someone else to bounce ideas off of. I

am deeply grateful for your friendship and for the experiences that I will carry with me because of you. I wish you a successful rest of your graduate career and scientific career from thereafter.

Yuran Xie: You were the first, and longest lasting lab member to join after I did. We shard just over 4 years together and I could not have asked for a better co-worker and friend. You were always there to offer advice, assistance, or a laugh which was always welcomed. You single-handedly made my graduate school career more worthwhile. I wish you the best in your career, I know you will only succeed.

Collaborators:

Dr. Shields: Thank you for the opportunity to work in your lab and your support for our imaging studies. My fellowship would not have been possible if not for you.

Kirk Douglas: Thank you for all your help and time that you spent with me during my *in vivo* studies. You helped everything run much smoother than it normally would have.

Cancer Biology Program:

Dr. Larry Matherly: Thank you for the opportunity to carry out my Ph.D. within such a wonderful program that you helped create. You were vital in every aspect of my career, here at Wayne State.

Dr. George Brush: Thank you for your guidance early on to set my graduate curriculum. You were a very valuable asset for students who just entered the program.

Nadia Daniel: Thank you for everything that you do; not only for me but also for the program. You kept everything running smoothly and helped me with any help that I needed: from graduation, to travel support or registration.

Cancer Biology Steering Committee: Thank you for keeping abreast on my situation and progress throughout my career. I am very appreciative of the financial support that you helped to award me.

Cancer Biology Students: Thank you for the support and fun the past four and a half years. You were all very friendly and willing to offer assistance if I needed. I wish you all the best in the rest of your careers.

TABLE OF CONTENTS

LIST OF TABLES

LIST OF FIGURES

LIST OF ABBREVIATIONS

AFM	Atomic Force Microscopy
AF488	Alexa-fluor 488
CD	Circular Dichroism
CLSM	Confocal Laser Scanning Microscopy
CMC	Critical Micelle Concentration
DLS	Dynamic Light Scattering
EGFR	Epidermal Growth Factor Receptor
EOC	Epithelial Ovarian Cancer
FCS	Fluorescent Correlation Spectroscopy
FRα	Folate Receptor Alpha
FRβ	Folate Receptor Beta
FRδ	Folate Receptor Delta
FRγ	Folate Receptor Gamma
GPI	Glycosylphosphatidylinositol
HLB	Hydrophilic-Lipophilic Balance
LPS	Lipopolysaccharide

MyD-88	Myeloid Differentiation Factor 88
PCL	Polycaprolactone
PEI	Polyetheyleneimine
PEG	Poly(ethylene glycol)
PTX	Paclitaxel
RISC	RNAi Induced Silencing Complex
siRNA	Small Interfering RNA
SPECT	Single-Photon Emission Computed Tomography
TLR4	Toll-like Receptor 4
TEM	Transmission Electron Microscopy
TNFα	Tumor Necrosis Factor-α

CHAPTER 1 – INTRODUCTION

1.1 Introduction to Nanomedicine

Over the past decade, a boom in new therapeutics has emerged in the industry and academic sector that are coined under the term “nanomedicine”. Nanomedicine has attracted a lot of attention in the clinical setting. This new wave of scientific interest employs nanotechnology, or nano-sized tools, for the purpose of diagnosis, treatment, and even prevention of diseases ranging from cancer to sexually transmitted diseases.(1-3) Backing this development of nanomedicine is the combination of multiple fields, including biology, chemistry, material science, engineering, and clinical practice.(2) Nanoparticles offer the advantage of accessing diseased organs or cells with the ability to be engineered to perform more efficiently than non-modifiable chemical or biological molecules.(1, 4) Although this recent trend of molding these fields together has grown exponentially in publications within the last decade, the first example of researchers using nanomaterials for a therapeutic purpose actually originated well before this surge. One of the first studied concepts of the field of nanomedicine used liposomes for drug delivery. Subsequently, the first FDA approved nanomedicine was a liposomal delivery system also.

Liposomes are spherical lipid vesicles which have a hydrophilic core. They are made of a similar amphiphilic bilayer structure as the one that comprises a cellular membrane.(5, 6) Therefore, liposomes can readily cross cell membranes and be used to package drugs within their aqueous core. Researchers first became aware of liposomes and their drug loading capabilities in 1965.(2, 7) Liposomes offer the unique ability to load both hydrophobic drugs within the bilayer and hydrophilic drugs within their core. Their ability to load drugs within their structure to form solid dispersions alleviates the issue of solubilizing very hydrophobic drugs, such as doxorubicin, within harsh organic solvent solutions to use in patients.(7-9) Since the 1960s, multiple variations

of the liposome structure have been introduced paralleled by an increase regarding the variety of drugs that can be loaded into the inner core and membrane. One popular modification to the surface of the liposome was the use of polyethylene glycol (PEG) to coat the outer layer with the aim of increasing biocompatibility, evading phagocytosis by immune cells, and decreasing aggregation and the binding to serum proteins.(7, 10) In 1995, the first nanoparticle based therapy was approved by the FDA which utilizes a PEGylated liposome that encapsulates doxorubicin. Doxil, as it was termed, has been approved in the clinic to treat Kaposi's sarcomas and ovarian epithelial cancers.(7, 11, 12) Liposomes, such as Doxil, rely upon the so-called enhanced permeation and retention effect (EPR effect) to localize within the tumor due to leaky blood vasculature and retain within the tumor interstitium for a prolonged period of time due to insufficient lymph drainage.(13, 14)

The EPR effect allows for nanoparticles to preferentially accumulate within the tumor due to the abnormal and chaotic growth of blood vessels which result in larger and less ordered fenestrations within the blood vessel wall.(15, 16) This passive accumulation mechanism is also utilized by the FDA approved drug Abraxane. Abraxane is a nanoparticle of albumin-bound paclitaxel used to treat a variety of cancers such as breast and lung cancer.(17, 18) These two nanoparticle based drugs allow researchers to avoid the use of harsh organic solvents which would be required for drugs being administered as a solution. However, by encapsulating them in nanoparticles, these harsh solvents, which normally cause biocompatibility concerns, are not needed. Encapsulating them onto and within nanoparticles allows for normally water insoluble drugs to no longer require harsh organic solvents which are necessary if solutions of the drugs are administered. Furthermore, passive targeting of nanoparticles based on the EPR effect has been shown to decrease off target toxicity in the heart and kidneys after administration of doxorubicin

and toxic neutropenia commonly caused by paclitaxel.(12) Additionally, due to the inherent accumulation within tumors, Abraxane dosing regimens allow for lower doses of the drug to be administered to achieve the same clinical responses.

Taken together, the two currently approved nanoparticle based treatments, Doxil and Abraxane, demonstrate the efficacy and the need for nanoparticles in the clinic which can ultimately decrease off target toxicity caused by common chemotherapy.

1.2 Targeted Nanomedicine

Traditional chemotherapeutic compounds have been in use since the 1950s. Many of these chemotherapy agents are still being used today; however, they have several drawbacks. While most of these compounds kill cells by different mechanisms, they all share one common characteristic. All of these compounds target rapidly proliferating cells with no differentiation between healthy and diseased ones.(1, 8) The systemic activity of chemotherapeutics causes side effects such as hair loss, fatigue, decrease in blood cell count, and appetite loss. Therefore, a limitation of traditional chemotherapeutics is their upper dose limit that can be administered, above which serious off target toxicity becomes a concern for the patient. As described earlier, one way to overcome this barrier is through encapsulating chemotherapeutic drugs within nanoparticles which rely upon passive accumulation in the tumor. An alternative strategy to passive targeting is the concept of attaching a targeting ligand onto the surface of the nanoparticle. This approach, called active targeting, can increase the interaction between nanoparticles and the targeted cell and the likelihood of a more quantitative tumor targeted and specific uptake.(19-24)

Targeted nanomedicine offers the opportunity to treat patients in a more individualized approach. To date, there is a wide assortment of biomarkers that have been exploited by researchers to deliver a targeted payload to a tumor site. These functionalizations on the surface of the

nanocarriers include monoclonal antibodies, aptamers, ligands for cell surface receptors, and small peptides.(9, 25-28) Each of these is able to bind in a targeted manner to cellular specific biomarkers such as cell surface receptors. Current receptors being exploited for targeted delivery include, but are not limited to, folate receptor alpha and beta (FRα, FRβ), transferrin receptor, or integrin receptors.(29-31) Certain surface receptors, such as FRα and transferrin receptor, are significantly overexpressed in several cancers but display a very selective expression profile throughout the rest of the body. For example, FRα is reported to be over-expressed in greater than 85% of ovarian cancer patients and 80% of non-small cell lung cancers.(32, 33) Thus, attaching a ligand to the surface of nanoparticles creates a homing-like mechanism to deliver their payload in a targeted manner. When the nanoparticle binds to the receptor, a "Trojan-horse" type mechanism is used to hijack the receptors' natural ability to endocytose and to deliver the drug payload. This concept, along with the advantages of FRα targeting is elaborated upon more thoroughly in Chapter 3. Additionally, atomic force microscopy (AFM) techniques are utilized in Chapter 4 to assess the interaction between ligand and receptor in relation to competitive inhibition of targeted nanoparticles. Lastly, Chapter 5 addresses the nanoparticle biophysical changes that occur when the targeting ligand folic acid is attached to the surface of the delivery vector. The FRα targeting strategy is represented within Figure 1. Additionally, the AFM approach for analyzing ligand-receptor interaction can be seen in Figure 2.

There are four different isoforms of the folate receptor which can be found throughout the body; α, β, γ, and δ. Each isoform shares a highly conserved amino acid sequence which ranges between 68-79% similarity.(34, 35) All isoforms of the folate receptors have a high affinity for binding multiple folate compounds including folic acid, reduced folates, and antifolates to provide unidirectional transport into the cell. FR α and β have two N-glycosylation sites and bind folic acid

with high affinity with an equilibrium dissociation constant (K_D) of ~1 nM. These receptors bind their ligands and internalize them into the cell via receptor mediated endocytosis via caveolae coated pits.(34, 36-38) These pits completely evaginate into the cell and pinch off from the cellular membrane to create an endosome. As the endosome matures from an early to a late endosome, the pH inside the endosome drops considerably. Once the pH of the endosome has dropped, the ligand will be released into the cytoplasm of the cell through pH-dependent anion transporters or diffuses out of the intact endosomes.(33-35, 39) Substrates such as folic acid cannot be made *de novo* in the body and thus are required to be taken up by the cells for purine synthesis.

The encoding gene for folate receptors is found on the 11q13.3-q13.5 chromosome.(33) Of the four isoforms, FRα and β are a cysteine-rich glycophosphatidyl (GPI) anchored proteins which have a select expression throughout the body.(34, 35, 40) Folate receptor alpha (FRα) is expressed along the apical surface of the lung, the apical surface of the proximal tubules within the kidney, as well as within the choroid plexus. Due to its expression profiles in healthy tissues throughout the body, FRα is unable to recognize and bind circulating folates.(29, 40) However, these receptors have also been found to be over-expressed within multiple cancers which have direct access to the bloodstream; therefore, making them an attractive target for personalized therapy approaches.(26, 41, 42) FRβ expression profiles are limited to hematopoietic cells, such as activated macrophages, neutrophils, and the placenta.(43, 44)

Unlike the functions of FRα and β, the roles of FRγ and δ are lesser known. FRγ does not contain a GPI-anchored signaling domain and has been cited to be a secretory protein whose function is currently unknown.(45, 46) Lastly, FRδ plays an important role in fertilization of an egg. FRδ is found on the surface of mammalian egg cells and can recognize the sperm counterparts.

After recognition, FRδ expression is quickly decreased, possibly suggesting that FRδ also helps in egg cells ability to recognize only one sperm and prevent the occurrence of polyspermy.(47)

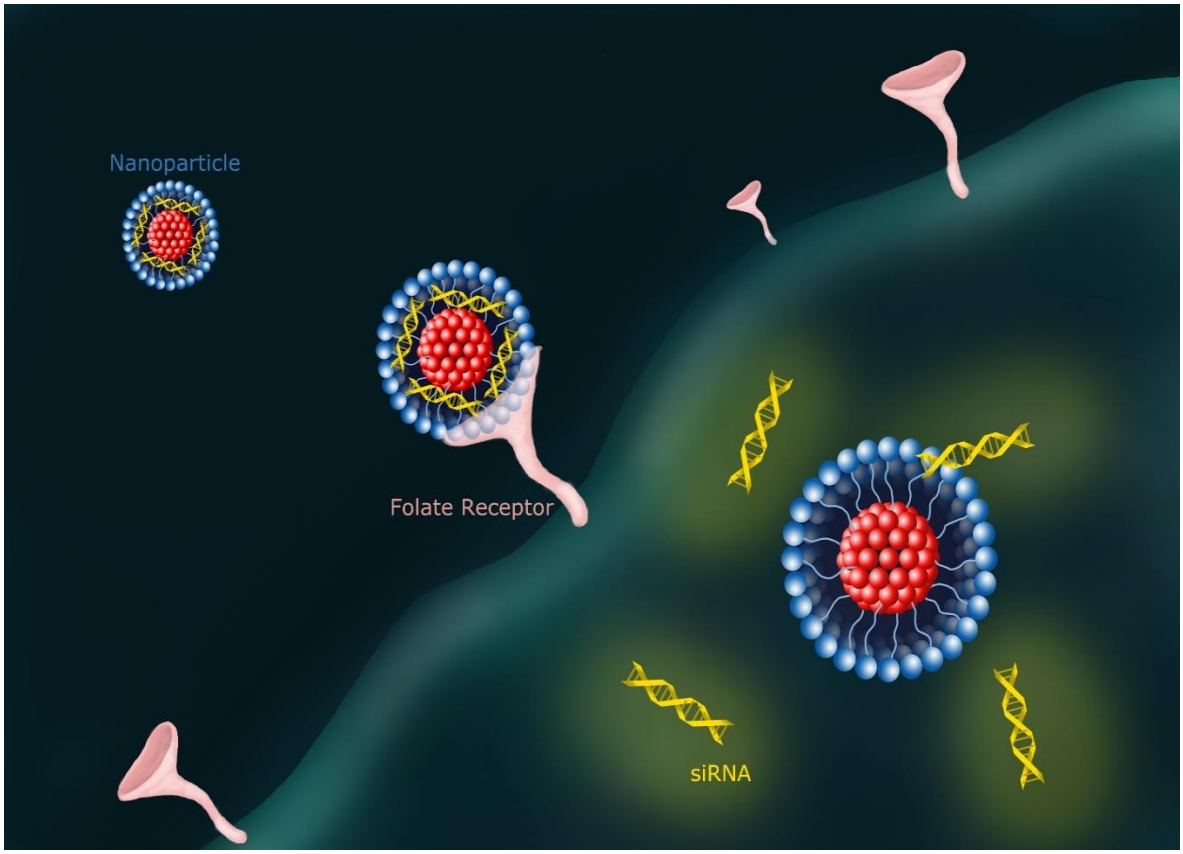

Figure 1.1: Graphical abstract of FRα targeted delivery of siRNA.(48)

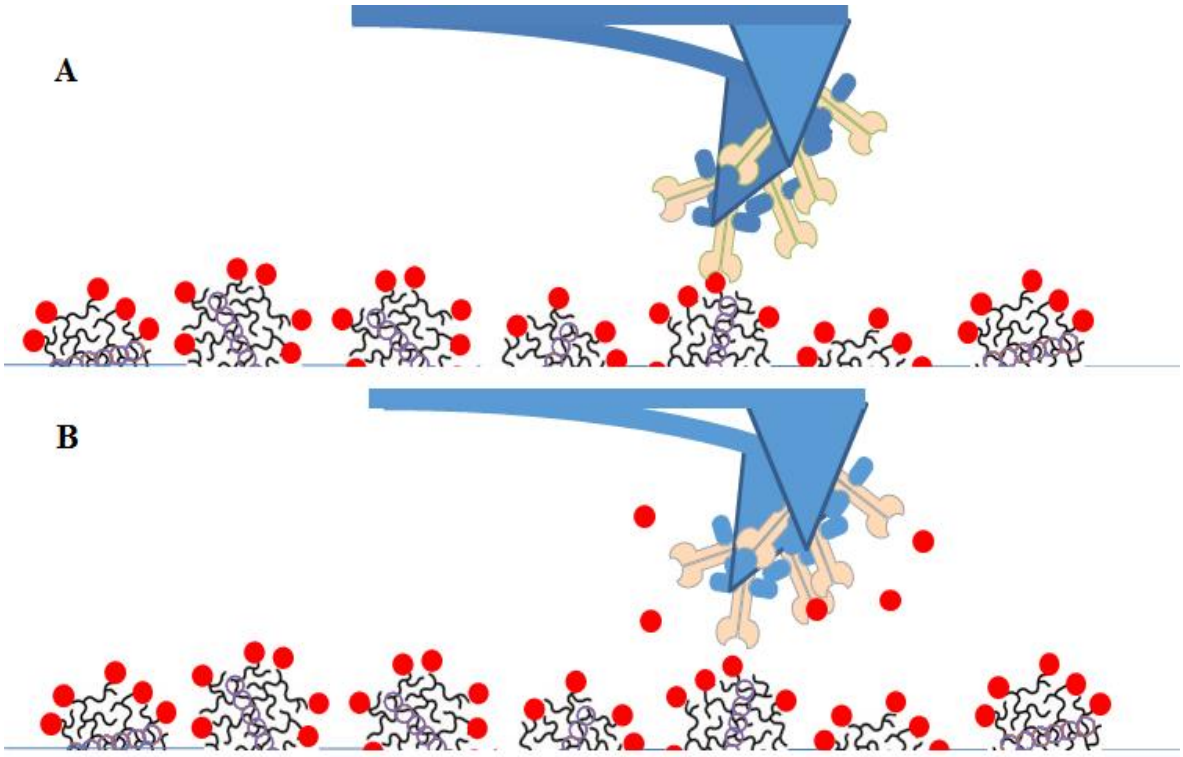

Figure 1.2: Graphical abstract of AFM FRα modified cantilever (in blue). Cantilever binding to folate decorated micelleplexes (bottom) without excess folic acid (red circles) (A) and excess folic acid (B).

Although targeted therapy offers many advantages over standard chemotherapy, it does have its limitations. One main challenge to this approach is that tumors are heterogeneous and it can be difficult to find biomarkers that are uniquely specific to the cells within the tumor. Additionally, inter-tumoral heterogeneity can arise creating more complexity.(49, 50) With heterogeneous populations found in tumors, alternative delivery strategies are considered due to their potent therapeutic effect and potential synergy they can offer to standard treatments. Nanoparticles, with their high modularity, have the capabilities to deliver a wide variety of drugs to various targets throughout the body. Very hydrophobic drugs, such as paclitaxel or cisplatin, can be packaged inside the bilayer of liposomes, thus, allowing these drugs to be administered in an aqueous formulation of a delivery vehicle.(51-53) Additionally, gene therapy based payloads, such as messenger RNA (mRNA), plasmid DNA (pDNA), and small interfering RNA (siRNA)

can be packaged inside polymeric nanoparticles through means of electrostatic condensation or precipitation.(54, 55) These packaging strategies are beneficial for the successful delivery of nucleic acids due to nucleic acids being large, negatively charged molecules and display poor cellular uptake capabilities. Payloads such as siRNA offer several therapeutic benefits over standard chemotherapy based drugs, which is why numerous companies are in the process of translating siRNA nanomedicine into the clinic.

1.3 Introduction to siRNA and Delivery

RNA interference (RNAi) was discovered in 1998 by Andrew Fire and Craig Mello when they first displayed the cells' natural ability to use double-stranded RNA to silence gene expression within the cytoplasm of the cell.(56, 57) They discovered that long double stranded RNA (dsRNA) can be cleaved by a ribonuclease, termed dicer, which cuts the double-stranded RNA into small interfering RNAs. These siRNAs can complex with the RNA induced silencing complex (RISC), a protein complex with endonuclease activity, which in turn can recognize and cleave mRNA that contains a homologous sequence. This decrease in functional mRNA leads to a transient protein knockdown within the cell. Soon after Fire's and Mello's discovery, this concept was exploited by researchers who demonstrated that synthetically made small interfering RNA (siRNA), delivered into the cytoplasm, could utilize the same mechanism while also achieving a protein knockdown.(16, 55, 56, 58) Synthetic siRNA molecules can be designed to recognize any target mRNA sequence. Therefore, theoretically, if administered properly, siRNA has the ability to silence any gene throughout the body. Due to its ease of modularity and its very potent therapeutic effects within the cell, siRNA delivery remains a very promising tool in nanomedicine.

Unfortunately, one of the major hurdles of siRNA therapy is the delivery of siRNA into the cytoplasm of the cell. Due to its large size and negative charge, naked siRNA cannot enter the

cell efficiently to achieve its therapeutic effects.(58, 59) Furthermore, naked siRNA is quickly cleared through the renal system and can easily be degraded in circulation by nucleases.(60) Therefore, researchers have created ways to package siRNA molecules into a variety of nanoparticles with the aim to increase its uptake profiles. Commonly used nanoparticles for siRNA delivery are made of, but are not limited to, lipid based, polymeric, dendrimer, and cationic materials. These types of nanomaterials are able to condense and protect the siRNA while aiding in the uptake efficiency of siRNA and increasing its gene knockdown efficiency.(61-63) In order to prolong the circulation profiles of the nanoparticles, and to increase the likelihood for them to reach the target site, PEG can be attached to the outer surface of nanoparticles. Additionally, as stated above, the surface of nanoparticles can be functionalized with targeting ligands such as folic acid. Folic acid as a targeting ligand has shown the capability to deliver payloads to ovarian cancer cells which overexpress the respective receptor. The ability to deliver siRNA to specific cells through active targeting helps bolster the therapeutic potential of siRNA nanomedicines. Overall, siRNA delivery has the ability to transiently knockdown specific genes which can give rise to disease progression or those which are aberrantly expressed.

1.4 Ovarian Cancer

With approximately 22,400 new cases each year, ovarian cancer is ranked the 17th most common cancer for women within the United States.(64, 65) Unfortunately, however, most of the patients who get diagnosed are already at the late stages of the disease progression where the cancer has already spread from the primary site of origination.(64, 66) For these patients, the survival rate is considerably lower. As a whole, ovarian cancer has a cure rate of approximately 30%. Ovarian cancer originates from three distinct areas: the ovary epithelium, fallopian tube epithelium, as well as the surface of the peritoneum.(64, 67) Once a tumor is established, it has a

fast disease progression with metastatic sites preferentially occurring within the peritoneum of the abdominal cavity. When theses metastatic sites take hold, they can choke off vital organs.(64) Standard treatment for ovarian cancers include tumor debulking, a full oophorectomy, and a combinational treatment regimen of a platinum agent (e.g. carboplatin) and a taxane agent (e.g. paclitaxel). (68, 69)

There are a few mutations that are common for ovarian cancer patients. It was estimated by Endocyte and the American Cancer Society (ACS) that more than 85% of ovarian cancer patients show a significant up-regulation of FRα.(70, 71) Additionally, as the histological grade of the cancer increases from 1-4, a corresponding trend of increased FRα expression is observed as well.(33, 71) This over-expression has been utilized by researchers and clinicians to help increase treatment and imaging efficacy.(72) Two main genetic alterations commonly found in ovarian cancer are p53 loss and BRCA 1 and 2 mutations.(73-78) Carrying a BRCA 1 or 2 mutation predisposes patients to ovarian cancer, as it is known for breast cancer. These individuals have a 40-60% chance to develop ovarian cancer.(79) Similarly, more than 80% of ovarian cancer patients that have serous ovarian carcinomas express a p53 mutation which ultimately loses its function.(64) These two mutations can create treatment problems as the tumors are likely not to respond to drugs and give rise to chemoresistant populations. Chapter 6 provides insight into FRα targeted nanoparticle delivery of siRNA within a clinically relevant orthotopic ovarian cancer mouse model using single-photon emission computed tomography (SPECT) and bioluminescence imaging (BLI).

Reoccurring and chemotherapy resistant ovarian cancer is a major hurdle that has not yet efficiently been addressed. Many ovarian cancer patients fall into either or both categories. Response rates for second line therapies can be as low as 10-30%.(64) Multiple pathways have

been cited to give rise to ovarian cancer chemoresistance. One mechanism of resistance is the over-expression of drug efflux pumps such as multi-drug resistance gene 1 (MDR1). (80-82) These pumps are one of a family of P-glycoprotein pumps that can export the drugs out of the cell before it can achieve its therapeutic effect.(83, 84) Additionally, anti-apoptotic proteins have been identified to give rise to ovarian cancer chemoresistance. These proteins, such as BCL-2 and BCL-xL, when overexpressed can inhibit efficacy of drugs by decreasing the likelihood of cells to undergo programmed cell death once treated.(75, 85) Both examples provide significant hurdles that need to be overcome in order to effectively treat ovarian cancer patients. Overcoming chemotherapy resistance within ovarian cancer models by interfering with Toll-like receptor 4 signaling via FRα targeting is addressed in Chapter 3.

Toll like receptors plays a vital role in the innate immune system surveillance with the ability to recognize bacterial pathogens.(86, 87) To date, 11 TLRs have been identified in humans and namely expressed on various immune cells. The TLR family maintains a conserved intracellular signaling domain along with a leucine-rich extracellular domain.(87, 88) TLRs are transmembrane proteins that most commonly signal through a myeloid differentiation factor 88 (MyD88) dependent pathway and promote inflammation and immune response.(89) Toll like receptor 4 (TLR4) can bind and recognize lipopolysaccharides (LPS) within bacterial cell walls which, in turn, promotes the production of proinflammatory cytokines such as IL-6, IL-12, and tumor necrosis factor-α (TNF-α).(88, 90) Several studies have demonstrated that increased inflammation and cytokine production within a tumor microenvironment can lead to a harsher microenvironment and promote tumor progression.(91-93) To date, TLR4 has been described to be involved with immune system surveillance and activation. However, recent studies have revealed a link of TLR4 activity with the tumor progression and chemotherapy resistance in

epithelial ovarian cancers (EOC).(88-90, 94) This link is driven by two factors: the first one being the expression of TLR4 and MyD88 dependent signaling in EOC, and secondly, PTX being identified as a TLR4 ligand. Subsequently, TLR4 activity through the MyD88 signaling cascade plays a role in EOC PTX chemotherapy resistance.(88, 90, 94) Therefore, it remains a promising target for therapeutically overcoming PTX chemotherapy resistance.

Current research using nanoparticles is attempting to combat this issue. Chemotherapy resistance has been more thoroughly studied in breast cancer. Therefore, within Chapter 2, we explore the major mechanisms that give rise to chemotherapy resistance and how nanomedicine can be utilized to combat and overcome them.

CHAPTER 2 – TACKLING BREAST CANCER CHEMORESISTANCE WITH NANO-FORMULATED SIRNA

Please note that this chapter has been taken and modified from the published Nature Gene Therapy review article in 2016. The authors include myself and Dr. Olivia Merkel. I am the first author on this review article. I performed the literature searches, compiled the literature, and wrote the review.

S. Jones, OM. Merkel. "siRNA Utilization in Breast Cancer Resistance Treatment" Nature Gene Therapy. 2016;23(12):821-8.

2.1 Introduction

Breast cancer is the leading cancer diagnosed in women and the second leading cause of cancer related deaths in women. It is estimated that 1 in 8 women will be diagnosed with breast cancer in their lifetime and over 40,000 women will die each year due to it (95). Early detection is key for patients; with a greater than 90% five-year survival rate for patients diagnosed at stages 0, I or II. Approximately 10% of patients present with stages III and IV, where treatment options are determined on an individual patient basis (96, 97). Neoadjuvent treatment can be used for localized invasive breast cancer. These include but are not limited to Herceptin (Her2 positive tumors only); a combination of an anthracycline-based and taxane based chemotherapy; hormone replacement therapy with an aromatase inhibitor; or inhibitors of the cyclin-dependent kinase (CDK) 4/6 (98). For advanced breast cancer, traditional chemotherapy and radiation can be used. However, these patients may never be "cured" after the cancer has spread into distant organs. Chemotherapy, radiation, bisphosphonates, Herceptin, and other treatments have all been used in these cases to treat the disease but do not cure it.

Current limitations to standard chemotherapy in the clinic are extensively researched. Typical problems with chemotherapy include their systemic treatment, a lack of tumor targeting and side effects in off-target tissues and organs, insufficient tumor deposition and penetration which would be necessary to achieve cell killing. Additionally, chemotherapy drugs can be very hydrophobic and poorly soluble which can limit their possible administration. Lastly, repeated treatments with the same drugs can give rise to tumors that are comprised of cancer cells which have become resistant to the drug. This phenomenon is called chemotherapy resistance. Resistance can arise through several factors; however, the most commonly published resistance mechanisms are associated with increased translation of anti-apoptotic proteins, such as Bcl-2, and of ATP binding cassette (ABC) transporters – more specifically, a family member known as p-glycoprotein (p-gp) drug efflux pumps (53, 99-101).

Since the discovery of RNA interference (RNAi), or small interfering RNA (siRNA), researchers have been able to selectively inhibit the expression of proteins within the cell. Considering that individual proteins have been described to give rise to multi-drug resistance (MDR) in breast cancer, many researchers have pursued the idea of targeted delivery of siRNA to combat and overcome chemotherapy resistance in cancer, and specifically in the context of breast cancer (102, 103). However, delivering siRNA intracellularly and specifically to cancer cells to knockdown the target gene can be difficult. Non-formulated, "naked" siRNA is easily degradable by ubiquitous RNases, it is a macromolecule that does not readily cross membranes, and siRNA is negatively charged and hydrophilic. Ongoing research has been evaluating the encapsulation of siRNA inside various delivery vehicles, its delivery and targeting to cancer cells in order to knock down oncogenes, genes associated with cell survival and anti-apoptosis, genes associated with chemoresistance to resensitize resistant cells, and many others. The reader is referred to several

excellent reviews which cover the current state of viral, non-viral, lipid, as well as other creative delivery systems for siRNA therapy (16, 58, 104). Various mechanisms of chemotherapy resistance and approaches to combat this problem with nanodelivery of siRNA have been described (105). One important approach is depicted in Figure 2.1, showing how siRNA can be coencapsulated with a chemotherapy drug to achieve maximum resensitization toward the drugs. The siRNA delivered can be used to target known pathways which give rise to chemotherapy resistance such as efflux pumps or anti-apoptotic protein Bcl-2. In this review, we are focusing on nanoformulation of siRNA for the fight against breast cancer chemoresistance.

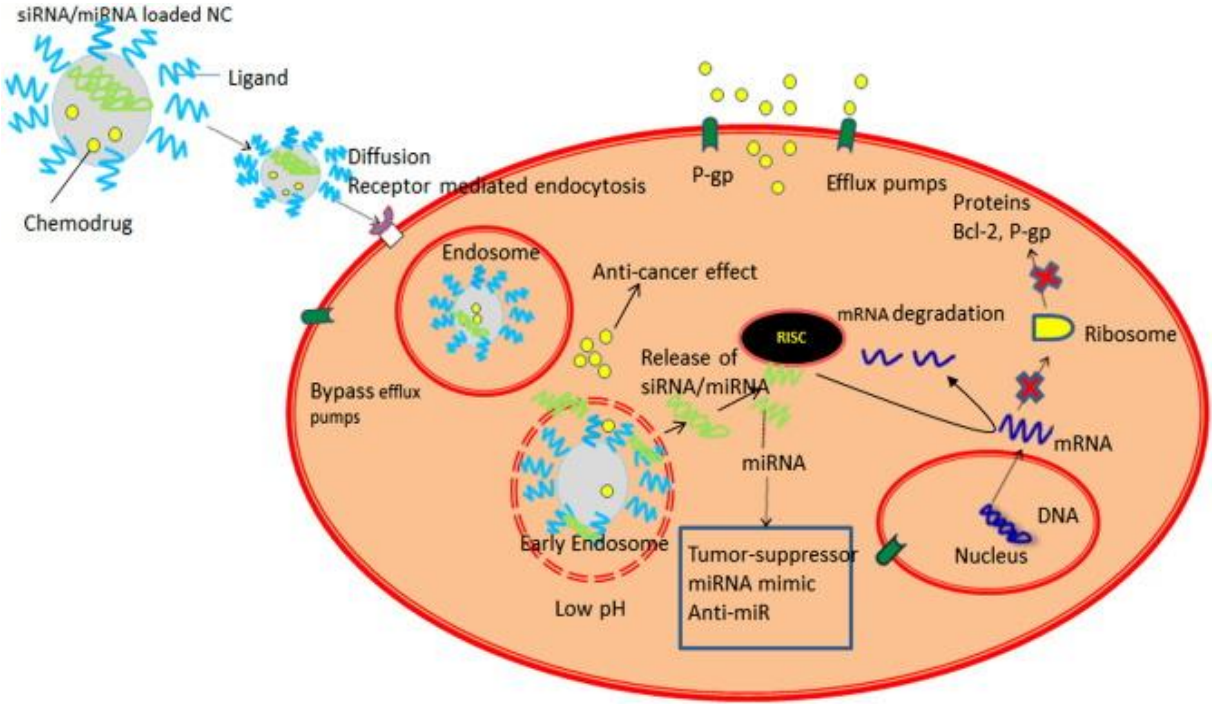

Figure 2.1: Combination approach of targeted delivery of siRNA and chemo drugs to the cytoplasm of a cancer cell to treat chemotherapy resistant breast cancer. By encapsulating both payloads with one nanoparticle, each drug is deposited inside the cell at the same time to achieve synergistic cytotoxic effects, e.g. gene silencing of p-gp pumps.

2.2 siRNA Delivery Challenges and Innovative Carriers

Multiple challenges oppose effective siRNA delivery. Due to its negatively charged and hydrophilic nature and susceptibility to degradation by nucleases, for successful delivery, siRNA

needs to be packaged inside a carrier in order to mediate its potent effects. Ideally, a carrier needs to be stable in circulation, have good cellular uptake and endosomal escape profiles, and be biocompatible and biodegradable, as well as be inherently non-toxic to the healthy cells (105). With a variety of "smart" vehicles being created and studied, these hurdles can be overcome. Successful siRNA delivery is reflected by efficient downregulation of specific proteins which give rise to multidrug resistance using nano-formulated siRNA.

Considering all the hurdles that need to be addressed in order to achieve safe and effective siRNA therapy, an abundant and wide range of carriers is being studied. Effective siRNA carriers for breast cancer therapy should have target specificity to the cancer cells which can be achieved with a targeting ligand to a receptor specifically expressed or overexpressed on the cell surface of breast cancer cells. Additionally, the final formulations of siRNA-bearing nanocarriers should have suitable sizes, charge, solubility profiles, encapsulation efficiency, as well as translational relevance in order to be potential candidates for clinical translation (106, 107). Wua et. al. and Wong et. al. were able to successfully co-encapsulate doxorubicin and siRNA against p-gp (108, 109). However, Wua et. al. used a folic acid targeting ligand on a PEG-b-(PCL-g-PEI)-b-PCL triblock copolymers which self-assembled into nanoparticles under 100 nm for delivery to MCF-7 cells, while Wong et. al. utilized a polymer-lipid hybrid nanoparticle (PLN) (108, 109). These dox loaded PLNs had an average size and zeta potential of 290 nm and -23.1 mV, respectively. The delivery systems of both groups were able to knockdown p-gp while employing a targeted vs. a non-targeted carrier system with different hydrodynamic diameters and zeta potentials. Considering that optimal sizes are often reported to be below 260 nm in order to avoid macrophage detection and phagocytosis, and optimal zeta potentials are described to be slightly positive to have an inherent interaction with the cell surface (110-113), the PLN characteristics could pose a

problem for *in vivo* delivery and efficacy. The use of folic acid on the surface of nanoparticles offers several benefits. The binding affinity of folic acid to FRα is characterized by an equilibrium dissociation constant being K_D=1 nM (114). This allows for a very strong and specific binding to the receptor. Coincidently, folate receptor alpha is primarily expressed on the epithelial surface throughout the body (ex. kidney, choroid plexus, lung) while several cancers show a significant overexpression of the receptor (29). This allows for folate receptor targeted nanoparticles to achieve a higher selectivity in cellular uptake along with a higher binding affinity or avidity. Another example of targeting a receptor on the cell surface was reported by Dou et. al (19). Their group targeted the HER-2 receptor on breast cancer cells by using positively charged protamine (F5-P) and attaching an anti-Her2 single-chain antibody fragment on the surface. The Her-2 targeting ligand displayed effective delivery to Her-2 positive cells BT474, but not to Her-2 null cells MDA-MB-231 (19). Utilizing a targeted approach with a single chain antibody offers the advantages of having a smaller size, of being cheaper and easier to produce, and the ability to functionalize in order to increase half-life (115).

Modifications to widely known polymers have been used to increase the efficacy of the latter or to increase their biocompatibility. Numerous groups have used polyethylene imine (PEI) as the cationic portion of their respective nanocarriers to condense siRNA for delivery. However, each group modified PEI differently in order to increase their carrier systems' biocompatibility. Navarro et. al. modified PEI with the phospholipid dioleoylphosphatidylethanolamine which resulted in particles of 127-187 nm in size, along with the ability to co-encapsulate p-gp siRNA and doxorubicin (116). In attempts to make PEI more biocompatible and to evade detection by the immune system, a common modification is the PEGylation of PEI. Meng et al. and Essex et. al. both PEGylated PEI in order to functionalize either a mesoporous silica nanoparticle with PEI-

PEG, or a DOPE-modified phospholipid PEI, respectively (117, 118). Meng's silica based nanoparticle achieved greater than 70% reduction of p-gp mRNA *in vivo,* as well as decreased off target cardiotoxicity after systemic doxorubicin treatment. On the other hand, by modifying a low molecular weight PEI with PEG, Essex et. al. exhibited an increase in circulation half-life of the nanocarriers which led to a deposition of 8% of the injected dose of siRNA in the tumor (117, 118). Lastly, low molecular weight PEI was designed by Lin et. al. with different alkylation groups and formed nanocarriers with clustered iron oxide nanoparticles. These nanocarriers were 80-130 nm in size with a zeta potential of +44 mV and were able to be imaged *in vivo*. Lin's iron oxide nanocarriers achieved a 50-60% downregulation of MDR1 *in vivo* after local administration (119).

Novel delivery devices and polymers have also been engineered and tested. Song et. al., for example, developed 270 nm thiolated glycol chitosan nanoparticles for anti-MDR1 siRNA delivery. Thiolating the nanoparticles helped increase their binding affinity and cross linking to form nano-complexes. This complex can be intravenously administered and shows 2.7x higher tumor targeting efficiency compared to non-chitosan-based nanoparticles (102). A unique approach to increasing doxorubicin's efficiency in treating triple negative breast cancer is the use of a layer-by-layer (LbL) nanoparticle film formation by alternately depositing siRNA and poly-L-arginine in layers atop a doxorubicin-loaded liposome. These nanoparticles were 120 nm in size with a zeta potential of -56 mV and could impressively hold 3,500 siRNA molecules per particle. In addition, the LbL nanoparticles had a circulation half-life of 28 hours, reduced MDR1 levels in the tumor by 80%, and increased doxorubicin's cell killing efficacy 4-fold (120). This approach, along with the Segovia et. al. approach of an oligo-peptide terminated pBAE nanoparticles embedded within a hydrogel scaffold, can lead to an increased half-life and a controlled release mechanism of siRNA to achieve a more sustained knockdown (121). Ultimately, several types of

carriers, ranging from well-established building blocks to novel compounds, have been studied and have shown promise. With all of the sophisticated carrier systems that have been developed, there has been a movement away from single payload delivery of siRNA to a co-delivery approach of multiple payloads to the cancer cell.

2.3 Common Targets to Overcome Resistance

In breast cancer research, several types of proteins are reported to lead to multidrug resistance. However, the most commonly studied form of MDR is caused by the overexpression of ABC transporters (122). In total, over 45 ABC transporter genes have been identified (123). These transporters actively transport various drugs through the plasma membrane and outside the cell. The most widely studied ABC transporter is ABCB1/MDR-1. Overexpression of MDR-1 can lead to an increase in the cells' resistance to certain drugs that are substrates to this efflux pump. The substrates for MDR-1 include, but are not limited to, generic chemotherapeutic agents such as anthracyclines, taxanes, and vinca alkaloids (109). However, even newer cancer drugs such as Gleevec (imatinib) can be a substrate (123). Numerous research groups around the globe have extensively studied the role of MDR1 in breast cancer (83, 103, 124, 125). Many of these groups have shown the effectiveness of inhibiting the overexpression of MDR1 with siRNA in order to resensitize breast cancer cells to various chemotherapeutic substrates of the protein pump. Other ABC family member transporters have been linked to giving rise to drug resistance in breast cancer. As demonstrated by Liang et. al., the inhibition of MRP-1/ABCC1 renders MCF-7 cells sensitive to doxorubicin (126). Furthermore, breast cancer resistance protein BCRP/ABCG2 was suppressed with siRNA in order to confer an increase in sensitivity to drugs such as methotrexate, doxorubicin, flavopiridol, and anthracyclines (127-129).

Additionally, several prosurvival and anti-apoptotic proteins have been linked to chemoresistance in breast cancer. Besides drug efflux pumps such as MDR1, prosurvival and anti-apoptotic proteins are the second most studied area in the breast cancer resistance field (53). Survivin, a small anti-apoptotic protein, can cause cells to avoid apoptosis when treated with paclitaxel. Salzano et. al described that when survivin is downregulated via siRNA treatment, cells became strongly resensitized to paclitaxel treatment and underwent significant inhibition of cell growth (130). Similar results were found with doxorubicin by Tang et. al. (51). By the same token, BCL-2, an anti-apoptotic protooncogene is overexpressed in at least 70% of breast cancers (131). By silencing more than 85% of BCL-2 expression in MCF-7 cells, Akar et. al. achieved efficient inhibition of cell growth and increased cell death (131). Other groups such as Li et. al. have studied NF-KB and its role in breast cancer chemoresistance (132). By co-delivering doxorubicin and siRNA against NF-KB, a significant decrease in doxorubicin's IC_{50} value was observed. Specifically, 80% of cells underwent apoptosis, and a greater than 95% positive synergy between the treatment with doxorubicin and anti-NF-KB siRNA was observed (132).

Besides the inhibition of MDR1 and anti-apoptotic proteins with siRNA, numerous other proteins have been published and linked to MDR within breast cancer. Liu et. al. revealed that fatty acid synthase (FASN) was overexpressed in breast cancers and gave rise to palmitic acid production which resulted in a decrease in apoptotic levels. Their work elucidates a potential new target for siRNA therapy to overcome chemotherapy resistance (133). Additionally, Gouazé et. al. provided a link to MDR through an overexpression of glucosylceramide synthase (GCS). By knocking down GCS, MCF7 cells exhibited a restored sensitivity to doxorubicin, vinblastine and paclitaxel (134). Members of the kinesin family have been linked to chemoresistance by Singel et. al. Two independent groups have shown that by knocking down the expression of Kif11 and Kif14,

resistance can be overcome in triple negative breast cancer (135, 136). This increase in kinesin family member proteins can be considered a potential biomarker for high-risk breast cancer tissue, according to Singel et. al. (135). Lastly, inhibition of angiogenesis in the context of breast cancer has been studied by knocking down VEGF with nano-formulated siRNA. Successful inhibition of VEGF was shown to inhibit the growth of tumor spheroids *in vitro*, while also showing efficacy *in vivo*. When combined with low dose doxorubicin, tumor microvessel density was inhibited, along with an increase in overall survival (137). Although less studied compared to MDR-1 or BCL-2, these alternative targets hold promise in the battle to overcome breast cancer resistance.

2.4 Epigenetic Targets

In an approach to better understand the development of chemoresistance, histone modifying and DNA methylating enzymes, so-called "epigenetic enzymes" have been reported to play important roles not only in cancer development (138, 139), but also in cancer chemoresistance (140). Calcagno et al. described that histone hyper acetylation is the reason for upregulation of ABCG2 in doxorubicin-selected cancer cell lines, including MCF7 breast cancer cells, and mediates their resistance. The authors employed Oligofectamine, a commercially available transfection reagent, to deliver siRNA against ABCG2 and observed that a 40-fold decrease in the ABCG2 levels led to 85% restored sensitivity compared to the parental MCF7 cells (140). But epigenetic changes can also cause chemoresistance via pathways independent of p-glycoproteins. As described above, pro-survival signaling can prevent the effectiveness of chemotherapy also. Accordingly, Almeida et al. reported that NFκB signaling can cause histone modifications which in turn mediate chemoresistance in head and neck squamous cell carcinoma (HNSCC) via histone deacetylation. The authors showed that knockdown of IKKα and IKKβ, which represses NFκB, resulted in induced acetylation of tumor histones and reduced chemoresistance against cisplatin

(141). Even though this study was conducted in HNSCC cells, similar pathways may be found in breast cancer cells, as well. In breast cancer, however, other epigenetic changes have already been described. Mungamuri et al. investigated epigenetic changes that lead to overexpression of Her-2/neu, an EGFR family receptor. The authors observed that methylation of H3K4me3 mediates resistance toward trastuzumab and that silencing of Wdr5 with shRNA, one of the four structural components of the H3K4 methyltransferase complex, decreased Her-2/neu levels and chemoresistance (142). shRNA was also used to silence DNA methyltransferase 3b (DNMT3b) in hypermethylator breast cancer cell lines BT549, and Hs578T and caused sensitization toward doxorubicin, paclitaxel, and 5-fluorouracil (143). DNMT3b and DNMT1 were also the subject of other studies that used commercially available transfection reagents to deliver siRNA (144, 145). However, to our knowledge, so far no studies have been published employing nanoformulated siRNA to silence epigenetic targets.

2.5 Co-delivery of Payloads and Alternative Approaches

Recent literature has stated that simultaneous delivery of siRNA and a chemotherapeutic agent yields more synergistic results and more cell killing than separate or stand alone treatment (53). This technique of encapsulating chemotherapeutic drugs within carriers offers the advantages of encapsulating poorly soluble drugs, eliminating off target effects caused by harmful organic solvents needed to dissolve hydrophobic drugs and replacing the use of viscous emulsions. Encapsulating chemotherapeutic agents within the core of a micelle or liposome allows for the opportunity to add a targeting ligand to change the delivery profile from systemic non-targeted to targeted therapy. Additionally, delivering both payloads at the same time ensures that both agents reach the tumor simultaneously instead of relying on the pharmacokinetic circulation profiles, and

targeting efficiency of each separate drug. Several groups have used this approach to their advantage to overcome resistance in breast cancer.

Due to the frequent overexpression of p-gp in breast cancer, several groups have co-encapsulated anti-siRNA p-gp with doxorubicin. Examples of this strategy were described by Wua et al. and Wong et. al. Both groups demonstrate that co-delivery of both payloads can reduce off target toxicity and resensitize MCF-7 and MDA-435 cell lines (108, 109). Using a different carrier, Jiang et. al. synthesized a modified RGD (argininine-glycine-aspartic acid) targeted peptide liposome encapsulating p-gp siRNA and doxorubicin. These liposomes were less than 200 nm in size and *ex vivo* imaging studies showed the accumulation of siRNA and dox within the tumors at the same site. Furthermore, co-delivery of these two agents showed significant inhibitory effects on tumor growth (146). Peptide-based targeting moieties, such as integrin targeting RGD can bind to their respective receptors throughout the body. Peptides inherently are easy to synthesize, biocompatible, and smaller than antibodies, and have a wide variety of targeting receptors (147). A tabulated summary of co-delivery approaches is shown in Table 2.1, adapted from Gandhi et al. (105). This table depicts various approaches utilizing nanoparticles to co-deliver a chemotherapeutic drug, along with a nucleic acid based payload in order to treat a variety of cancers. These results emphasize the potent synergy between co-administration versus single dosing.

An alternative approach to overcoming resistance is packaging two separate siRNA sequences for different targets, as well as encapsulating selenium. Zheng et al., prepared layered double hydroxide (LDH) nanoparticles that were 116 nm in size and were able to selectively deliver siRNA against p-gp and *b*-tubulin III. This approach was shown to inhibit cell mitosis, spindle formation but also induced apoptosis in MCF-7/ADR cells (148). Additionally, other

groups have described the approach of using two siRNA sequences to silence multiple ABC transporters in MCF-7 cells. In a study by Li et al., ABCG2 and ABCB1 sequences were simultaneously delivered inside a pH-sensitive carbonate apatite nanoparticle. The dual targeted siRNA approach led to an enhanced toxicity (above 45-50% cell killing) when treated with cisplatin, paclitaxel and doxorubicin. While the single delivery of siRNA did slightly resensitize the cells, the dual targeted siRNA approach had a greater cytotoxicity (149).

Table 2.1

Co-delivery of siRNA in combination with chemotherapeutic drug and/or nucleic acid based reagent for the treatment of cancer.

siRNA/ miRNA	**Drug**	**Type of nanocarrier**	**Cell lines**	***In vivo* model**	**Targeting**	**Targeting moiety**	**Ref.**
siRNA targeting BCL2 and MRP-1	DOX/ CIS	Mesoporous silica nanoparticle	A549 human lung adenocarcinoma	Murine A549 lung cancer Orthotopic model	Active	LHRH peptide	(13)
siRNA targeting P-gp	DOX	mesoporous silica nanoparticles	MDR KB-V1 human cervical carcinoma	–	Passive	–	(62)
siRNA targeting P-gp	DOX	PEI-PEG functionalized mesoporous silica nanoparticles	MCF-7/MDR—breast cancer	Murine MCF-7/MDR breast cancer Xenograft model	Passive	–	(27)
siRNA targeting mTERT	PTX	HTCC nanoparticles	LLC—lewis lung carcinoma	–	Passive	–	(63)
siRNA targeting GFP	DOX	G(4)-PAMAM-PEG-DOPE dendrimers	C166 cells—yolk sac endothelial	–	Passive	–	(64)

siRNA targeting Luc gene	DOX	(G3) poly (l-lysine) OAS dendrimer	U-87 glioblastoma	–	Active	RGD peptide	(13)
siRNA targeting BCL-2	Docetaxel	PEG-PLL-PLLeu cationic micelles	–	Murine MCF-7 breast cancer Xenograft model	Passive	–	(65)
siRNA targeting MCL-1 and GL2	SAHA	TLO cationic liposomes	KB epithelial cancer	Murine KB epithelial cancer Xenograft model	Passive	–	(13)
siRNA targeting VEGF	PTX	PDMAEMA–PCL–PDMAEMA cationic micelles	PC-3 human prostate cancer and MDA-MB-435-GFP breast cancer	–	Passive	–	(66)
siRNA targeting VEGF and c-Myc	DOX	Lipid polycation DNA nanoparticles	MDR NCI/ADR-RES ovarian tumor	Murine NCI/ADR-RES ovarian cancer xenograft model	Passive	–	(67)
siRNA targeting c-Myc	DOX	Liposome-polycation-DNA nanoparticles	HT-1080 fibrosarcoma	Murine HT-1080 fibrosarcoma xenograft model	Active	PEGylated NGR (aspargine-glycine-arginine)	(68)
siRNA targeting BCL2 and MRP-1	DOX	DOTAP cationic lipid nanoparticles	MDR lung cancerMDR A2780/AD ovarian cancer	–	Passive	–	(13)
siRNA targeting MCl-1	MEK inhibitor PD032590	Cationic liposomes	KB epithelial cancer	Murine KB epithelial cancer xenograft model	Passive	–	(69)
siRNA targeting	CIS	PEI complexes	–	Murine A549	Passive	–	(13)

VEGFR and EGFR				NSCLC xenograft model			
siRNA targeting X linked inhibitor of apoptosis	PTX	Deoxycholic acid-PEI complexes	HCT-116 colorectal cancer	Murine HCT-116 xenograft model	Passive	–	(70)
siRNA targeting BCL-2	DOX	Cationic PEI-PCl nanoparticles	C6 Glioma Bel-7402 human hepatoma	Murine C6 glioma xenograft model	Active	Folic acid	(71)
siRNA targeting P-gp	PTX	PLGA-PEI nanoparticles	JC mouse mammary cancer	Murine BALB/c JC breast cancer xenograft model	Active	Biotin	(72)
siRNA targeting MCL-1	PTX	Cationic solid lipid nanoparticles	KB epithelial cancer	Murine KB epithelial cancer xenograft model	Passive	–	(73)
siRNA targeting Plk1	PTX	PEG-b-PCL-b-PPEEA micelleplex	MDA-MB-435 breast cancer	Murine MDA-MB-435 s breast cancer xenograft model	Passive	–	(74)
siRNA targeting BCl-2	S-1	Lipoplexes	DLD-1 colorectal adenocarcinoma	Murine DLD-1 colorectal adenocarcinoma xenograft model	Passive	–	(75)
iMdr-1-shRNA iSurvivin-shRNA	DOX	Poly (b-amino esters) based nanoparticles	MCF-7 human breast adenocarcinoma	Murine BALB/c MDR MCF-7 breast adenocarcinoma	Passive	–	(42)

				xenograft model			
siRNA targeting HMD2<comma>c-Myc	VEGF siRNA	Lipid coated calcium nanoparticles	A549 adenocarcinoma and H460 lung carcinoma	Murine A549 and H460 NSCLC xenograft model	Passive	–	(76)
siRNA targeting c-Myc and MDM2	VEGFR mir-24a	Liposome-polycation-hyaluronic acid	–	Murine B16F10 melanoma xenograft model	Active	scFv	(77)

2.6 Animal Models

In order to move the various delivery systems, siRNA targets, and disease states closer to the clinic, numerous animal models have been employed to investigate overcoming multidrug resistance in a more complex *in vivo* setting. For the past four decades, several previous models have been utilized *in vivo* for breast cancer research (102, 108, 121). Current breast cancer models which are applied can be spontaneously forming tumors, mainly in larger animals, genetically modified models, and xenografts. Additionally, all of the various subtypes of breast cancer such as triple negative, invasive ductle carcinoma or inflammatory breast cancer are studied. However, new models needed to be developed in order to specifically analyze the re-sensitization of chemotherapy resistant cells in laboratory animals, mainly in mice.

Numerous research groups have created isogenic cell lines that are sensitive and resistant to various chemotherapeutic agents. Montazeri et al. used a xenograft nu/nu nude mouse model with MDA435 sensitive and resistance cells injected subcutaneously into the right flank of the mice (150). This model, along with the authors' work delivering VEGF siRNA and doxorubicin to mice, helped elucidate a decrease in tumor blood vessels which allowed for an increase in life

span of the tumor bearing mice. Commonly, MCF-7 cells are used in breast cancer *in vivo* xenograft models due to being extensively researched, being easily available, and for having resistance to commonly used agents such as doxorubicin. A multitude of independent groups have all utilized MCF-7 cells to study chemotherapy resistance and demonstrate their treatments efficacy on overcoming MDR *in vivo* (102, 119, 137, 151, 152). Similarly, triple negative breast cancer cell lines such as MDA-MB-231 and MDA-MB-468 can be injected into immune-suppressed mice in order to study the response of triple negative breast cancer to siRNA therapy (107, 153-155). Besides varying cell lines in order to study a wide variety of breast cancer subtypes, different injection sites have been described. While the most common injection site for studies employing nano-formulated siRNA to tackle chemoresistance in breast cancer is the subcutaneous area at the flank (102, 150, 154), other models mimic metastases in the axilla region (137, 152), or primary orthotopic tumors in the mammary fat pad of the mice (107, 119, 153). So far, no spontaneous tumors or genetic models have been used for siRNA delivery to breast cancer in the fight against chemoresistance. The lack of more relevant models may explain the large amount of pre-clinical but the very small amount of clinical studies.

2.7 Clinical Trials of siRNA Utilized in Breast Cancer Treatment

Since the discovery of siRNA, researchers have been trying to transition this technology to the clinic. Advances have been made since the discovery of the RNAi mechanism, however, the transition into clinical trials and into the clinic has remained challenging. There have only been a handful of RNAi based clinical trials translated into the clinic for treatment of solid tumors, and hardly any for breast cancer. In 2008, Calando Pharmaceuticals started a clinical trial with their drug CALAA-01 for solid tumors, including breast cancer (24). Their study used a transferrin targeted cyclodextrin-containing polymer which carried an anti-R2 siRNA sequence. Transferrin-

targeting utilizes a recycling pathway involving a clatherin-coated pits method of internalizataion which can be exploited to help delivery payloads into the cell while also achieving a tumor targeting approach. Several cancers such as breast, pancreas, colon, lung, and bladder have demonstrated an increased expression of transferrin receptors, including several drug resistant tumors (24). This transferrin-targeted clinic trial was performed to study the safety and tolerability of a nanoparticle and siRNA based injection in patients and has been subsequently terminated due to not meeting their primary or secondary outcome measures (156). Lately, M.D. Anderson Cancer Center has been recruiting participants for their EphA2 gene targeting study using a liposomal siRNA delivery agent. This study also assesses the safety of their liposomal formulation. Data such as dose-limiting toxicity and hematologic toxicity are being recorded (157). On the other hand, ever since the discovery of ABC transporters, such as MDR1, several clinical trial studies have investigated inhibitors of ABC transporters. These clinical trials range from the early 1990s until recently. Although these trials do not include siRNA, but rather small-molecule inhibitors of the transporter pumps, they have been studied in several cancers, including breast cancer, and have been shown to increase overall survival in patients (100). The knowledge obtained through these clinical trials could in fact be a promising basis for subsequent trials with siRNA for the inhibition of ABC transporters. Overall, siRNA based therapies have not yet reached the clinic, but with further development of multiple targets, sophisticated delivery systems, and combination treatments, hopefully a breakthrough can be achieved.

2.8 Conclusion and Outlook

Resistance to chemotherapy is a challenging obstacle that needs to be addressed and overcome in the clinic. One mechanism that has been used to resensitize cells has been targeted delivery of siRNA. Since the discovery of RNA interference, researchers have been trying to

exploit its benefits in order to provide therapeutic gene knockdown of target proteins. This approach yields several advantages, especially in combination with standard chemotherapy. For years it has been known that several proteins (namely ABC transporters and anti-apoptotic factors) are over-expressed in breast cancer leading to resistance toward chemotherapy drugs such as doxorubicin or paclitaxel. Effective siRNA delivery can selectively knock down the over-expression of such proteins, thus resensitizing the cells to treatment. While this review touched heavily upon resistant mechanisms derived from MDR expression, anti-apoptotic factors, angiogenesis, and epigenetic factors, there are a variety of alternative pathways and factors that can give rise to multidrug resistance. Due to the scope of this review, those factors such as tumor microenvironment mediated drug resistance will not be addressed in this chapter. However, in order to effectively deliver siRNA, a carrier needs to be used. One of the major advantages is that these carriers can encapsulate multiple payloads for a combination treatment. It has been shown that combination treatment of drugs such as doxorubicin and siRNA have a greater therapeutic efficacy than the delivery of single agents. This approach has shown significant promise both *in vitro* and *in vivo*. Albeit multiple studies have been shown to achieve significant therapeutic efficacy with nanoformulated siRNA therapies, there are hurdles that need to be addressed in the future. For a more in depth analysis on the toxicity and off target effects of siRNA and nanoparticles, the authors refer the reader to several in depth reviews on the matter (158-161).

The transition of siRNA therapy into the clinic has yet to be achieved. Only a handful of clinical trials have used siRNA, and only a small fraction included breast cancer patients. It is expected that with newer targeted delivery agents, the most common hurdles for specific and efficient siRNA delivery can be overcome. If successful, siRNA treatment has a promising future in the clinic, especially for chemoresistant breast cancer patients.

CHAPTER 3 – FOLATE RECEPTOR TARGETED DELIVERY OF SIRNA AND PACLITAXEL TO OVARIAN CANCER CELLS VIA FOLATE CONJUGATED TRIBLOCK CO-POLYMER TO OVERCOME TLR4 DRIVEN CHEMOTHERAPY RESISTANCE

Please note that the entirety of this chapter has been published as a research article in Biomacromolecules in 2015. The Authors include myself, Vincent Lizzio, and Olivia Merkel. Within this publication, I designed and executed the experiments, as well as wrote the chapter.

S. Jones, V. Lizzio, OM. Merkel. "Folate Receptor Targeted Delivery of siRNA and Paclitaxel to Ovarian Cancer Cells via Folate Conjugated Triblock Co-polymer to Overcome Chemotherapy Resistance". Biomacromolecules 2015, doi: 10.1021/acs.biomac.5b01189.

3.1 Introduction

While healthy tissues outside of the kidneys, choroid plexus, lung generally do not express an abundance of folate receptor-α (FR-α) exposed to the bloodstream, several cancers have been found to significantly over express FR-α which are. Most notable, in approximately 85-90% of ovarian cancers, there is an over expression of FR-α with an increasing expression as the histological grade of the cancer increases.(69, 70, 162, 163) Outside of a full oophorectomy for early stage patients, treatments for late stage ovarian cancer includes radiation and a combination of platinum and taxane chemotherapeutic agents. Often times, late stage ovarian cancer patients experience a reoccurrence of their disease where resistance to first line treatment is seen.(164) To overcome challenges seen within the clinic, such as chemotherapy resistance, relapse of the disease, and off target toxicity, we are taking advantage of the over-expressed FR-α commonly observed in ovarian cancer patients by using folate receptor-targeted nanoparticles. Targeted nanoparticle delivery, formulated and designed specifically for enhanced tumor targeting and

uptake tackling chemoresistance could therefore become a novel approach for treating chemotherapy refractory ovarian cancer.

A new theory to treating cancer eventually within the clinic is the use of nanoparticles to deliver a targeted payload to the tumor, while decreasing uptake of the drug inside healthy tissues. Both Doxil and Abraxane are nanopartcles that are currently being used within the clinic to treat cancer.(68, 165) However, both of these nanoparticle formulations solely rely upon the enhanced permeation and retention effect (EPR effect) to passively target the tumor by means of extravasation out of the tumor's leaky blood vasculature.(14, 166) A targeted delivery, such as demonstrated within this dissertation, can be achieved by attaching a targeting ligand to the surface of the nanoparticle to increase its interaction with the tumor cell.(26, 167-169) The folate receptor is an excellent receptor to target tumors due to its nature of receptor-ligand interaction. FR-α is an internalizing transmembrane receptor which will endocytose once folic acid, its ligand, binds, and the receptor-ligand complex is internalized. The ligand, and anything conjugated to it is subsequently deposited into the cytoplasm, while the receptor is recycled back to the cell surface.(170-172) This provides a selective gate to deliver chemotherapeutics, but also macromolecules such as therapeutic RNA (siRNA) can be delivered into the cytoplasm of the cell where they can achieve their effect.(170) In order to overcome the hurdles commonly seen with ovarian cancer treatment, such as relapse and resistance, a wide variety of combinational therapies that include siRNA are currently being studied.(74, 173-178) However, our own approach incorporates targeted delivery of siRNA to ovarian cancer cells for therapeutic knock down of specific oncogenes that give rise to chemotherapy resistance, such as TLR4.(88, 90, 94, 179) We hypothesize that knock down of these proteins re-sensitizes ovarian cancer cells toward first-line chemotherapeutic agents. Our results show that folate-decorated nanoparticles can effectively

deliver siRNA into the cancer cells and achieve a drastic and sustained knockdown of TLR4. Our approach of using a tri-block copolymer that consists of polyethyleneimine-graft-polycaprolactone-block-poly(ethylene glycol), or folate-coupled PEI-*g*-PCL-*b*-PEG-Fol, overcomes typical obstacles of siRNA delivery, such as rapid clearance and degradation in circulation. PEI-*g*-PCL-*b*-PEG polymers have been shown to form stable micelles with siRNA that exhibit enhanced circulation time, and folate coupled PEI-*g*-PCL-*b*-PEG-Fol conjugates have been reported to transfect receptor overexpressing cells in a targeted manner.(59, 180-186) Within the polymer, PEI electro-statically condenses and shields the siRNA from degradation by nucleases, while the conjugated folic acid ligand on the particle surface provides specificity towards cells that over-express FR. In addition, the PCL block increases the hydrophobic content of the nanoparticle, which forms the inner core of the micelle where paclitaxel (PTX) can be encapsulated for combination therapy with the same particle.(180) Lastly, the addition of PEG increases the biocompatibility and acts as a stealth mechanism to avoid macrophage detection of the nanoparticles.(184) Collectively, these four components are hypothesized to effectively encapsulate their payload and yield a targeted delivery to the cancer cells of interest.

Altogether, our strategy within this project is to create an effective, targeted siRNA therapy to meet the following goals: 1) develop a biocompatible folate-decorated nanoparticle which can deliver siRNA in a targeted fashion to ovarian cancer cells that over-express FR-α; 2) achieve a targeted tumor uptake and specificity; 3) accomplish improved pharmacokinetic parameters such as bioavailability and prolonged circulation; and 4) overcome the barrier of chemotherapy resistance. In response to the aforementioned strategy, we hypothesize that by effectively delivering siRNA against TLR4 with our folate conjugated tri-block co-polymer to ovarian cancer

cells, we can achieve a targeted therapeutic effect in FR-overexpressing cells, decrease off-target toxicity, and overcome chemotherapy resistance in combination with PTX.

3.2 Materials and Methods

3.2.1 Reagents

Hetero-bifunctional poly(ethylene glycol) (HO-PEG-COOH, 3.5 and 5 kDa), as well as monofunctional poly(ethylene glycol) (CH3-PEG-COOH, 5 kDa) was purchased from JenKem Technologies (Plano, TX, USA). Hyper branched polyethylenimine (hyPEI, 25k Da) was obtained from BASF (Ludwigshafen, Germany). All other regents for synthesis were obtained from Sigma-Aldrich (St. Louis, MO, USA) and used without further modification. Dicer substrate double-stranded siRNA (DsiRNA) targeting the Enhanced Green Fluorescent Protein gene (EGFP siRNA, 25/27), siRNA for Toll-Like Receptor 4 (TLR4), and a scrambled nonspecific control (siNegCon) DsiRNA as well as Alexa Fluor-488 and TYE-563 labeled siRNA, were purchased from Integrated DNA Technologies (IDT, Coralville, IA, USA). Dulbecco's Modified Eagle's Medium (10x) without folic acid, Dulbecco's phosphate buffered saline (PBS), heat-inactivated fetal bovine serum (FBS), D-(+)-glucose, sodium bicarbonate, sodium pyruvate, 2-mercaptoethanol, dimethyl sulfoxide (DMSO, ≥99.7%), ethylenediaminetetraacetic acid (EDTA, 99.4−100.06%), trypan blue (0.4%, sterile filtered), and luciferin were purchased from Sigma-Aldrich (St. Louis, MO, USA).

3.2.2 Synthesis of Tri-block Copolymers and Characterization

The overall reaction scheme, adjusted from Liu et al, (187) can be found in Supplementary Scheme 1. The tri-block copolymers were synthesized by a six step reaction process consisting of coupling an azido functionalized folic acid (molecule A) with a heterobifunctional acrylate-PCL-*b*-PEG-alkyne (molecule B) via click chemistry reaction. This was followed by coupling the previous product of acrylate-PCL-*b*-PEG-Fol (molecule C) with *hy*-PEI (25 kDa), as previously

described.(187) A total of six different conjugates were synthesized consisting of two different PEG lengths (3.5 kDa or 5 kDa), varying grafting densities of PCL-*b*-PEG-Fol (10 µmol or 30 µmol per 10 µmol of PEI), as well as one null folate conjugate (Table 1). Compounds synthesized were characterized by ^{1}H NMR, UV spectroscopy, and a folate composition assay.

3.2.3 Folate Composition Assay

A UV spectroscopy assay was used for determining the folic acid concentration within each sample. Each sample was read in triplicates on a Synergy 2 microplate reader (BioTek Instruments, Winooski, VT, USA). Folic acid standards were dissolved in DMSO at a concentration of 2, 1, 0.5, 0.25, 0.125 and 0 mg/mL. Conjugates were weighed out and dissolved in water. Afterwards, 100 µL of each sample was added to a 96 transparent well plate and read at 360 nm. Blank values of DMSO and water were used to eliminate any background signal. Results were analyzed by Graphpad Prism 5.0 and are displayed as mean values.

3.2.4 Cell Culture

SKOV-3 cells are a human ovarian cancer cell line and were obtained from ATCC (LG Promochem, Wesel, Germany). The SKOV-3/LUC cell line was transfected to stably express the reporter gene luciferase as described before.(188) SKOV-3 ovarian cancer cells were cultured in folate-free DMEM cell culture medium (Sigma-Aldrich) supplemented with 0.584 gm/L of L-glutamine, 3.7 gm/L sodium bicarbonate, 10% fetal bovine serum (Thermo Scientific Hyclone), and 1% penicillin/streptomycin. Cells were grown in 75 cm^2 cell culture flasks (Thermo Scientific) at 37 °C and 5% CO_2 and passaged every 2-3 days when they had reached confluency.

A549 cells are a human adenocarcinoma alveolar based lung cancer cell line and were obtained from ATCC (LG Promochem, Wesel, Germany). A549 lung adenocarcinoma cells were cultured in DMEM cell culture medium (Sigma-Aldrich) and supplemented with 10% fetal bovine

serum and 1% penicillin/streptomycin. Cells were grown in 75 cm^2 cell culture flasks at 37 °C and 5% CO_2 and passaged twice a week when they reached confluency.

3.2.5 Preparation of PEI-g-PCL-b-PEG-Fol Micelleplexes

Each polymer was dissolved in water to yield a 1 mg/mL concentration based upon the PEI 25 kDa content. Once dissolved, samples were filtered through a 0.22 μm filter for sterilization. In order to prepare the micelleplexes, a specific ratio between the amine groups found within the polymer (N) and the phosphate groups of the siRNA (P) was chosen. The N/P ratios were calculated based upon the formula seen below:

$$m\ (polymer) = n(siRNA) \times 52 \times MW\ (protonable\ units) \times N/P\ ratio$$

In the equation listed above, m refers to the mass of the polymer needed, n refers to the amount of siRNA used per well, 52 represents the amount of phosphate groups within one 25/27 nucleotide siRNA molecule, the MW represents the molecular weight of the protonable unit found within the polymer (43.1 g/mol for *hy*-PEI), and the N/P is the desired ratio between amine groups on the polymer and phosphate groups on the siRNA.

3.2.6 SYBR Gold and Heparin Assays

The SYBR gold assay was used to assess the ability of each conjugate to successfully condense siRNA at varying N/P ratios (0-20). SYBR Gold is a fluorescent dye that intercalates with uncomplexed double-stranded nucleic acids and experiences a more than 1000-fold fluorescence enhancement upon intercalation. However, once siRNA is condensed within the micelleplex, the dye can no longer intercalate and exhibits very weak fluorescence. All conjugates were tested against *hy*-PEI (25 kDa) as a positive control. At varying N/P ratios (0-20), 50 μL of polymer dilution and 50 μL of 1 μM EGFP siRNA were added to each well in a total of 100 μL of a 5% glucose solution. Once mixed, solutions were incubated for 20 minutes at room temperature.

Afterwards, 30 μL of a 4x SYBR Gold solution (Life Technologies, Carlsbad, CA, USA) were added to each well and incubated in the dark for 10 minutes at room temperature. Samples were measured in triplicates for fluorescence at 495 nm (excitation) and 537 nm (emission) on a Synergy 2 microplate reader (BioTek Instruments, Winooski, VT, USA). Samples were normalized based upon the following criteria. The fluorescence level of 100 percent free siRNA was calculated based upon the fluorescence of free siRNA, non-condensed, with SYBR Gold dye. The fluorescence of zero percent free siRNA was calculated with SYBR Gold dye in glucose solution only at the absence of siRNA. Results were analyzed by Graphpad Prism 5.0 and are displayed as mean values and standard deviation.

Similarly, heparin assays were used to determine the stability of the micelleplexes the conjugates formed at a physiologically relevant pH (7.4), as well as at a lower pH to resemble the late endosome (4.5). The lowest N/P ratios which showed full condensation for each polymer (N/P 5) were used for testing the stability against increasing amounts of heparin (0-1.0 I.U.). The samples at pH 7.4 were made in 5% glucose solution while the samples measured at pH 4.5 were made in sodium acetate buffer. Samples were prepared as described for the SYBR Gold assay with the exception of adding 10 μL of Heparin solution at various concentrations (0-1 international unit (IU) per well). Samples were incubated for varying time points (30 min-4 hours) at room temperature. Afterwards, fluorescence was measured in triplicates at 495 nm (excitation) and 537 nm (emission) on a Synergy 2 microplate reader (BioTek Instruments, Winooski, VT, USA). Results of the heparin assays were analyzed as described for the SYBR Gold assays.

3.2.7 Hydrodynamic Diameter and Zeta (ζ) Potential Measurements

Measurements of the hydrodynamic diameters of micelleplexes were performed by dynamic light scattering (DLS) using a Zetasizer Nano ZS (Malvern Instruments Inc.,

Malvern, UK). Micelleplexes were made as described above and measured at N/P 5, 6, and 7, complexing 40 pmol of scrambled siRNA. Samples were diluted with 5% glucose to a total volume of 75 μL within a disposable cuvette. Each sample was read in triplicates with each run consisting of 15 scans. Results are represented as average size (nm) ± standard deviation. The samples were then diluted with 5% glucose to 800 μL, and transferred to disposable capillary cells, and ζ-potential measurements were taken. ζ-potential measurements were read in triplicates by laser Doppler anemometry (LDA), with each run consisting of 30 scans. Results are shown in mV ± standard deviation.

3.2.8 Transmission Electron Microscopy (TEM)

Transmission Electron Microscopy (TEM) was used in order to assess the size and morphology of the micelleplexes after siRNA condensation. For TEM analysis, micelleplexes were made, as described above, in a total volume of 20 μL of 5% glucose containing 20 pmol of siRNA. Samples were added dropwise to a copper-coated grid, air dried and imaged with a transmission electron microscope (JEOL 2010 TEM, JEOL, Tokyo, Japan).

3.2.9 Cellular Uptake of Micelleplexes by Flow Cytometry

In 24-well plates (Corning Incorporated, Corning, NY) 60,000 SKOV-3 cells were seeded and incubated overnight at 37 °C and 5% CO_2. In each experiment, freshly made micelleplexes containing 50 pmol of AF488 siRNA at varying N/P ratios were added per well. Negative controls consisted of blank/untreated cells, and cells treated with free siRNA. Positive control cells were transfected with Lipofectamine 2000 (Life Technologies, Carlsbad, CA, USA) following standard protocol. Unless otherwise stated, cells were transfected for 4 hours in 37 °C and 5% CO_2 with 50 μL of micelleplex solution containing 50 pmol siRNA within a total volume of 500 μL of serum containing cell culture media. In order to quench any extracellular fluorescence, the cells were

incubated with 100 μL of 0.4% Trypan Blue (Fisher Scientific). Results were compared between cells treated with and without Trypan Blue in order to gain insight into each polymer's uptake profile. Cells were then washed twice with 1X PBS + 2 mM EDTA, trypsinized and spun down at 350 g for 5 min. After centrifugation, the supernatant was decanted, and the cells were washed twice with 1X PBS + 2 mM EDTA. Samples were analyzed via flow cytometry (Applied Biosystems Attune Acoustic Focusing Cytometer), and the Median Fluorescence Intensity (MFI) was collected and recorded. Samples were run in triplicates, with each sample consisting of a minimum of 10,000 viable cells. The siRNA was excited at 488 nm, and emission detected using a 530/30 band-pass filter set. Analysis and presentation of the data were performed by GraphPad Prism 5.0 software calculating mean values and standard deviations.

3.2.10 Monensin Assay

To determine the extent of siRNA being trapped within the endosome, a monensin assay was utilized with flow cytometry. In 24-well plates 60,000 SKOV-3 cells were seeded and incubated overnight at 37 °C and 5% CO_2. Freshly made micelleplexes containing 50 pmol of AF488 siRNA were added per well. Negative controls consisted of blank/untreated cells. Cells were transfected for 24 hours in 37 °C and 5% CO_2 with 50 μL of micelleplex solution containing 50 pmol siRNA within a total volume of 500 μL of serum containing cell culture media. In order to quench any extracellular fluorescence, certain cells were incubated with 100 μL of 0.4% Trypan Blue while others were treated with monensin. Results were compared between cells treated with and without Trypan Blue and monensin in order to gain insight into each polymer's uptake profile. Cells were then washed twice with 1X PBS + 2 mM EDTA, trypsinized and spun down at 350 g for 5 min. After centrifugation, the supernatant was decanted, and the cells were washed once with 1X PBS + 2 mM EDTA and incubated at 4 ˚C for 30 minutes with 50 μM monensin.

Afterwards, cells were washed once with 1X PBS + 2 mM EDTA and were analyzed via flow cytometry; the Median Fluorescence Intensity (MFI) was collected and recorded for each sample. Samples were run in triplicates, with each sample consisting of a minimum of 10,000 viable cells. The siRNA was excited at 488 nm, and emission detected using a 530/30 band-pass filter set. Analysis and presentation of the data were performed by GraphPad Prism 5.0 software calculating mean values and standard deviations.

3.2.11 Confocal Scanning Laser Microscopy

SKOV-3 cells were seeded in a Permanox 8 chamber slide (Nunc, Fisher Scientific, Waltham, MA, USA) at a density of 25,000 cells in a total volume of 300 μL and allowed to incubate over-night in 37 °C and 5% CO_2. Micelleplexes were made as described above using 40 pmol of labeled siRNA. After incubating the cells with the micelleplexes for 4, 12, or 24 h, the supernatants were decanted. Following this, the cells were washed with 300 μL of PBS for 2-3 minutes each while shaking. Afterwards, cells were fixed with 4% paraformaldehyde solution in PBS for 20 minutes at room temperature. This solution was then discarded, and cells were washed twice with 300 μL of PBS for 2-3 minutes each while shaking. The nucleus was stained with DAPI at a concentration of 175 ng/mL (Life Technologies, Carlsbad, CA, USA) for 20 minutes at room temperature while shaking. Cells were then washed twice with 300 μL of PBS. The chambers were then removed, the slides were blotted to remove any excess wash solution with a Kimwipe, and 1 drop of Fluorsave (CalBiochem, San Diegeo, CA, USA) was added per coverslip. The coverslips were mounted and allowed to sit for 1-2 hours in the dark. For excitation of TYE-563, an excitation wavelength of 570 nm was used while emission was detected with a spectral detector at 590 nm. DAPI staining was excited with a UV laser that had an excitation wavelength of 364

nm, and emission was detected at 385 nm. Images were recorded using a Zeiss LSM 780 confocal microscope and overlaid with brightfield light to gain information about cellular structures.

3.2.12 Protein Knockdown by Western Blot and Luciferase Assay

SKOV-3 and A549 cells were seeded in 6 well plates with a seeding density of 300,000 cells per well and allowed to attach overnight at 37 °C and 5% CO_2. For the assessment of TLR4 expression, SKOV-3 and A549 cells were harvested after 24 hours of incubation. For transfection of SKOV-3 cells, micelleplexes were formed as previously described containing 100 pmol of TLR4-targeted siRNA. Cells were incubated with micelleplexes for 48 and 72 hours to assess protein knockdown. Afterwards, they were washed twice with ice cold PBS, followed by a 2 minute incubation in 100 μL of RIPA lysis buffer. The lysis solution was collected, transferred to a conical tube, and pipetted up and down to ensure complete cell lysis. Cells were incubated on ice for 30 minutes, followed by sonication and centrifugation at 15,000 g for 20 minutes at 4 °C. Once centrifuged, the pellet was discarded and samples were analyzed via a Pierce BCA Protein Assay Kit (Life Technologies, Carlsbad, CA, USA) to determine the protein concentration.

The samples were prepared for loading the 10% polyacrylamide gel by denaturing 30 μg of protein by adding 1X final concentration loading buffer (4% SDS, 10% 2-mercaptoethanol, 20% glycerol, 0.004% bromophenol blue, and 0.125 M Tris-HC), β-mercaptoethanol, and by diluting them to 35 μL with a radioimmunoprecipitation assay buffer (RIPA). Samples were added to a dry heat bath (at 95 °C) for five minutes before loading onto the gel. Once loaded, samples were run at 110 V for approximately 1-2 hours at room temperature. The gel was then transferred to a PVDF membrane by running at 0.4 A current for 1 hour at room temperature. In order to keep the box cold, it was placed on ice. The membrane was then blocked in 5% milk in phosphate buffered saline containing Tween-20 (PBST) for 1 hour at room temperature followed by overnight

incubation with 1:1000 diluted primary anti-TLR4 antibody 76B357.1 (Abcam, Cambridge, MA, USA) at 4 °C. On the next day, the membrane was washed three times for 10 minutes each with PBST, followed by incubation with a secondary antibody (goat anti mouse IgG-HRP SC-2005 diluted 1:10,000) (Santa Cruz Biotechnology, Dallas, Texas, USA). Samples were incubated at room temperature for 1 hour. This was lastly followed by another set of three washes of PBST for 10 minutes each. Afterwards, the membrane was imaged using an ImageQuant LAS4000. Membranes were also probed for β-actin with a mouse monoclonal antibody 3700P (Cell Signalling Technology, Beverly, Massachusetts, USA) in order to test for proper loading controls.

Protein knockdown was also measured with a luciferase knockdown experiment. SKOV-3/LUC cells which have a NF-KB binding site on the CMV luciferase promoter were used in this experiment. In 24 well plates, 60,000 SKOV-3/LUC cells were seeded per well and incubated overnight at 37 °C and 5% CO_2. Micelleplexes were made as described previously with 50 pmol of TLR4 targeted or scrambled siRNA. Cells were incubated at 37 °C and 5% CO_2 with the micelleplexes for 24 hours before adding 1000 nM Paclitaxel to each well for an incubation period of 48 hours. After 48 hours, cells were washed twice with 200 μL of PBS and treated with 300 μL of lysis buffer (Cell Culture Lysis Reagent, CCLR, Promega, Madison, WI, USA) per well. Each well was scraped with a pipette to effectively dislodge cell debris on the bottom of the well. The plate was then rocked for 5 minutes at room temperature. Cell lystates were transferred to conical tubes and set on ice. Each tube was vortexed for 10-15 seconds and then centrifuged at 12,000 g for 2 minutes at 4 °C. The supernatant was collected, and 20 μL of each sample was added to a white 96-well plate to be analyzed for luminescence using a Synergy 2 microplate reader (BioTek Instruments, Winooski, VT, USA). Each well was injected with 100 μL of luciferase assay reagent containing 10 mM luciferin (Sigma-Aldrich, St. Louis, MO, USA) by the plate reader immediately

before the measurement. Samples were measured in triplicates and analyzed using GraphPad Prism 5.0 software.

3.2.13 MTT Assays

SKOV-3 cells were seeded at a density of 10,000 cells per well in 200 µL of medium in a 96 well plate and incubated overnight at 37 °C and 5% CO_2. Lipofectamine and each conjugate were diluted to varying concentrations from 0-16 µg mL^{-1} and added to SKOV-3 cells and incubated for 24 hours at 37 °C and 5% CO_2. Upon 24 hours of incubation, 20 µL of a sterile 5 mg/mL MTT solution was added to the cells and incubated for 4 hours at 37 °C and 5% CO_2. The media was then removed and 200 µL of DMSO was added to each well for 10 minutes. The plate's absorbance was read at 540 nm using a Synergy 2 microplate reader (BioTek Instruments, Winooski, VT, USA). The percentage of viable cells was calculated by the ratio of absorbance of treated cells compared with untreated cells. Samples were measured in triplicates and analyzed using GraphPad Prism 5.0 software.

For assessment of resensitization of SKOV-3 cells toward PTX, SKOV-3 cells were transfected with the micelleplex containing 780 nmol TLR4 siRNA within a T-75 flask for 24 hours at 37 °C and 5% CO_2 – day 0. On day 1, 6,000 SKOV-3 cells were seeded per well within a 96 well plate for the MTT assay in 200 µL of media. Subsequently on day 2, the cells were treated with PTX at concentrations ranging from 0-1000 µM for 48 hours in 200 µL of media. Upon 48 hour incubation, on day 5, 20 µL of a sterile 5 mg/mL MTT solution was added to the cells in serum-free media and incubated for 4 hours at 37 °C and 5% CO_2. The media was then removed and 200 µL of DMSO was added to each well for 10 minutes. The absorbance of each well was read at 540 nm using a Synergy 2 microplate reader (BioTek Instruments, Winooski, VT, USA).

Samples were run in triplicate and the data was analyzed with GraphPad Prism 5.0 software for IC_{50} values.

3.2.14 Annexin Assays

SKOV-3 cells were seeded at 60,000 cells per well in 24 well plates and incubated overnight at 37 °C and 5% CO_2. Micelleplexes were made as described previously with 50 pmol of TLR4 targeted or scrambled siRNA. Cells were incubated at 37 °C and 5% CO_2 with the micelleplexes for 24 hours before adding paclitaxel (0-1000 nM). Cells were incubated for another 48 hours. Afterwards, cells were washed with PBS while keeping each supernatant. Cells were trypsinized for 3-5 minutes, fresh media was added to each well, and the supernatant was added to each tube. Samples were centrifuged at 350 g for 10 min, and the supernatants were decanted. According to the Alexa Fluor 488 Annexin V/Dead Cell Apoptosis Kit, 1X Annexin Binding Buffer was prepared consisting of 10 mM HEPES/NaOH, 140 mM NaCl, and 2.5 mM $CaCl_2$ at pH 7.4. Cells were resuspended in 100 μL of 1X Annexin Binding Buffer followed by the addition of 5 μL of Alexa Flour 488 annexin V and 1 μL of 100 μg/mL of Propidium Iodine (PI). Cells were incubated at room temperature for 15 minutes and then diluted with 400 μL of 1X binding buffer. Samples were kept on ice and analyzed by flow cytometry at excitation of 488 nm and emission at 530 nm. Samples were measured in triplicates and analyzed using GraphPad Prism 5.0 software.

2.2.16 Statistics

All statistical analyses within this dissertation were performed in triplicates. Results are given as mean values ± standard deviation (SD) values. GraphPad Prism 5.0 software was utilized to address significance by means of either a one or two-way ANOVA.

3.3 Results and Discussion

3.3.1 Synthesis of PEI-PCL-*b*-PEG-Fol Conjugates

The first step in this project was to synthesize several tri-block co-polymers and to characterize them via several criteria. Two different molecular weight blocks of hetero-bifunctional PEG chains were used in order to start the synthesis, namely 3.5 kDa and 5 kDa. Both were heterobifunctional with a hydroxyl and carboxylic acid group at either end. Two different groups of co-polymers were synthesized with either molecular weight of PEG. Additionally, the grafting degree of PCL-*b*-PEG-Fol was varied in terms of two different molar ratios per fixed amount of PEI, namely equimolar or 3-fold molar excess. One co-polymer was synthesized to bear 10 μmol of the grafted *PCL-b-PEG-folate* chains per 10 μmol of PEI, and the other one was grafted with 30 μmol per 10 μmol of PEI. Furthermore, we synthesized a *PEI-g-PCL-b-PEG* null folate polymer which had a monofunctional mPEG chain and no folic acid attached, and a mixed conjugate which had both 3.5 kDa and 5 kDa PEG blocks in the *PCL-b-PEG-folate* chains. Interestingly, the feed ratio of PCL-b-PEG-folate chains did not have a significant influence on the polymers' final structure. Both equimolar ratios and 3-fold excess yielded in copolymers with statistically about 5 PCL-b-PEG-folate chains per molecule PEI. It is possible that especially in the reactions of equimolar ratios a large amount of unreacted PEI or PEI with just one PCL-b-PEG-folate chain were present but were lost during the purification of the polymers by ultrafiltration with a 30 kDa MWCO membrane. A folate concentration assay was performed on each of the five conjugates which were made with folic acid attached to the PCL-PEG chain. The average amount of folate was 1.313×10^{-5} mol folate/mg of polymer. This was similar, and in some cases higher, than what has been previously reported in the literature.(187) Table 1 describes each polymer's composition along with its corresponding and designated name. Diagrams of these

polymers can be seen in Scheme 1 (Supplementary data). Furthermore, conjugates were successfully characterized by ^{1}H NMR (D_2O) as described before;(187, 189, 190) and the spectra were as follows: δ (ppm) = 8.6, 8.0, 7.6, 6.8 peaks characterizing the folate terminus; strong singlet peak at 3.6 (OCH_2CH_2O); and a broad but weak peak 1.6-1.2 ($COCH_2CH_2CH_2CH_2CH_2O$) (Supplementary Spectrum 1).

Name	PEG Chain Size (kDa)	PCL Chain Size (kDa)	*Hy*-PEI (kDa)	Feed Ratio of PCL-b-PEG(-folate)	Statistical (final grafting degree)	Folate (mol per mg polymer)
3.5k 10 µmol	3.5	1000	25	10 µmol	5	2.4E-06
3.5k 30 µmol	3.5	1000	25	30 µmol	5.5	3.1E-06
5k 10 µmol	5	1000	25	10 µmol	5	1.2E-05
5k 30 µmol	5	1000	25	30 µmol	4.7	8.9E-06
Mixed Conjugate	3.5 and 5	1000	25	10 µmol	0.5	3.9E-05
Null Folate	5	1000	25	10 µmol	2.5	0

Table 3.1: All six conjugates synthesized with the proposed scheme.

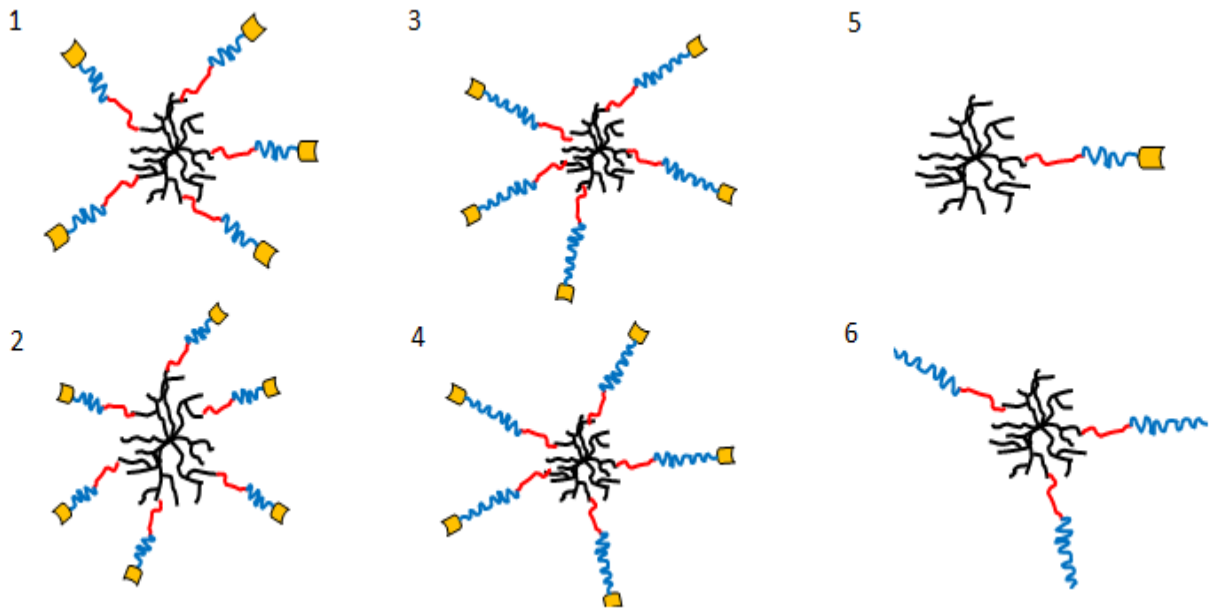

Schematic Table 3.2: Schematic representation of all synthesized folate decorated conjugates. Numbers 1-6 are all screened for siRNA condensation as shown in figure 3.1. Red depicts PCL, while blue and yellow signify PEG and folic acid, respectively.

3.3.2 siRNA Condensation Ability and Retention

As explained above, our approach utilizes a PEI block to electrostatically condense and protect the siRNA from nuclease degradation *in vitro* and *in vivo*. Therefore, we tested whether the tri-block co-polymers were still able to effectively condense the siRNA compared to unmodified, hyperbranched *hy*-PEI as described previously.(191) In order to do this, SYBR Gold assays were carried out with each polymer at varying polymer:siRNA (N/P) ratios ranging from 0-20. **Figure 3.1 A** shows that the grafting of PCL-PEG-Fol did not decrease the co-polymers' ability to condense the siRNA. In order to mimimize toxic side effects that could result from an excess of free polymer in the micelleplex suspension, the ideal N/P ratio was defined as the lowest one which fully condenses the siRNA. The SYBR Gold assays showed the optimal N/P ratios of all conjugates to be between 5 and 7. Therefore, these N/P ratios were continuously used for all subsequent experiments.

Additionally, the appropriate retention and release of siRNA are critical for effective delivery. Therefore, heparin assays were utilized in order to mimic release of the siRNA during circulation (pH 7.4) and in the late endosome (pH 4.5).(183, 192) Heparin is a polyanion and in the presence of the micelleplexes can be used to mimic competition for the electrostatic binding with the polymer. It is known that the presence of polyanions in serum can cause premature release of the siRNA from merely electrostatically self-assembled polyplexes.(193) Each conjugate was tested at N/P 5 in the presence of increasing amounts of heparin (0-1.0 I.U.). These data, seen in **Figure 3.1 B**, demonstrate that the copolymers only released 3-12% of the total siRNA in presence of the competing poly-anion heparin at pH 7.4, whereas PEI polyplexes released up to 20% siRNA in the concentration range of heparin tested here. Conversely, micelleplexes need to have good release profiles at low pH values in order to be released from the polymer to achieve optimal protein knockdown. Based upon our hypothesis that our micelleplexes are internalized within the cell by means of folate receptor-mediated endocytosis, the micelleplexes have to escape out of an endocytic vesicle to deposit the siRNA into the cytoplasm. Thus, the same heparin assay was run with similar conditions as before, except at pH 4.5 to mimic the pH of the late endosome. **Figure 3.1 C** demonstrates that all micelleplexes were able to successfully release more than 95% of the siR2.NA, while unmodified PEI only released about 50%. Collectively, these data indicate that all six co-polymers would not only be stable in circulation (see release at pH 7.4, Figure 3.1 B), but could efficiently release siRNA into the cytoplasm upon being endocytosed (see release at pH 4.5, Figure 3.1 C). Release of siRNA is into the cytoplasm is hypothesized to occur due to the "proton sponge" effect which results in bursting of the endosome and subsequent siRNA deposition into the cytoplasm. Evidence for siRNA deposition and action within the cytoplasm is reflected in the protein knockdown data that is discussed later in this dissertation. Similar assays were performed

to assess siRNA release over time while in the presence of heparin. It was found that after 30 minutes, the release profiles did not change, but were comparable to the curves in **Figure 3.1 C** (Data not shown).

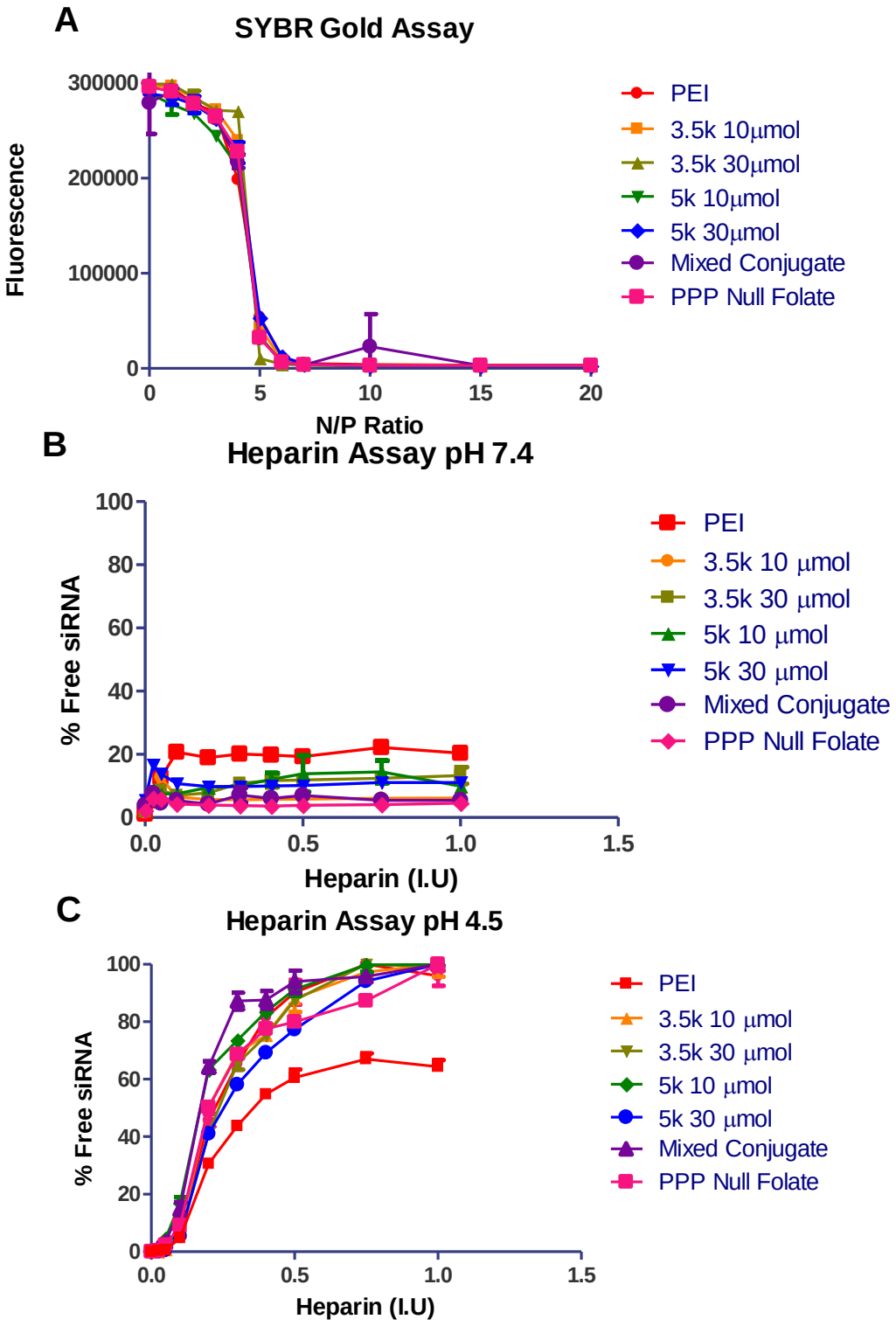

Figure 3.1 A-C: SYBR Gold assays for each conjugate in comparison to PEI. The conjugates' abilities to electrostatically condense siRNA were analyzed from N/P 0-20 (A). Heparin assays at pH 7.4 mimic the pH during in vivo circulation. Each conjugate was tested at N/P 5 and incubated in the presence of heparin for 30 minutes (B).

Heparin assays at pH 4.5 mimic the late endosome. Each conjugate was tested at N/P 5 and incubated in the presence of heparin for 30 minutes (C).

3.3.3 Characterizing nanoparticle morphology, hydrodynamic diameter, and zeta potential

Two important characteristics for nanoparticle delivery are their sizes and zeta potentials. An effective carrier should form nanoparticles within the nanometer scale with a slightly positive zeta potential to increase the likelihood of cell binding and consecutive endocytosis.(178, 181, 194-197) Maintaining small sizes of nanoparticles is important for permeation out of the blood vessels and into the tumor as well as avoiding detection from the host's natural defense mechanisms, such as macrophages. In the lung, an optimal size to avoid macrophage detection and subsequent endocytosis is 260 nm (196, 198). However, optimal sizes of nanoparticles that are administered intravenously should also be below 260 nm, if not smaller, in order to avoid macrophage detection and phagocytosis, along with other side effects.(194, 195, 197) Here, micelleplex formulations with 50 pmol of siRNA at N/P 5, 6, and 7 were characterized by dynamic light scattering (DLS). As seen in **Figure 3.2 A**, at N/P 5, the hydrodynamic diameters were all below 150 nm, and slightly increased as the N/P ratio increased. At the higher N/P ratios, (6 and 7) the hydrodynamic diameters were either at or below 260 nm. The sizes determined here with DLS measurement are smaller than other folic acid chitosan low molecular weight PEI delivery systems reported in literature (220-250 nm).(199) Conversely, other previously published folic acid targeted delivery systems utilizing platinum based nanoparticles have much smaller hydrodynamic diameters.(200) Collectively, this suggests that our micelleplexes have adequate sizes to evade the host immune system and easily permeate out of the blood vessel and into the tumor interstitium and correspond adequately with what is published.

Furthermore, the zeta potentials of the micelleplexes are important for delivery as the cell membrane carries a slight negative charge. If the micelleplexes are negatively charged, they can

be electrostatically repelled by the cell membrane, and the siRNA uptake would suffer. Conversely, with a slight positive charge to the micelleplex, attraction between the cell membrane and micelleplexes is expected which helps promote binding to the cell membrane and non-specific, adsorptive uptake. However, a micelleplex that is strongly positively charged can be toxic to the cells, which is a common problem with polycation delivery vectors for siRNA. Ideally, this toxicity should be avoided. In case of targeted nanoparticles, a strong positive zeta potential is not necessary, since uptake is promoted by receptor-mediated endocytosis. A slight positive charge, however, can be helpful to orient the particles in close proximity of the cell membrane and receptor. In our experiments, the corresponding zeta potentials for every micelleplex at every N/P ratio were all positive, and below +20 mV. Although there has not been a reported threshold for cationic polymers zeta potential in correlation to toxicity, generally the less cationic nanoparticles are, the fewer cytotoxic effects will be seen within the cell. Most N/P formulations for each micelleplex were around +8-12 mV; corroborating other nanoparticle formulations which are published.(201) **Figure 3.2 B** represent the average zeta potential for each micelleplex containing siRNA. Cytotoxicity studies were carried out with an MTT assay comparing lipofectamine, a known toxic transfection reagent, against our conjugates. The MTT assay was carried out at concentrations at which lipofectamine was used for transfections. However, our conjugates are used at much lower concentrations and additionally exhibit higher IC_{50} values, thus suggesting that there is little toxicity concerns when transfecting with our folate-decorated micelleplexes (**supplementary Figure 3.1**). This has been seen in literature with similar PEI-PEG/siRNA delivery systems.(188) Based upon the data acquired from zeta potential measurements, our micelleplexes should exhibit a slight attraction to the cell membrane and not be inherently toxic.

Additionally, TEM was used to validate our findings obtained with dynamic light scattering in terms of micelleplex sizes. TEM imaging serves to learn more about the size but also the morphology of our micelleplexes. As presented in **Figure 3.2 C-D**, the sizes determined by TEM corroborate extremely well with DLS measurements. In addition, the micelle formation of the inner core and outer corona is clearly shown. Concluding these results, all conjugates formed micelleplexes with the siRNA with adequate sizes (100-200 nm) and zeta potentials (+8-12mV). Based on these data, our micelleplexes contain optimal characteristics to condense siRNA and allow for interaction with the cellular membrane.

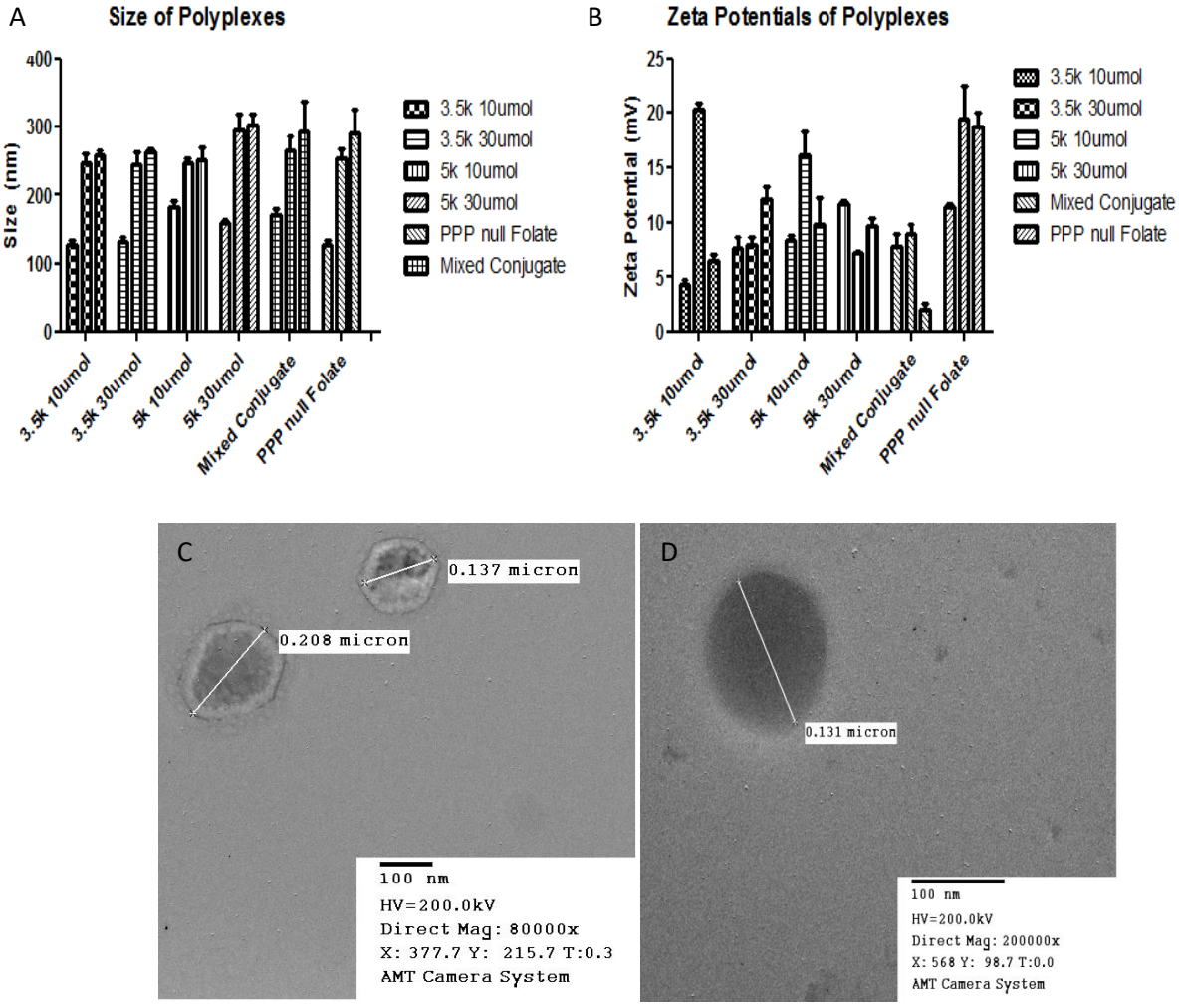

Figure 3.2: Characterizing nanoparticle morphology, size, and zeta potential. Each micelleplex's hydrodynamic diameter was tested at N/P 5, 6, and 7 with 50 pmol of siRNA (A). Each micelleplex formulation was then diluted to measure zeta potentials via LDA (B). TEM images of 5k 30 μmol (C) and mixed conjugate (D) are shown.

3.3.4 Assessing siRNA uptake and targeted delivery

After the appropriate characterizations were performed to assess our micelleplexes' size, zeta potentials, and siRNA release/retention profiles, flow cytometry was utilized to perform siRNA delivery studies. For all siRNA uptake flow cytometry experiments, unless otherwise stated, Alexa fluor 488 labeled siRNA was used. In order to identify which conjugate worked the best, all folate decorated micelleplexes were tested against one another, as well as compared with PEI and lipofectamine. As seen in **Figure 3.3 A**, comparable results to PEI were obtained, while slightly less transfection efficiency was seen in comparison to lipofectamine. Although there seemed to be no statistical difference in the initial screen between all conjugates, we did notice a trend that the 10 μmol conjugates performed better than their 30 μmol counterparts. Due to this, the three most promising conjugates appeared to be PEI grafted with 10 μmol of the chains containing 3.5 kDa PEG (3.5k 10 μmol), PEI grafted with 10 μmol of the chains containing 5 kDa PEG (5k 10 μmol), and the mixed conjugate. With this small selection, we determined the optimal N/P ratio for each conjugate's siRNA delivery. Due to the smaller sizes obtained at N/P 5 and no difference in uptake with higher N/P ratios, siRNA was formulated with the co-polymers mentioned at N/P 5, which may also reduce any possible toxicity seen with excess polymer at increasing N/P ratios (Data not shown). Once delivery conditions were optimal, folate-decorated conjugates were compared against a null folate conjugate to assess targeted FRα-mediated uptake. First, a time course analysis was carried out comparing the three best folate-decorated conjugates and the null-folate conjugate seen in **Figure 3.3 B**. Each micelleplex was transfected and allowed to incubate for 24, 48, 72, and 96 hours before harvesting cells for flow cytometry. At each time point, every folate-decorated conjugate outperformed the null folate polymer in SKOV-3 FRα

positive cells. This led us to believe that there are two possible mechanisms for uptake of our micelleplexes. As one possibility, non-receptor mediated, but charge-mediated adsorptive endocytosis across the cellular membrane could occur due to sedimentation of the micelleplexes over a period of time and might be promoted by their amphiphilic properties. Secondly, the folate decorated micellepexes are able to be endocytosed utilizing the folate receptor mediated endocytosis pathway. With this in mind, we hypothesized that our folate decorated micelleplexes can take advantage of both mechanisms, thus resulting in a more significant uptake over time.

The next step was to test whether the uptake that was demonstrated in **Figure 3.3 B** was folate receptor driven. To answer this question, two experiments were performed. First, we analyzed the micelleplexes' siRNA delivery at 37˚ C and 4˚C. When cells are incubated at 4˚C, the lower temperature inhibits active uptake such as FRα mediated endocytosis, but leaves receptor-mediated binding or charge-mediated binding to the cell still an available option for cell associated fluorescence. **Figure 3.3 C** shows that significant inhibition of active uptake occurs for SKOV-3 cells incubated with folate decorated micelleplexes at 4˚C in comparison to 37 ˚C. Conversely, the folate null micelleplexes showed little decrease between the two conditions, thus suggesting no receptor-mediated but possibly adsorptive endocytosis was inhibited for this conjugate. Most interestingly, the uptake efficacy of the targeted formulation (3.5k 10 μmol) was significantly higher than that of the non-targeted micelleplexes (Null folate) if incubated at 37˚ C. However, if incubated at 4˚ C, the uptake of both formulations was comparable. Additionally, competitive inhibition of receptor-mediated uptake was analyzed after pre-incubating SKOV-3 cells with an excess of the receptor substrate, free folic acid (FF).

The recycling rates of FRα vary depending upon the tissue and tumor cell line. However, on average, the in vivo recycling rate is just under 5.7 hours, and recycling of a receptor previously

blocked with free folic acid renders the former available for binding folate-conjugated nanoparticles.(202) Therefore, our studies were performed at early time points with or without pre-incubation of free folic acid to get a better picture of whether the targeted micelleplexes are binding with FRα.(70, 202) **Figure 3.3 D** demonstrates that when excess free folic acid was added (20 µg), there is no significant drop in siRNA uptake for neither the folate decorated micelleplex nor the non-folate micelleplex. Excess folic acid concentrations were used based upon previous studies with similar concentrations and findings.(167, 203, 204) Benoit et. al. did not observe any competitive inhibition in the presence of 10 µg/mL of free folic acid.(167) Conversely, at higher concentrations, above 1 mM, uptake was inhibited as shown by Arima et. al.(203) Tied into the fact that a non-specific inhibition was seen across the board with our folate-decorated micelleplexes, as well as the non-decorated ones at concentrations above 1 mM of free folic acid per well (data not shown), we have seen a different result of competitive uptake than that reported by Arima et. al. The lack of competition with low amounts of free folic acid could be due to the fact that our micelleplexes are multivalent, and thus have a stronger binding avidity to the receptor when compared to the affinity of a monovalent folic acid to the receptor. Therefore, it is expected that the folate-decorated micelleplexes will easily out compete folic acid for the folate receptors binding sites. At higher concentrations of free folic acid, uptake can be inhibited but the observed inhibition is not necessarily an inhibition of receptor mediated endocytosis.

Taken together, these results imply that uptake of these micelleplexes by means of diffusion does not explain the difference of targeted vs. non-targeted formulations, while the folate-decorated micelleplexes are able to utilize FRα-mediated uptake for siRNA delivery if 1) energy-dependent endocytosis is possible, and 2) the receptor is not blocked by free competing ligand. These data were further reinforced by confocal microscopy showing significantly more

siRNA deposition within the cell by the folate-decorated nanoparticles. As seen in **Figure 3.4**, all folate-decorated nanoparticles (**C-E**) were able to effectively delivery siRNA more efficiently than their null folate counterpart (**F**). At first glance PEI seemed to deliver a significantly larger amount of siRNA to the cells. However, the fluorescence may arise from PEI complexes merely bound to the surface of the cell due to the strong electrostatic interaction and not effectively being endocytosed into the cell. When analyzed with flow cytometry and using trypan blue to quench the extracellular fluoresecence, the MFI for PEI drops significantly in comparison to targeted micelleplexes, indicating that a higher percentage of polyplexes is not internalized but only cell-bound. Additionally, PEI/siRNA polyplexes that are taken up into an endosome may not release siRNA as efficiently into the cytoplasm as the micelleplexes do due to the very strong binding of the polymer to siRNA (**Figure 3.1 C**). Taken together, these results appear different from the flow cytometry data in **Figure 3.3 A**. Due to CLSM being a different type of measurement revealing information on spatial siRNA deposition in the cell, it is not surprising that there is a discrepancy seen here. This could also be attributed to self-quenching of the fluorescently labeled siRNA molecules when in close proximity to other fluorophores which could be stronger for the Tye-563 dye than observed with Alexa Fluor 488.(205) However, our CLSM data strengthen our previous observations that folate decorated micelleplexes can utilize a receptor-mediated mode of uptake while the null folate micelleplexes cannot, thus resulting in greater siRNA delivery ability.

To determine if the micelleplexes are taken up by endocytosis into acidic vesicles, a monensin assay was performed. Fluorescence was measured after transfection in three distinct ways: without any treatment for total fluorescence, after treatment with trypan blue to quench any extracellular fluorescence, as well as after treatment with monensin to quench any fluorescence located within acidic vesicles. With this technique, we are able to elucidate where in the cell the

fluorescent signal originates from. As shown in Figure 3.3 E, the majority of the fluorescence is intracellular for both folate-targeted and non-targeted micelleplexes. At 24 h, the overall uptake was higher for targeted vs. non-targeted micelleplexes, which is in line with **Figure 3.3B**. Interestingly, a higher extent of targeted particles was trafficked into acidic vesicles compared to non-targeted ones. This observation can be explained by the intracellular trafficking of the folate receptor which can either be recycled at the early endosome stage or ripen to a late endosome. Most importantly, however, the targeted micelleplexes are shown to be more efficient in terms of delivery to the cytoplasm, which is the site of action for siRNA. These results are also in line with our observations based on confocal microscopy which, especially in **Figure 3.4D**, show siRNA in the cytoplasm, rather than in vesicles. The percentage of particles that is trapped in vesicles, however, may not result in a bright signal in the CLSM images, however, and therefore explain the discrepancy with the flow cytometric results.

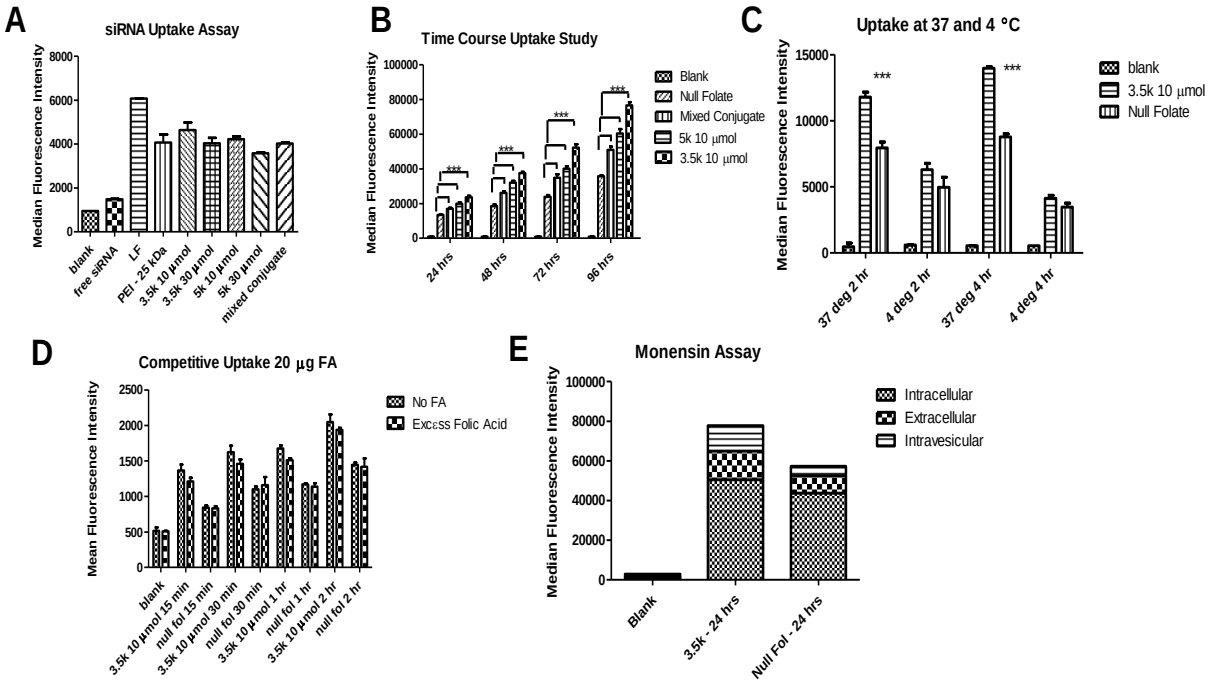

Figure 3.3: siRNA uptake studies using flow cytometry. Uptake study across all folate decorated conjugates using Alexa Fluor 488 for 4 hrs (A). Time course uptake study with the three most promising conjugates against folate null conjugate (B). Uptake in SKOV-3 cells incubated for 2 or 4 hrs at 37 ˚C versus 4 ˚C (C). Uptake study with and without an excess of free folic acid to determine competitive inhibition of binding (D). Uptake study with trypan blue and monensin treatment to assess localization of siRNA (E). Significance values were determined with a two-way ANOVA. *** = $p < 0.05$, **** = $p < 0.01$

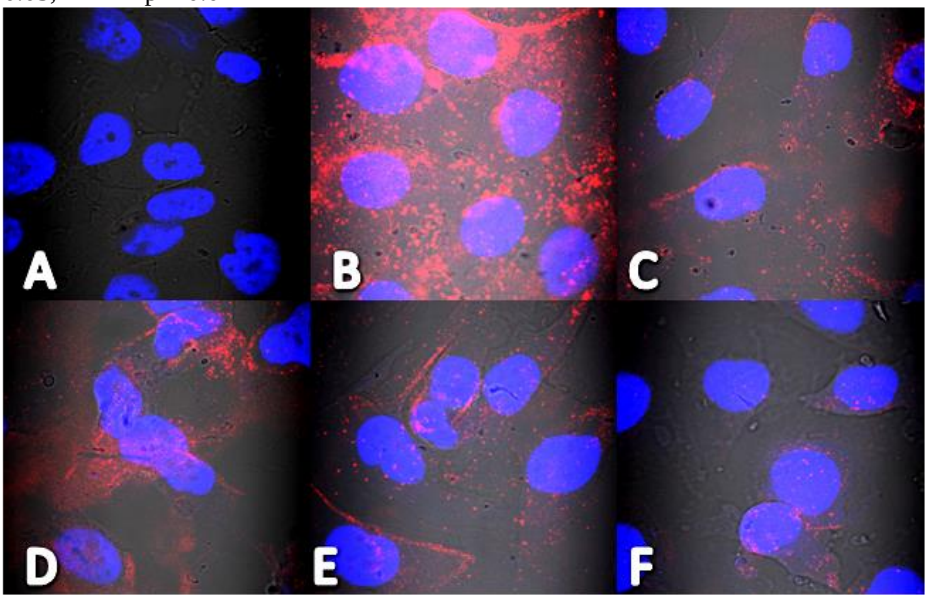

Figure 3.4: siRNA uptake studies using confocal laser scanning microscopy. Uptake study across the three most promising folate decorated conjugates compared to *hy*-PEI and null folate for 4 hrs. Cell nuclei are stained with DAPI. In order, images are of blank cells (A), PEI treated (B), 3.5k 10 µmol (C), 5k 10 µmol (D), mixed conjugate (E) and null folate (F).

3.3.5 Protein Knockdown *in vitro* and Resensitization Towards Paclitaxel Treatment

Ultimately, the main goal of siRNA delivery is to be able to achieve protein knockdown. Furthermore, our objective was to mediate protein knockdown in a targeted manner to achieve PTX re-sensitization. For preliminary experiments, we chose SKOV-3 cells that are PTX resistant and FRα over-expressing, in comparison to a PTX sensitive cell line, here A549, which have only a basal FRα expression. The TLR4 expression in both cell lines was assessed via Western Blot analysis and found to be about 4-fold increased in SKOV-3 cells, as compared to A549 cells, seen in **Figure 3.5 A**. Previous literature studying ovarian cancer suggests that a rise in TLR4 expression leads to increased chemo-resistance.(88-90, 94) Subsequently, we transfected SKOV-3 cells with siRNA against TLR4 using the 3.5k 10 µmol conjugate and lipofectamine as a positive control and determined the gene knockdown after 48 and 72 hours via Western blot analysis. **Figure 3.5 B** shows significant knockdown of TLR4 at 48 hours and knockout at 72 hours for both lipofectamine and the 3.5k 10 µmol conjugate.

To further elucidate the impact of TLR4 knockdown, we used a SKOV-3 luciferase cell line with luciferase expression controlled by a CMV promoter with a NF-KB binding site. In this cell culture model, NF-KB activation results in enhanced luciferase activity. Combined with the fact that PTX treatment causes NF-KB activation downstream through activating the TLR4 pathway, this model allows determining the effects of TLR4 knockdown on chemosensitivity of SKOV-3 cells toward PTX through measuring luciferase expression.(89) **Figure 3.5 C** shows that the luciferase expression of SKOV-3/LUC cells is clearly upregulated upon treatment with PTX, unless TLR4 is down regulated upon TLR4 knockdown by the 3.5k 10 µmol micelleplex. In this

case, a dramatic decrease in luciferase expression is observed compared to cells not treated with PTX. However, cells treated with PTX upon transfection with a scrambled siRNA or polymer only showed an increase of luciferase expression, thus demonstrating no knockdown of TLR4 occurred. Interestingly, TLR4 knockdown did not affect the basal luciferase expression of SKOV-3/LUC cells when this expression was not triggered by treatment with PTX. Thus, **Figure 3.5** demonstrates three processes: 1) if SKOV-3 cells are treated with PTX, NF-KB is activated and pro-survival genes may be activated; 2) if TLR4 is knocked down, NF-KB activation is inhibited; and 3) NF-KB is not necessary for basal luciferase expression but strongly triggers the latter. Taken together, **Figure 3.5** demonstrates that the 3.5k 10 μmol conjugate is able to successfully knockdown TLR4 protein with a therapeutically relevant effect on PTX treatment.

Figure 3.5 A: Western blot. Western Blot analysis of TLR4 levels within SKOV-3 and A549 cells.

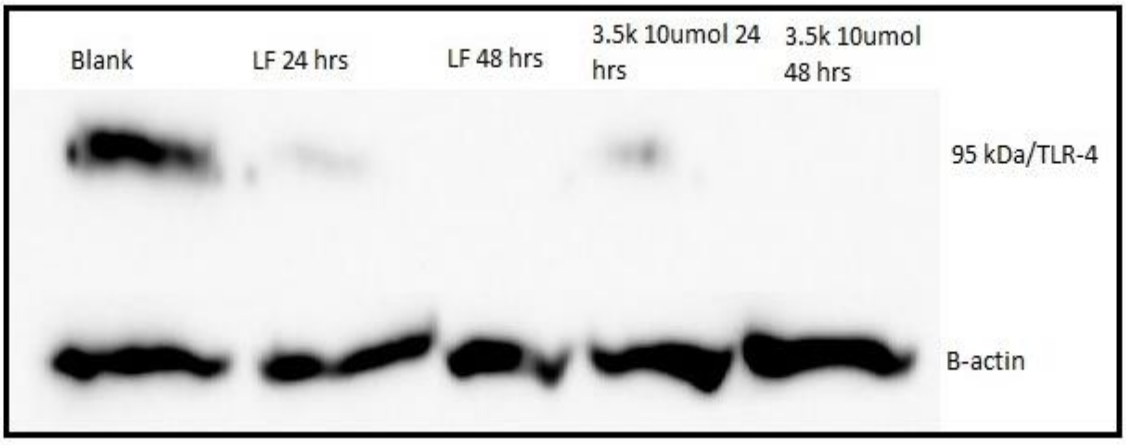

Figure 3.5 B: Western blot. Western Blot analysis of TLR4 knockdown at 24 and 48 hours using lipofectamine and 3.5k 10μmol.

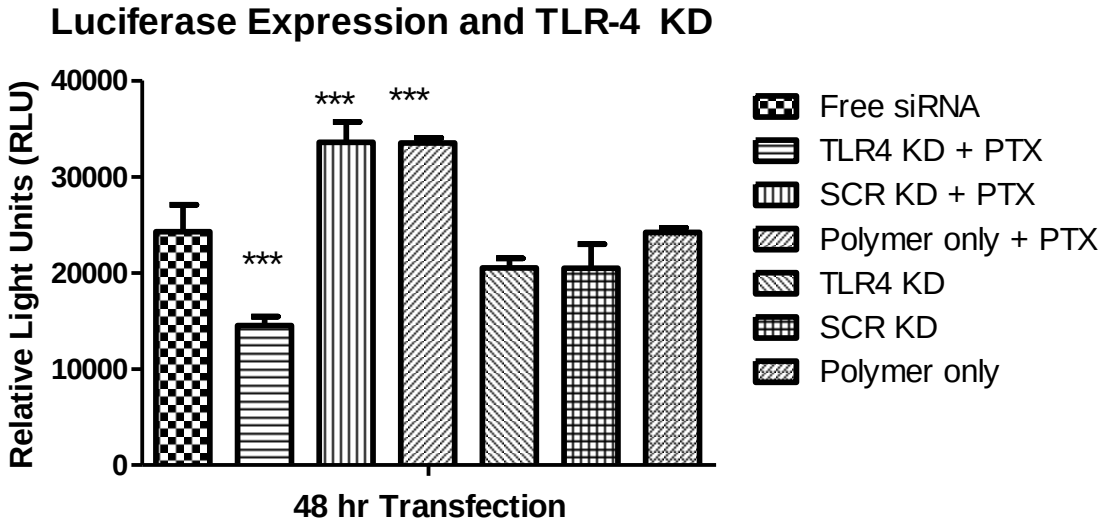

Figure 3.5 C: Luciferase assay. Luciferase assay in SKOV-3/LUC cells assessing TLR4 knockdown on luciferase expression 48 hrs post transfection when treated with 1000 μM of PTX. Significance values were determined with a two-way ANOVA.*** = $p < 0.05$.

Lastly, cells were transfected with the 3.5k 10 μmol conjugate containing TLR4 siRNA, followed by treatment with PTX in order to assess SKOV-3 re-sensitization to PTX. MTT cell viability assays confirmed that TLR4 knockdown resulted in a decrease in IC50 value for PTX in comparison to cells not transfected with micelleplexes containing TLR4 siRNA (**Figure 3.6 A**). Their corresponding IC_{50} values were 9.34 and 21.72 nM, respectively. In addition, cells were analyzed via flow cytometry to assess the percentage of apoptotic cells between different treatments. **Figure 3.6 A/B** shows that pre-treatment with 3.5k 10 μmol micelleplexes containing TLR4 siRNA caused a re-sensitization of SKOV-3 cells at varying concentrations of PTX. This effect was most drastic at higher PTX concentrations. At 1000 nM, only 27% and 23% of cells were apoptotic or dead if the cells underwent no pre-treatment or if they were transfected with 3.5k 10 μmol conjugate containing scrambled siRNA, respectively. Conversely, when TLR4 specific siRNA was used, more than double the cells stained positive for annexin V binding to phosphatidyl serine on the cellular surface - a marker of apoptosis. Collectively, SKOV-3 cells that were pre-

treated with 3.5k 10 μmol micelleplexes containing TLR4 siRNA before PTX treatment resulted in a significant increase in cell death. A loss in TLR4 activity has been cited in the literature render SKOV3 cells sensitive to PTX treatment. Szajnik et. al showed that by using siRNA to knockdown TLR4 there was a 2-3 fold increase in cell death upon PTX treatment.(90) Other groups using shRNA to stably knock down TLR4 have displayed similar resensitization, namely a 3-fold increase in caspase activity, upon PTX treatment. (88) Our results are in line with these published results; however, our approach utilizes a targeted micelleplex delivery system to focus the TLR4 knockdown to cells that overexpress FRα.

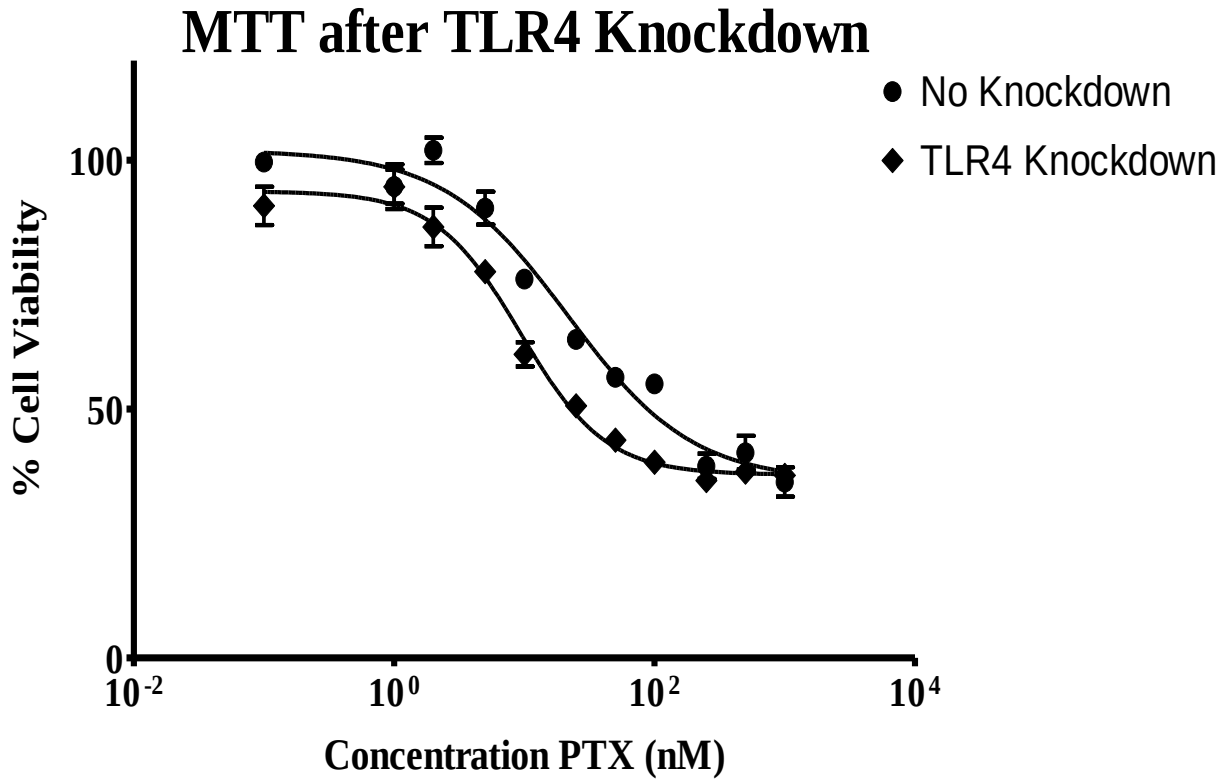

Figure 3.6 A: MTT assay. MTT assay of SKOV-3 cells after TLR4 knockdown at 48 hours.

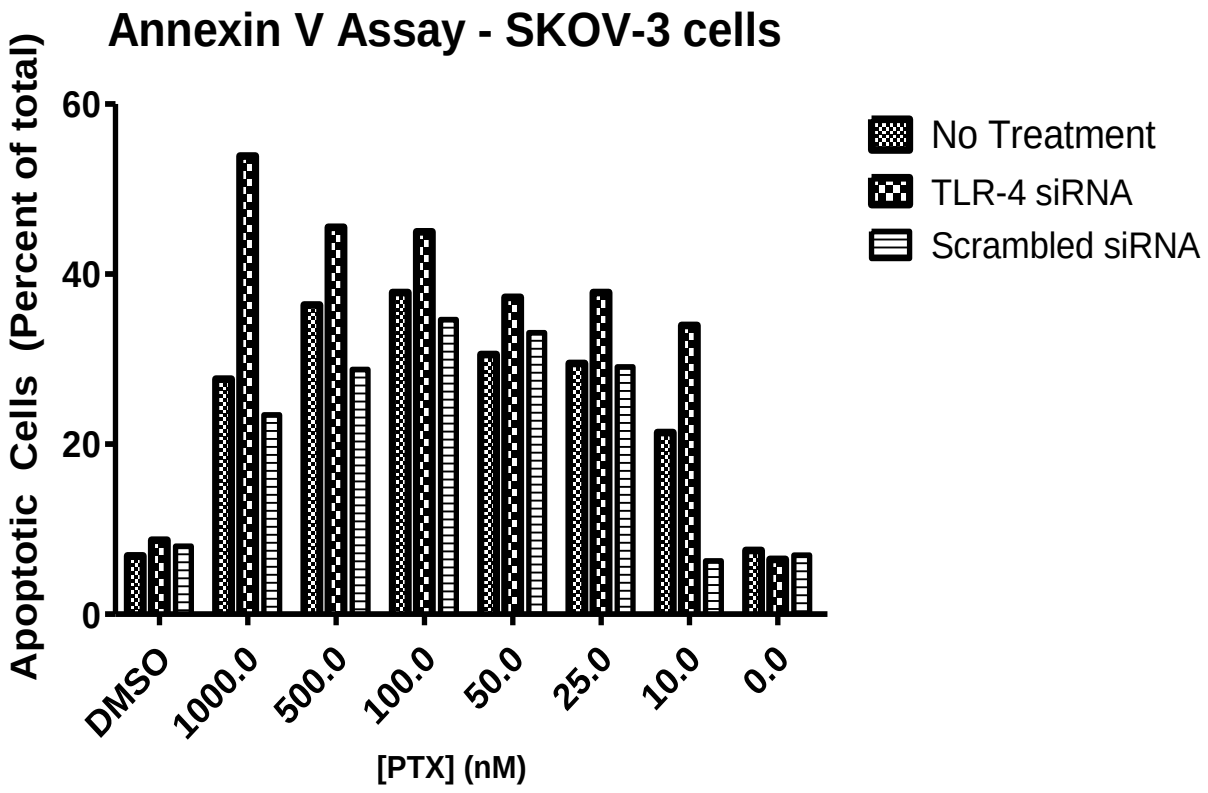

Figure 3.6 B: Annexin Flow cytometry stain. Flow cytometry analysis of cell death via Annexin V staining for apoptosis.

3.4 CONCLUSION

The over-expression of FRα in ovarian cancer cells offers the ability to specifically target and deliver siRNA in a Trojan-horse like mechanism explicitly to these cancer cells. Utilizing polymer based siRNA delivery systems for therapeutic purposes offers a very wide range of possibilities due to the modularity of this approach. Theoretically, as long as a sequence is available for a protein's mRNA, complementary siRNA sequences can be made against that protein to abrogate its expression. The delivery system discussed in this chapter has the opportunity and ability to target cancer cells through FRα overexpression for example found in ovarian cancer cells. Furthermore, targeted micelleplexes, as seen here, have the ability to provide beneficial therapy to patients while decreasing off target toxicity which is commonly seen with

most chemotherapy treatments. Our tri-block co-polymer, consisting of PEI-PCL-*b*-PEG-Fol has shown impressive ability to condense and protect siRNA, along with favorable release profiles at acidic pH values as found in late endosomal vesicles. Furthermore, several physical techniques such as DLS, and TEM were utilized to show adequate sizes (100-200nm), zeta potentials (0-30 mV), and a core-corona structure. Utilizing fluorescently labeled siRNA and flow cytometry, transfection conditions were optimized, and the micelleplexes were demonstrated to utilize FR-mediated endocytosis for cellular uptake. Protein knockdown with 3.5k 10 μmol micelleplexes was analyzed by Western blots and luciferase assays. Both demonstrated efficient protein knockdown of TLR4. Upon knockdown of TLR4, a re-sensitization occurred for SKOV-3 cells to PTX treatment and a significant increase in apoptotic cells was detected with flow cytometry. This approach displays similar therapeutic effects to those in the published literature but utilizes a targeted delivery mechanism. Collectively, these findings based on cell culture models suggest the feasibility of targeted gene knockdown of TLR4 and re-sensitization of PTX resistant cells toward PTX therapy. Currently, in vivo targeting and therapeutic efficacy are being tested.

CHAPTER 4 – REVISITING THE VALUE OF COMPETITION ASSAYS IN FOLATE RECEPTOR-MEDIATED DRUG DELIVERY

Please note that this chapter has been modified from the submitted entry in 2017. The authors include myself, Anwesha Sarkar, Dr. Peter Hoffman, and Dr. Olivia Merkel. I am the first author on this paper and I performed all *in vitro* experiments, designed and prepared all AFM experiments, as well as wrote the manuscript.

Steven K. Jones, Anwesha Sarkar, Daniel P. Feldmann, Peter Hoffmann, Olivia M. Merkel, Revisiting the value of competition assays in folate receptor-mediated drug delivery, Biomaterials, Volume 138, September 2017, Pages 35-45, ISSN 0142-9612, https://doi.org/10.1016/j.biomaterials.2017.05.034.

4.1 INTRODUCTION

Smart personalized cancer therapies utilize the molecular profiles of the tumor of individual patients as the basis of treatment and can selectively target malignant cells over healthy ones. A promising approach, which has already been utilized by drugs approved by the FDA, is based on targeting cellular receptors which are over-expressed on the surface of malignant cells. Several studies have been described which utilize receptor targeting to deliver a wide variety of payloads to multiple disease states.(206, 207) Several cancers such as ovarian cancer, non-small cell lung cancer, kidney cancer, and colorectal cancer have a significant over-expression of folate receptor alpha (FRα) (32, 41, 71). In ovarian cancer patients, it has been noted that as the histological grade of the cancer increases, so do the FRα expression levels (37). Several factors have made FRα over-expression in malignant cells a promising target for receptor targeted drug delivery: one being very low expression throughout the rest of the body, healthy tissues expressing

FRα on the apical side of the cell therefore not accessible to the bloodstream, and malignant cells displaying high degrees of overexpression that can be targeted through the bloodstream.(32, 37, 114) Furthermore, once FRα binds its ligand, it internalizes the receptor-ligand complex via receptor-mediated endocytosis. This process has the capability to endocytose the ligand and what is conjugated to it. Therefore, FRα internalization can be exploited by hijacking the internalization process with a drug payload which is conjugated to folic acid (FA). (208, 209) Currently, several approaches to FRα-guided imaging and therapies are being utilized clinically and tested in clinical studies.

However, in order to improve and better understand FRα drug targeting, the mechanics behind the ligand-receptor interaction need to be better understood. With a variety of targeting strategies for FRα, the need to comprehend the advantages and disadvantages to designing a FRα-targeted approach is necessary and will lead to more successful therapeutic approaches. One key aspect that has been studied is the need for having a monovalent versus multivalent drug conjugate. Several studies, including the clinical studies performed by Endocyte have proven that monovalent studies can be successful and deliver their drug payload specifically to cells which over-express FRα, while decreasing any unwanted and off target side effects.(210-213) Conversely, many studies such as the ones by Silpe et. al. and Stella et. al., have demonstrated that a multivalent approach yields a more advantageous system.(41, 214) In the latter studies, the principle idea of adding multiple folic acid molecules on the surface of the drug carrier is aimed at promoting higher binding avidity and affinity to FRα than a monovalent folic acid delivery system. This idea relies on the fact that several FRα cluster on the cell surface within lipid rafts, and therefore, multiple ligands binding to multiple receptors increase and prolong ligand-receptor interactions and therefore increase the FRα internalization with the drug.(214-216) Studies performed by Silpe et.

al. and Leistra et. al. revealed that with multiple ligand binding domains, the binding strength to the receptor of the folic acid drug conjugates can increase from to several orders of magnitude up to 1,000-fold, respectively (214, 215). Conversely, it has been shown that multivalent agents, such as the nanobodies used by Movahedi et al. bind more strongly to off-target tissues.(28) There are abundant nanocarrier delivery systems that have been used for FR-targeted delivery of a payload, such as siRNA. Of these systems, previous studies with block copolymers consisting of three components, namely polyethylene imine (PEI), polycaprolactone (PCL), and poly ethylene glycol (PEG), or PEI-PCL-PEG, have demonstrated effective siRNA delivery. Previous *in vitro* and *in vivo* work has shown that micelles made of PEI-PCL-PEG can effectively shield and condense nucleic acids in so-called micelleplexes at suitable sizes and zeta potentials, co-encapsulate hydrophobic drugs with the siRNA, achieve substantial knockdown of the target protein, and have stable and long circulation profiles within the bloodstream.(180, 181, 183, 217) Additionally, when this PEI-PCL-PEG platform was further modified with a folic acid targeting moiety, the self-assembling nanoparticles can selectively target and deliver siRNA to cancer cells which over-express FRα. (25, 48) Moreover, these FRα targeted nanoparticles exhibited stable circulation profiles as well as accumulation in FRα positive ovarian cancer xenografts, which was not achieved with the non-targeted formulation. (25)

This chapter focuses on better understanding the interaction of these multivalent FRα targeted nanoparticles with the receptor. In order to advance nanoparticle and small molecule therapies which utilize receptor-mediated drug delivery, a thorough understanding of the receptor-ligand interaction is imperative. Here, we assess this interaction with multiple *in vitro* cell-based and biophysical techniques including atomic force microscopy and flow cytometry. Collectively, we are demonstrating that excess monovalent free folic acid cannot outcompete targeted

multivalent micelleplexes for the binding to the clustered FRα and that by adding multiple ligands to the surface of the nanoparticle, a higher binding avidity is achieved. Additionally, the presence of high concentrations of competing ligand can cause instability problems or aggregation of the delivery system. These effects must be taken into consideration while validating targeted delivery with nanoparticles. Here, we demonstrate that pretreatment with excess ligand may not be the best approach in determining the specificity of targeting effects and alternative approaches are offered.

4.2 MATERIALS AND METHODS

4.2.1 Materials: PEI-PCL-PEG and PEI-PCL-PEG-FA copolymers were synthesized as described before.(48) Briefly, ring opening polymerization of polycaprolactone (PCL) and hetero-bifunctional (HO-PEG-COOH, 3.5 and 5 kDa) PEG was performed for the targeted polymer. For non-targeted PEI-PCL-PEG, monofunctional (CH3-PEG-COOH, 5 kDa) PEG (JenKem Technologies, United States) was used instead. Acrylate-PCL-*b*-PEG-alkyne or acrylate-PCL-*b*-mPEG was reacted with hyper branched polyethylenimine (hyPEI, 25k Da, BASF, Ludwigshafen, Germany) in a Michael addition, and azido functionalized folic acid was coupled to the alkyne-modified PEG in a click reaction. Firefly luciferase (FLuc) dicer substrate double-stranded siRNA (DsiRNA), and Alexa Fluor-488-labeled siRNA were purchased from Integrated DNA Technologies (IDT, Coralville, IA).

4.2.2 Preparation of PEI-g-PCL-b-PEG-Fol micelleplexes for *in vitro* use: Each polymer was dissolved in sterile water to yield a 1 mg/mL concentration of the PEI block of the polymer. Once dissolved, samples were filtered through a 0.22 μm filter for sterilization. In order to prepare the micelleplexes, a specific ratio of the amine groups found within the polymer (N) to the phosphate groups of the siRNA (P) was chosen, as described before. (48)

To prepare the micelleplexes, equal volumes of diluted polymer and siRNA were pipetted together, vortexed quickly, and incubated at room temperature for 20 minutes. After 20 minutes, the freshly formed polyplexes were characterized or used in cell culture experiments.

4.2.3 Hydrodynamic Diameter and Zeta (ζ) Potential Measurements: Measurements of the hydrodynamic diameters of micelleplexes were performed by dynamic light scattering (DLS) using a Zetasizer Nano ZS (Malvern Instruments Inc., Malvern, UK), as described previously. (48) Micelleplexes were made as described above in 1X PBS and measured at N/P 5 complexing with 40 pmol of siRNA. Samples were diluted with 1X PBS solution to a total volume of 75 μL within a disposable cuvette. Each sample was read in triplicate with each run consisting of 15 scans. Results are represented as average size (nm) ± standard deviation. The samples were then diluted with 1X PBS to a final volume of 800 μL, and transferred to a disposable capillary cell where ζ-potential measurements were performed. ζ-potential measurements were read in triplicates by laser Doppler anemometry (LDA), with each run consisting of 30 scans. Results are shown in average mV ± standard deviation.

4.2.4 Cell Culture: SKOV-3 and IGROV-1 cell lines are human ovarian cancer cell lines which were obtained from ATTC (LG Promochem, Wesel, Germany). Additionally, SKOV-3/LUC cells stably expressing the reporter gene luciferase were established as described before.(188) All three ovarian cancer cell lines were cultured in folate free DMEM cell culture medium (Sigma-Aldrich) supplemented with L-glutamine, sodium bicarbonate, 10% fetal bovine serum (Thermo Scientific Hyclone), and 1% penicillin/streptomycin. Cells were allowed to grow at 37 °C and 5% CO_2 and were passaged every 2-3 days when they had reached confluency.

4.3.5 Folate Receptor Alpha Receptor Expression Profiles by Flow Cytometry: Human ovarian cancer SKOV-3 and IGROV cells were grown in folate free DMEM medium and

subcultured as described previously.(48) For receptor expression experiments, 200,000 cells were harvested per tube and centrifuged at 350 g for 5 min. After the cells were pelleted, the supernatant was decanted, and the cells were washed twice with 1X PBS + 2 mM EDTA. Following an additional centrifugation step, 20 µL of primary monoclonal mouse anti-human Folate Receptor α antibody (MOV18 Enzo Life Sciences, Farmingdale, NY, USA) was added to their appropriate tubes. Samples were vortexed and incubated for 25 minutes at 4˚ C in the dark. Cells were washed with 1X PBS + 2 mM EDTA, centrifuged and washed one more time. The supernatant was decanted and 20 µL of a secondary goat anti-mouse IgG pacific blue conjugate antibody (Invitrogen, Carlsbad, CA, USA) was added to the tubes. After addition, samples were vortexed and incubated for 25 minutes at 4˚ C in the dark. Following this incubation step, samples were washed with 1X PBS + 2 mM EDTA twice. Samples were analyzed via flow cytometry (Applied Biosystems Attune Acoustic Focusing Cytometer), and the Median Fluorescence Intensity (MFI) was recorded. Samples were run in triplicate, with each sample consisting of a minimum of 10,000 viable cells. The secondary antibody was excited at 410 nm, and emission detected using a 450/40 band-pass filter set. Analysis and presentation of the data was performed in the GraphPad Prism 5.0 software calculating mean values and standard deviations.

4.2.6 Cellular Uptake of Micelleplexes by Flow Cytometry: In a 24-well plate (Corning Incorporated, Corning, NY), 60,000 SKOV-3 cells were seeded and incubated overnight at 37 °C and 5% CO_2. In order to remove any folic acid in the well, cells were washed two times with ice cold acid wash solution (150 mM NaCl, 10 mM sodium acetate, pH 3.5), followed by three washes with ice cold HBSS buffer (pH 7.4). Afterwards, serum-free and folate-free DMEM media (Sigma-Aldrich, St. Louis, MO, USA) was added to each well for samples treated in the absence of folic acid to avoid any source of folic acid. Samples that were treated with excess free folic acid (in

varying concentrations) were treated with serum-free DMEM media containing the specific quantity of folic acid. Samples were incubated in the new media for 30 minutes before transfection. For transfection, 50 μL of freshly made micelleplexes containing 50 pmol of AF488 siRNA at varying N/P ratios were added per well. Negative controls consisted of blank/untreated cells while positive control cells were transfected with Lipofectamine 2000 (Life Technologies, Carlsbad, CA, USA) following the supplier's standard transfection protocol. Unless otherwise stated, cells were transfected for 4 hours in 37 °C and 5% CO_2 with 50 μL of micelleplex solution containing 50 pmol siRNA within a total volume of 500 μL of serum free and folate free DMEM media (Sigma-Aldrich, St. Louis, MO, USA). After incubation, media was removed, and 100 μL of 0.4% Trypan Blue (Fisher Scientific, Waltham, MA, USA) was added to each well in order to quench any extracellular fluorescence. Cells were then washed twice with 1X PBS + 2 mM EDTA, trypsinized and spun down at 350 g for 5 min. After centrifugation, the supernatant was decanted, and the cells were washed twice with 1X PBS + 2 mM EDTA. Samples were analyzed via flow cytometry, and the Median Fluorescence Intensity (MFI) was recorded. Samples were run in triplicate, with each sample consisting of a minimum of 10,000 viable cells. The siRNA was excited at 488 nm, and emission detected using a 530/30 band-pass filter set. Analysis and presentation of the data were performed in GraphPad Prism 5.0 software calculating mean values and standard deviations.

4.2.7 Protein Knockdown by Luciferase Assay: Protein knockdown was measured with luciferase knockdown experiments. SKOV-3/LUC cells stably transfected with a CMV-luciferase plasmid were used in this experiment. In 24 well plates, 60,000 SKOV-3/LUC cells were seeded per well and incubated overnight at 37 °C and 5% CO_2. To remove any folic acid in the wells, cells were washed two times with ice cold acid wash solution as described above, followed by

three washes with ice cold HBSS buffer. Afterwards, serum-free and folate-free DMEM media was added to each well for samples treated in the absence of folic acid. Samples that were tested in the presence of excess free folic acid were treated with serum-free DMEM media containing the specific quantity of folic acid in order to match the concentrations used in the uptake studies. Samples were incubated in the new media for 30 minutes before transfections. Micelleplexes were made as described previously with 50 pmol of luciferase targeted siRNA. Cells were incubated at 37 °C and 5% CO_2. After 48 hours, cells were washed twice with 200 μL of PBS and treated with 300 μL of lysis buffer (Cell Culture Lysis Reagent, CCLR, Promega, Madison, WI, USA) per well. Each well was scraped with a pipette to effectively dislodge cell debris on the bottom of the well. The plate was then rocked for 5 minutes at room temperature. Cell lysates were transferred to conical tubes and set on ice. Each tube was vortexed for 10-15 seconds and then centrifuged at 12,000 g for 2 minutes at 4 °C. The supernatants were collected, and 20 μL of each sample was added to a white 96-well plate to be analyzed for luminescence using a Synergy 2 microplate reader (BioTek Instruments, Winooski, VT, USA). Each well was injected with 100 μL of luciferase assay reagent containing 10 mM luciferin (Sigma-Aldrich, St. Louis, MO, USA) by the plate reader immediately before the measurement. Samples were measured in triplicate and analyzed using GraphPad Prism 5.0 software representing average values and standard deviations.

4.2.8 Monensin Assay: To determine the extent of siRNA being trapped within the endosome, a monensin assay was utilized and analyzed via flow cytometry. In 24-well plates, 60,000 SKOV-3 cells were seeded and incubated overnight at 37 °C and 5% CO_2. Freshly made micelleplexes containing 50 pmol of AF488 siRNA were added per well. Negative controls consisted of blank/untreated cells. Cells were transfected for 24 hours in 37 °C and 5% CO_2 with 50 μL of micelleplex solution containing 50 pmol siRNA within a total volume of 500 μL of serum-

containing cell culture media. In order to quench any extracellular fluorescence, triplicates of cells were incubated with 100 μL of 0.4% Trypan Blue while other triplicates were treated with 50 μM monensin. Cells were then washed twice with 1X PBS + 2 mM EDTA, trypsinized and spun down at 350 g for 5 min. After centrifugation, the supernatant was decanted, and the cells were washed once with 1X PBS + 2 mM EDTA and incubated at 4 ˚C for 30 minutes with 50 μM monensin. Afterwards, cells were washed once with 1X PBS + 2 mM EDTA and were analyzed via flow cytometry; the Median Fluorescence Intensity (MFI) was recorded for each sample. Samples were run in triplicate, with each sample consisting of a minimum of 10,000 viable cells. The siRNA was excited at 488 nm, and emission detected using a 530/30 band-pass filter set. Analysis and presentation of the data were performed in the GraphPad Prism 5.0 software calculating mean values and standard deviations. Results were compared between cells treated with and without Trypan Blue and monensin in order to gain insight on the targeted and non-targeted micelleplex uptake profile.

All statistical analyses within this chapter were performed in triplicates. Results are given as mean values ± standard deviation (SD) values. GraphPad Prism 5.0 software was utilized to address significance by means of either a one or two-way ANOVA.

4.2.9 Atomic Force Microscopy (AFM): Atomic Force Microscopy was used in order to assess the size and morphology of the micelleplexes after siRNA condensation. Additionally, binding events of folate decorated polyplexes compared to folic acid on a folate receptor-modified cantilever were measured as described below. For AFM size and morphology measurements, micelleplexes were prepared at N/P 5 with 40 pmol of non-fluorescent siRNA in a total volume of 20 μL in 5% glucose. That suspension was added to a glass coverslip and let dry overnight. Lastly, micelleplexes for AFM force measurements with a FRα-modified cantilever were prepared as

described above with 75-fold higher amounts of siRNA and polymer in order to obtain a 3 mL suspension with the same polymer and siRNA concentration in 5% glucose solution, as used for all other AFM experiments.

4.2.10 Modification of Cantilevers with Folate Receptor: Cantilevers (MLCT-Bio, Bruker) were incubated within a cleaning solution (Cell cleaning solvent for UV/VIS, Agilent Technologies) for 2 h. The cantilevers were cleaned with ultra deionized water afterwards. Organic contaminants were removed through ozone treatment for 20 min. Afterwards, 5 mL of a 1 mM solution of silane PEG NHS (3400 Da, ThermoScientific) in 95% ethanol and 5% DI water was prepared, and the cantilever was incubated in this solution for 2 h. After rinsing, the cantilever was incubated in a solution of 0.15 mL recombinant human folate receptor α (FOLR1) protein (EZ Biosystems, College Park, MD, USA) for 1 h. Afterwards, the cantilever was preserved in 1×PBS solution until the experiments were performed within the following 24 h.

4.2.11 Immobilization of Folic Acid or Folate-Decorated Particles on the Substrate: Small silicon square pieces (15×15 mm) were rinsed with ultra DI water and UV glued to the bottom of a 60 mm sterile petri dish. The petri dish and substrate were further cleaned with DI water. The silicon substrate was incubated in a 5 mL solution of 1 mM silane PEG NHS (3400 Da, Thermo Scientific) in 95% Ethanol and 5% DI water for 2 h, followed by incubation in either 5 mL DMSO solution of 5 mg/mL folic acid or a suspension of folate decorated particles (16.38 μM of folic acid) for 5 h. The substrate was then washed with DI water and preserved in 1× PBS buffer until the experiment was performed.

4.3 Results and Discussion

The strategic design of the targeting aspect of the triblock copolymers used here for siRNA delivery relies upon the inherent over-expression of FRα in a variety of cancers. The American

Cancer Society (ACS) estimates that over 85% of ovarian cancers significantly over-express FRα, and that the expression has a positive correlation with the histological grade of the cancer. (37) Therefore, FRα levels have been studied in ovarian cancer cell lines such as IGROV-1 and SKOV-3 also by others. Both cell lines show significantly upregulated FRα expression levels when compared to normal epithelial tissues and other cancerous cell lines such as A549 adenocarcinomia alveolar basal epithelial cells. (33, 218). Figure 4.1 shows FRα expression levels in the specific cell lines used here and clearly demonstrates that both ovarian cancer cell lines IGROV1 and SKOV-3 showed an increase in FRα status. It should be noted that with varying FRα expression profiles, the receptor recycling rate does not change between cell lines. Therefore, SKOV-3 cells were utilized in all *in vitro* experiments to be consistent with previously published results.(25, 48)

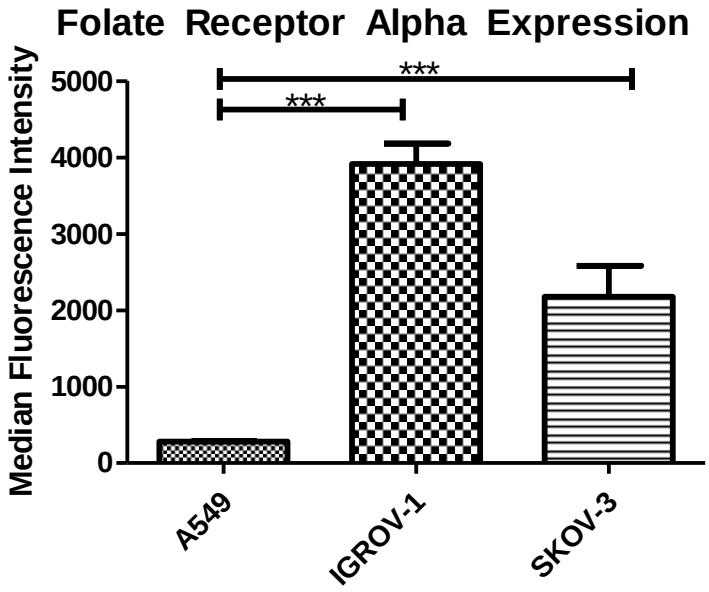

Figure 4.1. Folate Receptor Alpha (FRα) Expression for Ovarian Cancer Cell Lines: Two ovarian cancer cell lines which are known to over-express FRα were tested for their FRα expression levels via flow cytometry compared to a lung cancer cell line which is known to express only basal levels of FRα. Each sample was stained with a primary FRα specific antibody followed by a fluorescent secondary antibody, Significance values were determined with a two-way ANOVA.***$p<0.05$.

For successful delivery with nanoparticles, two important characteristics that need to be considered are their hydrodynamic diameters and zeta potentials. The polymers used here for nanoparticle formation were previously characterized by ^{1}H NMR, UV spectroscopy, and absorbance measurements. (48) The polymers used in this study were selected for the following reasons: 1) the targeted polymer previously showed the most efficient intracellular delivery of siRNA; 2) the polymer termed "mixed conjugate" contains, which contains 3.5 and 5 kDa PEG chains, also comprises the highest folic acid weight percentage; 3) a null folate conjugate not containing any folic acid was necessary as a negative control. (48) Due to the conditions required for AFM force measurements, the hydrodynamic diameters and zeta potentials of micelleplexes prepared with all three polymers were determined in PBS buffer. As shown in Figure 4.2 A, in all cases, hydrodynamic diameters were slightly larger than observed in 5% glucose solution (48) but still at or below the 260 nm threshold reported in the literature to favor evasion of recognition by macrophages. (110-112) It was not surprising that the hydrodynamic diameter increased when changing the dispersant from 5% glucose to a buffer with higher ionic strength where the hydrodynamic diameter is affected by the presence of a larger amount of counter ions that move with the diffusing particles. The sizes of the micelleplexes are comparable with other folate receptor-targeted nanoparticles. Bhattacharya, Li, and Esmaeili et. al. all have successfully prepared nanoparticles around 100-200 nm in size, while others such as Krais and Su et. al. reported sizes greater than 300 nm. (22, 219-222) Interestingly, the polydispersity indices (PDIs) were smaller than observed in glucose dispersion with 0.11, 0.12, and 0.04 for targeted, mixed conjugate, and null folate micelleplexes, respectively. The low PDI for each micelleplex confirms that size distribution around the average hydrodynamic diameter is very narrow, and that no large aggregates were observed. The same suspensions were utilized for zeta potential measurements.

The micelleplexes made with all three conjugates had a slightly positive charge, between +1.5 and +3 mV as shown in Figure 4.2 B. This positive charge can support the initial interaction between the negatively charged cellular membrane and the positive charge of the outer shell of the micelleplex but should not over shadow the desired targeting effect of the folic acid ligand. Taken together, in PBS, the three chosen conjugate formulations had hydrodynamic diameters and zeta potentials that were comparable to previous findings, which demonstrates initial promise towards an effective siRNA nanoparticle delivery approach based on size and zeta potential criteria.

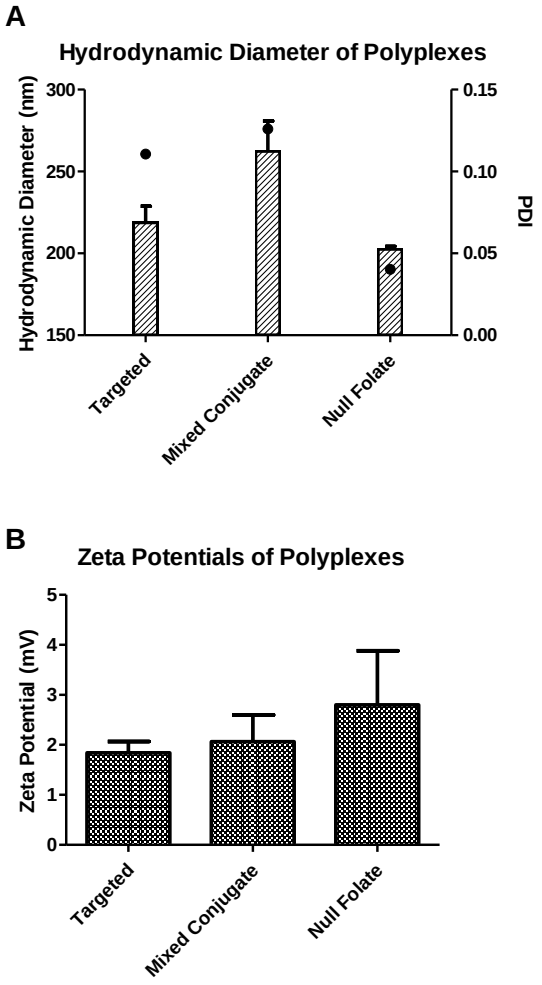

Figure 4.2. Hydrodynamic diameter (with polydispersity index, PDI, measurements) and Zeta Potential Measurements: Micelleplexes made of three different triblock copolymers were analyzed by dynamic light scattering (DLS) and LDA at N/P ratio 5 in PBS. Formulations made with two

folate decorated copolymers (targeted and mixed conjugate) as well as a null folate copolymer were analyzed. Hydrodynamic diameters and PDIs are presented in Figure 4.2 A, and zeta potentials are shown in Figure 4.2 B. Error bars represent stand deviation of error between triplicates.

When assessing receptor targeting, a common way to determine specificity and receptor-mediated endocytosis is to inhibit the uptake with an excess of the free endogenous ligand of the receptor. (48, 167, 203, 204, 223, 224) Accordingly, in regard to folate receptor targeting, free folic acid has been used as the substrate to demonstrate competitive inhibition for the binding and internalization for folate decorated therapies. Within recent literature, concentrations of excess folic acid used to inhibit nanoparticle binding and uptake have ranged from as low as 100 μM up to 5 mM. However, due to folic acid being a small molecule with only one possible binding interaction with the receptor, and the nanoparticles used here being multivalent, the aim of this project was to better understand the potential inhibition of nanoparticle binding to the folate receptor that free folic acid can mediate. Therefore, we used a concentration range of free folic acid that covers the concentrations reported in the literature. As shown in Figure 4.3, we compared micelleplexes made with the targeted polymer against null folate micelleplexes with and without excess competing free folic acid. Hypothetically, the folic acid-decorated micelleplexes would experience an inhibition in their uptake via FRα in the presence of an excess folic acid, while the null folate conjugates uptake profiles would not be affected. However, due to the multivalent nature of the conjugates, we did not expect strong inhibition of their binding or uptake due to their stronger binding avidity to FRα compared to monovalent folic acid. As described in our previous work, as well as in Figure 4.3 A, only a slight inhibition of uptake of the targeted nanoparticles is observed, while the uptake of the null folate micelleplexes is unaffected at low excess FA concentrations. (48) This slight inhibition at low concentrations corroborates what has been demonstrated by the Stayton group. (167) However, as the concentration of the free folic acid

increased to 500 μM and above (Figure 4.3 B-D), not only was the targeted nanoparticle uptake diminished, but also that of the null folate nanoparticles. It should be noted that uptake was studied 4 h past transfection. After such a short incubation time, the full targeting advantage of the targeted micelleplexes over the null folate ones is not yet expected. Collectively, the data in Figure 4.3 illustrate that at low concentrations of folic acid, a minor inhibition of the targeted micelleplexes occurred, while not affecting the null folate micelleplexes which are taken up by routes other than receptor-mediated endocytosis.

Alternatively, when treated with higher concentrations of free folic acid, it is possible that the hydrophobic folic acid destabilizes all micelles, no matter if they are targeted or not, which leads to decreased siRNA delivery for all nanoparticles.(5) It is also possible that the DMSO-containing solvent in which folic acid is dissolved changes the viscosity of the media, the micelle stability, or affects the cells. This decrease in nanoparticle uptake of targeted and non-targeted formulations after addition of high amounts of FA to the system has been observed before with folate targeted liposomes by Lee et al.(5) In order to overcome the stronger binding affinity observed in the case of multivalent particles, excess amounts of folic acid, above 1 mM were required. However, at these high concentrations, inhibition of the uptake of non-targeted liposomes was measured as well, which corroborates the results shown here in Figures 4.3 B-D. (5, 225) Lee et al. reasoned that with excess folic acid in solution, a disruption of the cationic lipid/nucleic acid complex stability occurred. Also in the case of our micelles, disruption and premature release of siRNA in the presence of excess folic acid was considered but was not observed (data not shown). However, at excess folic acid concentrations as low as 250 μM, hydrodynamic diameters of higher than 600 nm were measured, and steadily continued to increase with the folic acid concentration. These hydrodynamic diameters measured by DLS clearly suggest that aggregation is occurring in

the presence of free folic acid. It should be noted, however, that folic acid has been described to form dimers and trimers at higher concentrations within a system. These dimers and trimers, if formed, are then unable to bind to FRα to compete with the uptake of targeted nanoparticles. (226) Therefore, as shown in the literature, higher concentrations of folic acid on the surface of multivalent FA-modified nanoparticle may not necessarily yield a greater targeting advantage but rather hinder the targeting system. Reddy et. al. revealed that only 0.03 molar percent of folic acid on a liposome is needed to gain a targeting advantage. With higher molar percentages of FA on the surface of nanoparticles, it is possible that the problem of FA dimer and trimer formation is encountered. (225) The binding advantage of multivalent particles was demonstrated in uptake studies using SKOV-3 cells *in vitro*. However, when an excess concentration of free folic acid is used to saturate the receptors to outcompete for the binding of the targeted micelleplexes, no competition is detected. This observation falls in line with the hypothesis that multivalent micelleplexes cannot easily be displaced from FRα binding sites by monovalent folic acid. In comparison to the studies performed by Liu et. al. who showed efficient uptake inhibition at low excess amounts of FA added, the micelles demonstrated here carry more FA on their surface.(25) The discrepancy in competitive inhibition can therefore be explained by the difference in valency which determines the affinity and avidity with the receptor and the ability of these multivalent nanoparticles to be displaced by a monovalent ligand or not. Similar observations have been reported not only *in vitro***,** but even *in vivo*.(28) However, when high amounts of folic acid are added to the system, the decrease in uptake affects both targeted and non-targeted formulations. This suggests that the inhibition occurring is not due to blocking the receptor binding, but perhaps affecting all nanoparticle uptake due to a cellular event or a physical destabilization of the cationic condensation of the nucleic acids, or aggregation of the micelles, as Reddy hypothesized.(225)

Further experiments should therefore be performed in parallel to competiton studies to better understand this effect. Thus, when performing competitive inhibition studies, the concentration of folic acid in the experiment should be considered and optimized for maintained stability of the delivery system. Furthermore, competition assays may not necessarily be the most efficient route of addressing receptor targeting specificity; especially if the delivery system's physical and chemical properties are affected due to the presence of excess ligand.

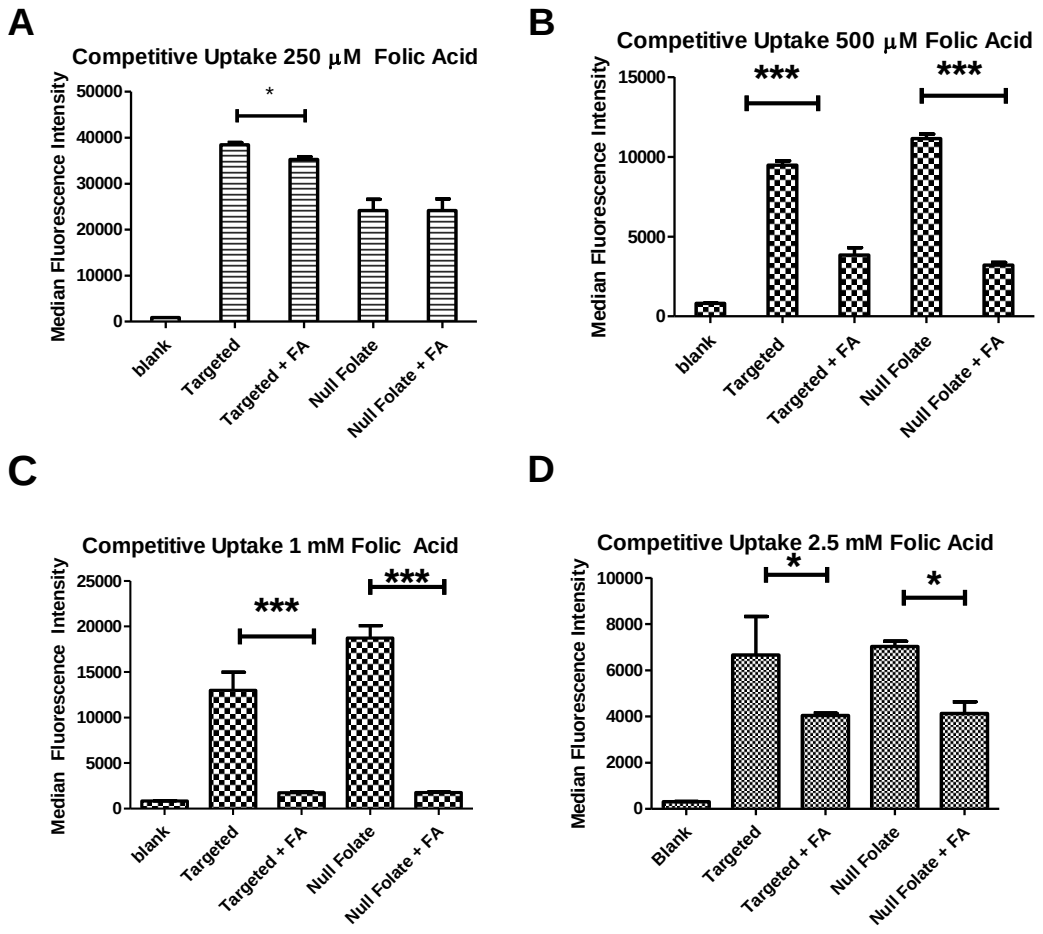

Figure 4.3. Micelleplex Competitive Uptake Studies Using Flow Cytometry (A-D): Uptake Studies in SKOV-3 cells compared for targeted and null folate micelleplexes at varying

concentrations of free folic acid. Samples were run in triplicates. Significance values were determined with a two-way ANOVA.*$p<0.05$, ***$p<0.01$.

After assessing the uptake profiles with and without excess free folic acid, the next step was to determine whether or not protein knockdown was affected by the inhibited uptake. We hypothesized that if the uptake is inhibited for the folate receptor-targeted micelleplexes, the knockdown of protein should be inhibited as well. By performing this test, we were able to assess whether the slightly inhibited uptake was reflected in only a slightly inhibited pharmacologic effect or if uptake mechanisms other than receptor-mediated endocytosis would skew the uptake results but would lead to endosomal entrapment of the particles, taken up by mechanisms other than receptor-mediated endocytosis reflected in a large inhibition of gene knockdown. SKOV-3/LUC cells were incubated with and without 250 μM and 1 mM of free folic acid, while being transfected with siRNA against Firefly Luciferase. After 48 hours, the luciferase knockdown was analyzed. In both data sets, the targeted micelleplexes achieved a significantly greater protein knockdown than the non-targeted micelleplexes. The more efficient gene knockdown mediated by the targeted micelleplexes could be due to the recycling parameters of FRα. The majority of FRα, once it binds and internalizes the ligand, will be recycled back to the cell surface. (202) This prevents many micelleplexes from becoming trapped inside the endosome and counteracts the degradation of the siRNA before it can cause protein knockdown. It is also possible that exocytosed particles may be endocytosed again at a later time point. Data shown in Figure 4.4 A demonstrate that when there was little uptake inhibition with 250 μM free folic acid, as shown in Figure 4.3 A, there was no knockdown inhibition. This demonstrates that over a prolonged time period, although a slight uptake inhibition occurred at 250 μM excess folic acid after 4 hours, the overall multivalent binding approach eventually overcomes whatever slight inhibition occurs early on and therefore

negates any offset in knockdown expected. Conversely, Figure 4.4 B demonstrates that a large excess folic acid (1 mM) can not only inhibit the uptake of both targeted and non-targeted nanoparticles, it can also impede the subsequent knockdown of luciferase as it generally inhibits nanoparticle uptake, no matter if the intended mechanism would have been receptor-mediated endocytosis or other uptake mechanisms. These data agree with the uptake results, demonstrating that uptake and knockdown seem to be inhibited when high concentrations of folic acid are added to the system due to micelle aggregation or a possible decrease in their stability. It should be noted that due to the relatively slow recycling rate of FRα, most folate receptor ligands remain on the cell surface or recycle through the cell without unloading their cargo into the cytoplasm.(202) The release from the receptor is expected to occur in the endosome after receptor-mediated endocytosis. Therefore, it may take longer for the targeted particles to achieve knockdown, and only a slight benefit of receptor targeting regarding gene knockdown is observed at 48 h post transfection versus non-targeted micelleplexes.

Theoretically, if the folate-decorated micelleplexes bind with FRα and become internalized, the receptor, ligand and nanoparticle will be taken up into the early endosome and undergo the endosomal ripening process starting from early endosomes and eventually merging with lysosomes. However, since the mechanism of action of the RNAi machinery is within the cytoplasm, the micelleplexes were designed to escape the endosome. A monensin assay is able to delineate where the siRNA loaded micelleplexes are located after transfection. With trypan blue treatment in addition to monensin, observations can be made as to where specifically the siRNA loaded micelleplexes are localized after transfection. As shown in Figure 4.5, after 48 hours, the folic acid-decorated particles (targeted) display significantly higher association with SKOV-3 cells than the null folate particles. However, much of the siRNA seems to be present extracellularly and

intravesicularly. The small difference of intracellular siRNA after delivery between the targeted versus non-targeted micelleplexes at the 48 h time point clearly explains the small benefit of targeting on gene knockdown efficacy at the same time point. These data could be explained by the relatively slow recycling kinetic of FRα. As most FRα is recycled back to the cell surface with the folic acid ligand still attached to the receptor, this represents a challenge for FRα mediated targeting strategies. If drugs are not able to escape the endosome after their first internalization, they do not reach the cytoplasm of the cell on first pass into the cell. The recycling of the targeted nanoparticles back to the cell surface, combined with the slow internalization kinetics of FRα, could explain the increased extracellular and intravesicular signals detected over time. However, these tri-block micelleplexes were designed to hijack the cells' natural receptor-mediated endocytosis mechanism and to escape the endosome to deliver siRNA to the cytoplasm. Receptor-mediated internalization can only be utilized by the folate decorated particles. It has been previously demonstrated that the uptake profiles of receptor mediated endocytosis is slower than adsorptive endocytosis and that the targeting benefit of these polyplexes is more clearly observed at later time points.(48) Additionally, it has been shown that FRα endocytosis of folic acid and FRα-targeted nanoparticles utilize caveolae mediated endocytosis within lipid rafts, whereas non-targeted particles are likely to enter the cell via clathrin-coated pits through adsorptive endocytosis.(227) Due to the nature of the different uptake mechanisms, the difference in intravesicular signal could be attributed to the uptake kinetics of the particles. Non-targeted particles may enter the cell at a faster rate than via the FRα mechanisms but may not be able to escape the endosome as efficiently as their targeted counterparts. Therefore, it is likely that the non-targeted particles were degraded within 48-hour past transfection. This hypothesis is supported by the results in Figure 4.4 A where the targeted particles demonstrated a more efficient

knockdown profile. These differences in kinetic and uptake mechanistic profiles can help explain the difference between their compartmental distribution shown in Figure 4.5.

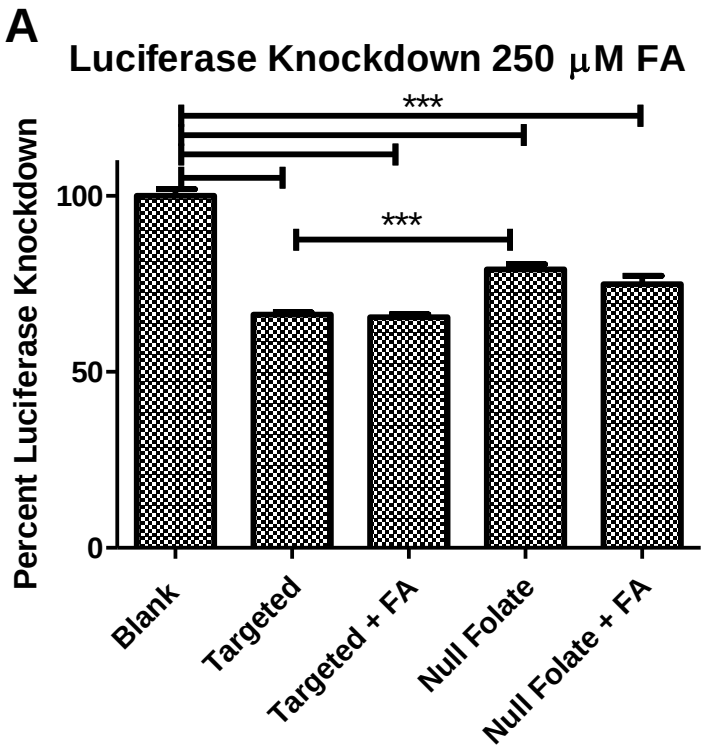
A
Luciferase Knockdown 250 μM FA
Percent Luciferase Knockdown
100
50
0
***
***
Blank
Targeted
Targeted + FA
Null Folate
Null Folate + FA

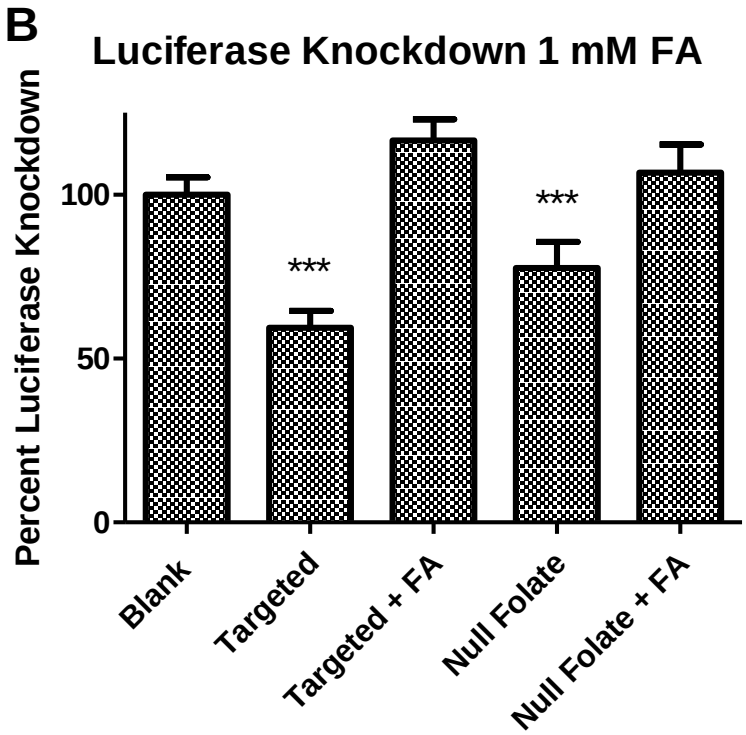
B
Luciferase Knockdown 1 mM FA
Percent Luciferase Knockdown
100
50
0
***
***
Blank
Targeted
Targeted + FA
Null Folate
Null Folate + FA

Figure 4.4. Luciferase Knockdown under Competition: Luciferase assay in SKOV-3/LUC cells assessing firefly luciferase knockdown 48 h post transfection at 250 µM (A), and 1 mM (B) of free folic acid. Samples were run in triplicates. Significance values were determined with a two-way ANOVA. *** $p < 0.05$

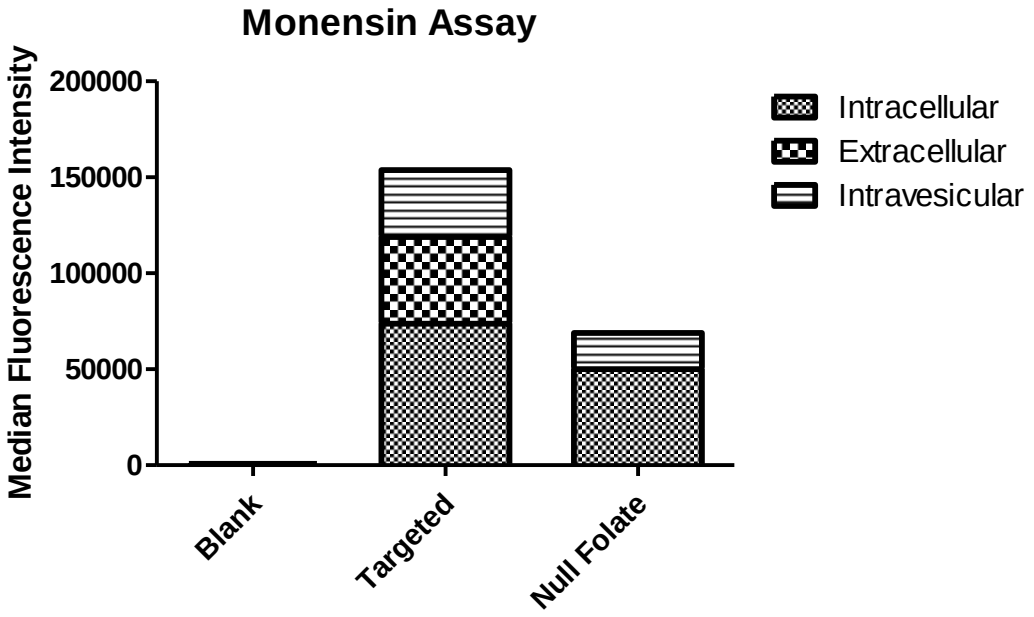

Figure 4.5. Monensin uptake assay: Uptake study with trypan blue and monensin treatment to assess localization of siRNA within SKOV-3 cells 48 h after transfection. Samples were run in triplicates.

To measure size and morphology of the conjugates, we imaged randomly dispersed micelleplexes which were air-dried on a glass coverslip. A uniform particle polydispersity with an average particle size of 152± 22 nm was observed, as shown in Figure 4.6. These sizes are consistent with the hydrodynamic diameters of micelleplexes determined in previously published work using a DLS.(48) These sizes, albeit slightly smaller than in Figure 4.2 A, are in agreement with the hydrodynamic diameters of micelleplexes prepared in 5% glucose instead of a PBS solution, emphasizing the role of counter ions diffusing with the particles in a higher ionic strength dispersant which increase their hydrodynamic diameters.

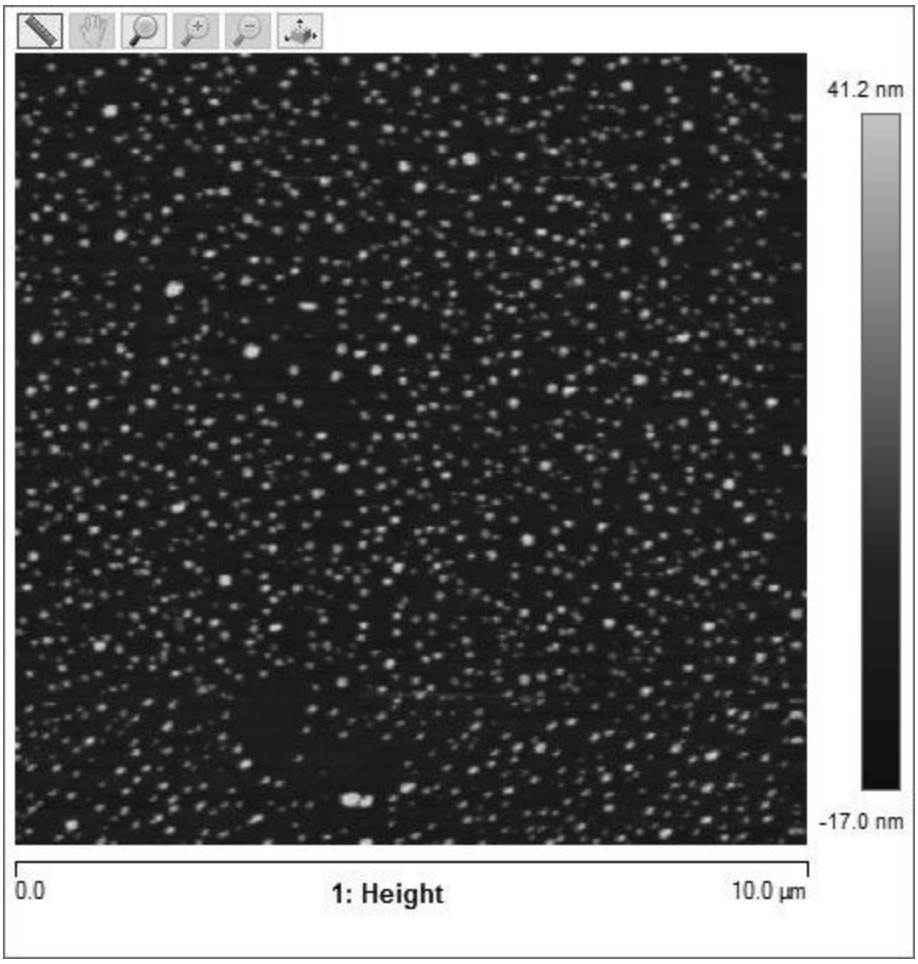

Figure 4.6. AFM images of micelleplexes: Topographical image of micelleplexes on a 25*25 mm glass coverslip with scan size of 10 µm.

In order to assess and compare binding probability of FRα with folic acid and folate-decorated micelleplexes, we performed AFM force measurements. The AFM cantilever was first functionalized with an active FRα and experiments were run with varying substrates on a glass cover slip. Control experiments were performed with folate receptors on the cantilever tip and a clean non-functionalized silicon substrate. In this case, there was little to no specific adhesion to the receptor; the binding probability for a blank substrate was 0.009. Next, over 1000 force measurements were recorded for each substrate with the FRα-modified cantilever. In each case, the binding probability was determined by the number of force curves that show at least one rupture

event divided by the total number of force measurements performed on the substrate. The binding probability for folic acid-modified substrates to the folate receptors attached to the cantilever was 0.462. Conversely, the binding probability for the folate-decorated micelleplexes to the active folate receptors attached to the cantilever was 0.573. The rupture force distributions on both folic acid and folate-decorated micelleplexes at a 2 μm/s retract speed were also recorded. Rupture force histograms for folic acid and folate-decorated micelleplexes are shown in Figure 4.7 A and B, respectively. For folate-decorated micelleplexes, we found a most probable rupture force of 215.8 pN. This binding force was significantly ($p<10^{-22}$) higher compared to the most probable rupture force of 78.6 pN, which was observed for free folic acid only. This large difference is most likely due to multiple bonds formed on the folate-decorated micelleplexes, leading to a higher binding probability and binding avidity of the multivalent folate-decorated micelleplexes versus the affinity of folic acid to FRα. It should be noted that the same type of cantilever was functionalized under identical conditions for both experiments.

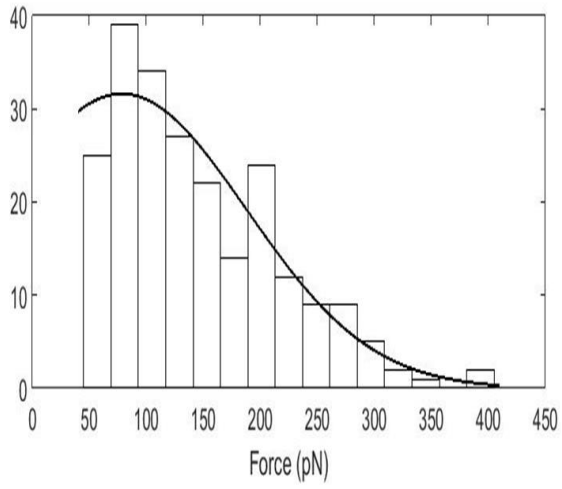

(a)

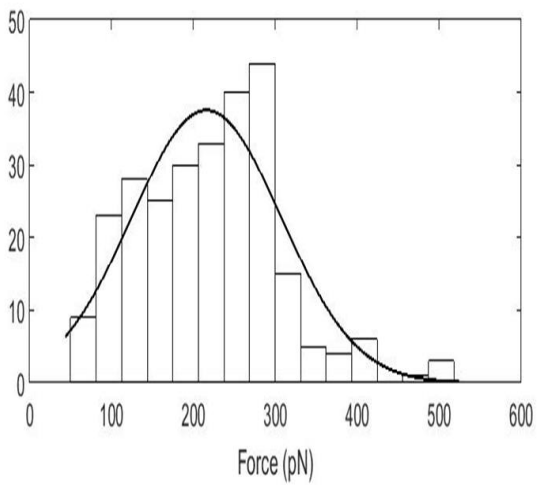

(b)

Figure 4.7. (a) Rupture force histogram plotted for substrate functionalized with free folic acid, (b) Rupture force histogram for substrate functionalized with folate-decorated nanoparticles.

Multiple studies have tried to use a competitive inhibition setup to demonstrate that the addition of free folic acid to the system outcompetes the folate-decorated nanoparticles regarding the binding to FRα. With this in mind, the kinetics of bond formation were observed between a FRα decorated cantilever and folate decorated micelleplexes. During the experiment, repetitive injections of free folic acid were added at fixed concentrations into the measurement cell. Figure 4.8 shows the binding probability of the decorated micelleplexes with FRα versus the injected folic acid concentration. Based on the cell uptake study shown in Figure 4.3, we hypothesized that low excess amounts of free folic acid could only slightly decrease the binding probability of multivalent folate decorated micelleplexes having multiple binding sites on the cantilever. Therefore, we expected that they could not be displaced efficiently from the receptor by monovalent folic acid. Accordingly, it was observed that injection of free folic acid into the flow cell did not decrease the binding probability significantly until about 250-300 μM free FA. However, as the concentrations of free folic acid increased, a precipitous decrease of the binding probability was observed. These results are in full agreement with the uptake study in Figure 4.3 A-D. Earlier published work with free folic acid around 100 μM showed no significant inhibition of siRNA uptake between targeted and non-targeted micelleplexes, which can be explained by the results in Figure 4.8. At 250 μM, a slight inhibition of binding probability can be observed correlated with a significant decrease in siRNA uptake for the targeted micelleplexes, but unchanged uptake in the non-targeted formulation. At this concentration, an optimal excess concentration seemed to be reached where the free folic acid inhibited the folate receptor dependent endocytosis while not decreasing micelleplex stability. Even if increased average hydrodynamic diameters of the particles were observed at this concentration of free folic acid,

apparently not all particles had aggregated and a large amount of particles was still in the size range for efficient endocytosis. As demonstrated at higher concentrations above 250 µM, the binding probability significantly drops in cell culture as the uptake of both targeted and non-targeted formulations was significantly inhibited. Overall, the precipitous drop of binding probability above 250 µM of free folic acid can easily be explained by micelleplex instability or aggregation in the presence of high concentrations of free folic acid. In case of dissociation of the micelleplexes, the valency is decreased from multivalent complexes to monovalent conjugates which can be displaced from the receptor by the presence of excess monovalent ligand. In case of aggregation, targeting ligands are lost in the core of the aggregates, and in cell culture, they reach sizes that are no longer conducive for endocytosis.

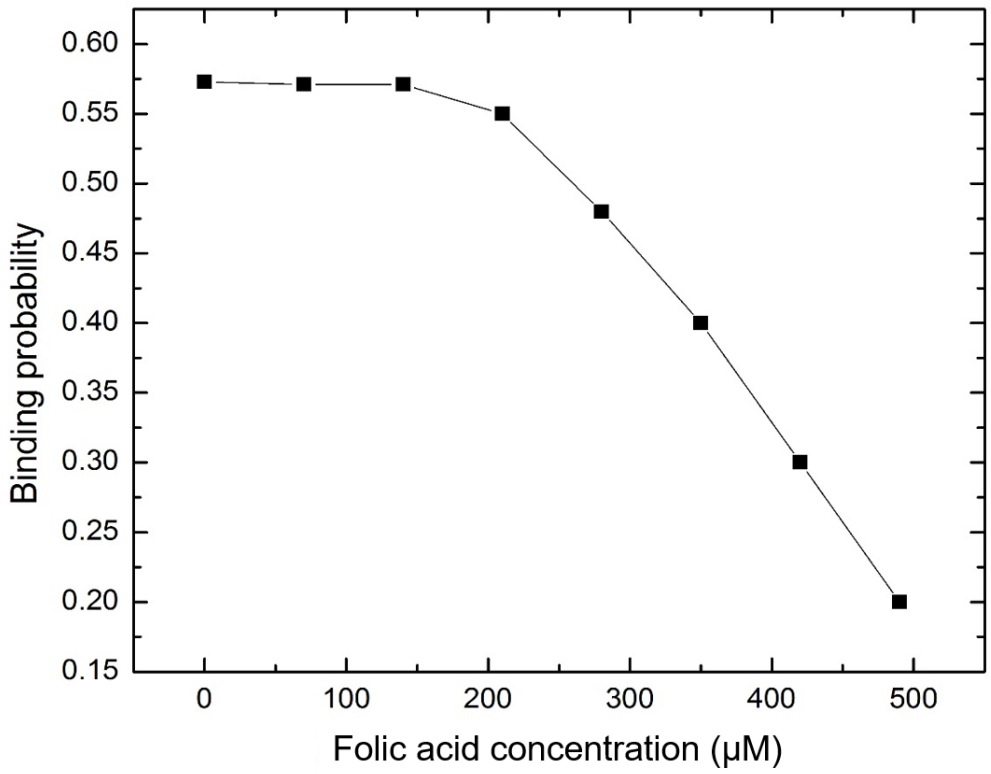

Figure 4.8. Binding probability versus concentration of folic acid after injecting folic acid in the flow cell of a substrate functionalized with folate-decorated nanoparticles with a folate receptor functionalized cantilever tip.

Limits of this AFM-based approach failed to take into account, or to verify, the clustering of FRα. On the apical surface of the cell, FRα tends to cluster together on lipid rafts which can not be mimicked through this AFM-based approach. In a biological state, if the FRα clusters together, the multivalency of folate decorated micelleplexes can utilize the proximity of other FRαs to create a tighter binding when compared to a free standing FRα. Unfortunately, with functionalizing the cantilever with FRα, receptor clustering can only be aimed for by adjusting the receptor concentration used for the functionalization.(36, 39) Lastly, in *in vitro* and *in vivo* experiments with FRα-expressing cells, the addition of free folic acid can have several pharmacological effects on the cells which could inhibit binding and uptake. However, with the AMF approach, we can only address any biophysical effects of receptor binding that happen.

4.4 Summary and Conclusion

Targeted therapy has been on the forefront of developing new treatment options for cancer in the clinic. The ability to selectively target cancer cells while avoiding toxicity toward healthy tissues has become the ideal outcome of drug delivery. Since the development of the field of nanomedicine in the late 2000's, the ability to easily modulate and alter delivery systems to fit the needs of one disease profile is achievable. It has been shown that multiple cell surface receptors are significantly over-expressed within a variety of disease states such as cancer and or inflammatory diseases. Examples of such receptors are folate receptor alpha and beta, HER-2, transferrin, and integrin receptors (30, 31, 48, 228). However, to target these receptors, specifically FRα, we believe that more optimization in the models is needed in order to confidently claim that receptor targeting is being utilized when a ligand is added to a nanoparticle. Multiple experiments

other than the excess addition of the targeting ligand, as discussed in this chapter, can further elucidate the multivalent targeting advantage gained when a targeting ligand (e.g., folic acid) is added to a drug delivery system. Here, FRα binding properties of micelleplexes made with folate-targeted triblock copolymers were evaluated. The sizes and zeta potentials of the micelleplexes were verified with DLS and AFM in a PBS suspension and compared with previously published results.(48) The sizes obtained with both techniques were within the range of 200-250 nm with a slightly positive zeta potential. The hydrodynamic diameters were slightly larger than previously reported due to the change in dispersant from 5% glucose to PBS. AFM data with a modified cantilever demonstrated that the multivalent micelleplexes bind at a higher probability and a with a stronger force than free folic acid. Receptor-mediated endocytosis and knockdown kinetics were studied with the monensin assay and luciferase assay. Due to the slow rate of FRα recycling, and the time required to observe protein knockdown with siRNA, later time points of 48 h post transfection were assessed. As shown, the targeted micelleplexes resulted in a greater accumulation in the cytoplasm over time which leads to a significant targeting advantage to luciferase knockdown after 48 hours when compared to the non-targeted micelleplex. Additionally, due to the slow recycling of the FRα over time as well as the propensity of the receptor to recycle back to the surface with its cargo, greater amounts of the micelleplexes were found extracellularly and intravesicularly over time. This difference could be greater for periods longer than 48 hours if particles are still located on the outer surface of the cell or not yet released from the intracellular vesicles after 48 h. Collectively, these data suggest that a simple design of adding excess folic acid ligand to an uptake study may not prove or disprove receptor-mediated endocytosis. Further studies, as described here, should be carried out to investigate a targeting advantage that is gained through ligand conjugation. In this chapter, the targeted micelleplexes

have a higher degree of binding and stronger binding than folic acid. This results in an inherent targeting advantage that cannot be overcome by adding excess ligand into the solution without jeopardizing the entire system. Currently, further biophysical approaches are being carried out to further assess the biophysical changes of triblock copolymer interaction with siRNA when a targeting ligand is conjugated and the differences of cellular interactions of targeted and non-targeted micelleplexes.

CHAPTER 5 – AN INSIGHT INTO THE BIOPHYSICAL CHARACTERISTICS OF FOLATE RECEPTOR ALPHA TARGETED SIRNA MICELLEPLEXES

5.1 INTRODUCTION

The number of nanomedicine publications has grown exponentially since the early 2000's. Within this field, nanoparticle therapies for drug delivery have only become more sophisticated. The first nanoparticle-based therapies to be approved in the clinic were doxil and abraxane. Both are non-targeted towards any tumor specific biomarker and solely relied upon passive uptake to treat cancer.(7, 18) Now, nanoparticles in the clinical pipeline include multiple delivery vectors such as liposomes, silica or gold nanoparticles, or polymeric micelles. These nanoparticles are used as imaging agents, and a wide variety of them are cancer therapeutics for solid and liquid tumors, as well as for auto-immune diseases.(3) Intelligently designed nanoparticle therapies could be one approach to overcome the complexities of diseases such as cancer. These nanoparticles are optimized in order to deliver the most payload possible to the target site. Polymeric nanoparticles, which can be easily modified, allow for multiple disease states to be targeted with various targeting ligands.(23, 41, 114, 204, 229-231) Nanoparticles have a wide variety of payloads that can be encapsulated or covalently attached. One of the types of payloads that researchers have utilized for nanoparticle delivery is the group of nucleic-acid based therapeutics, including mainly DNA and RNA, but also modifications such as peptide nucleic acids (PNAs) and locked nucleic acids (LNAs). Researchers have used gene delivery to introduce new genes or knock out specific genes in a safe and efficient way. After discovery of short interfering RNA (siRNA) in the late 1990's, it has been heavily investigated for its therapeutic properties to silence aberrant gene expression. However, naked siRNA is not able to circulate long in the bloodstream due to being renally excreted within minutes and being easily degraded by endonucleases.(60) Therefore, carriers are needed to safely deliver siRNA into cells in order to

achieve its promising therapeutic potential. However, these carriers ideally need to be stable to avoid premature release of the payload, allow for long circulation, have a low toxicity and immunogenicity profile, and to be biodegradable.

Since the discovery of the potential of nucleic acid and gene delivery, a special focus on developing a variety of nucleic acid vectors has developed. Researchers have created viral and non-viral delivery systems, all of which have shown considerable potential. Non-viral nanoparticles are comprised of lipids, peptides, polymers or blends and conjugates of the latter.(54, 232) Here, we chose to utilize a polymer-based nanoparticle delivery system with three components: polyethyleneimine (PEI), polycaprolactone (PCL), and poly(ethylene glycol) (PEG). The rationale for including PEI within the polymer backbone was its ability to electrostatically condense siRNA and provide the resulting polyplexes with a net positive charge for interaction with the cell membrane and intracellular delivery. PCL drives micelle formation and increases the hydrophobic content of the polymer.(62) However, a major disadvantage of high molecular weight PEI is its marked toxicity.(116, 117, 233) Therefore, PEG was added to the backbone in order to increase the biocompatibility, while also aiding in macrophage phagocytosis avoidance.(234) As previously reported, this triblock co-polymer effectively delivers siRNA and mediates protein knockdown. (48)

In order to target gene therapy to cancer cells and not healthy dividing cells, researchers have been exploiting options for conjugating targeting ligands on the surface of their nanoparticles. This creates homing mechanism which allows for the selective targeting of diseased cells over healthy ones. There have been several targeted therapies that have made their way into the clinic in the form of antibody-drug conjugates, or antibodies/antibody fragments.(27, 235, 236) Examples of these therapies are Herceptin, Zevalin, and Avastin which have all been approved by

the FDA.(19, 228, 237) Strategies to create targeted nanoparticles rely upon the same concept as attaching targeting ligands to small molecules, proteins, or antibodies/antibody fragments. However, attaching a ligand to a drug or a nanoparticle can affect many parameters such as molecular weight, hydrodynamic diameters, hydrophilicity, hydrophobicity, interaction with excipients, and many more. Therefore, here, we explore the biophysical effects of attaching folic acid targeting ligands on the surface of our micelleplex siRNA delivery system.

The benefits of using these targeted nanoparticles need to be better understood, and the effects of the targeting ligands can play a role in changing important properties of the nanoparticles. Several targeted nanoparticle drug delivery papers have been published which compare payload delivery efficiencies between their targeted and non-targeted delivery vectors. However, simple additions of any component within the nanoparticle structure can have drastic effects on the size, shape, charge, drug loading efficiency, and other physical or chemical parameters. All of these can either enhance or be detrimental to drug delivery. The same principle can be applied to a targeting ligand, in this case folic acid. Therefore, we sought to address whether or not a simple comparison between a targeted and non-targeted nanoparticle is truly a fair assessment. Accordingly, we assessed several biophysical properties of the different micelleplexes to determine if any basic biophysical property changes with the addition of a folic acid targeting ligand.

5.2 MATERIALS AND METHODS

5.2.1 Materials. Hetero-bifunctional poly(ethylene glycol) (HO-PEG-COOH), as well as monofunctional (CH3-PEG-COOH, 5 kDa), were purchased from JenKem Technologies (Plano, TX, United States) and utilized for chemical synthesis of siRNA delivery vectors. Hyper branched

polyethylenimine (hyPEI, 25k Da) (BASF) was included in the overall synthesis of the tri-block copolymer. All other chemical regents for synthesis were obtained from Sigma-Aldrich and used without any modification. Dicer substrate double-stranded siRNA (DsiRNA) targeting the Enhanced Green Fluorescent Protein gene (EGFP siRNA, 25/27), firefly luciferase (luc siRNA, 25/27), and a scrambled nonspecific control (siNegCon, 25/27) siRNA were purchased from Integrated DNA Technologies (IDT, Coralville, IA).

5.2.2 Synthesis of Tri-block Copolymers and Characterization. The tri-block copolymers consisting of PEI-PCL-PEG and PEI-PCL-PEG-Folic acid were synthesized based upon a previously published approach applying ring opening polymerizations, Michael's addition reactions, and folic acid decoration onto the triblock copolymer via click chemistry reaction.(48) Here, a targeted polymer with 3.5 kDa PEG chain length, a non-targeted one with 3.5 kDa PEG chain length, as well as a polymer with higher folic acid grafting degrees and mixed 3.5 kDa and 5 kDa PEG chains (mixed conjugate) were synthesized and characterized by ^{1}H NMR, UV spectroscopy, and a folate composition assay, as described before.(48)

5.2.3 Preparation of PEI-PCL-PEG-Fol micelleplexes. Each polymer was dissolved in water at 1 mg/mL based on the PEI content and sterilized with filtration. Polymers were stored at -4 ˚C. Micelleplexes were created using the same equation, as described before with these triblock co-polymers.(48)

To prepare the micelleplexes, equal volume amounts of polymer and siRNA were added together, vortexed, and incubated at room temperature for 20 minutes. Once the micelleplexes had been formed, suspensions were added to the samples for respective experiments.

5.2.4 Cell Culture. SKOV-3/LUC cell line is a human ovarian cancer cell line which was obtained by stably transfecting SKOV-3 cells, obtained from ATTC (LG Promochem, Wesel, Germany),

with a pCMV-luciferase plasmid. SKOV-3/LUC cells were cultured in folate free DMEM cell culture medium (Sigma-Aldrich) supplemented with L-glutamine, sodium bicarbonate, 10% fetal bovine serum (Thermo Scientific Hyclone), and 1% penicillin/streptomycin. Cells were allowed to grow in 37 °C and 5% CO_2, incubators and passaged when they reached confluency.

5.2.5 Transmission Electron Microscopy (TEM). Transmission Electron Microscopy was utilized to assess the size and morphology of the micelleplexes after siRNA condensation, as well as assessing localization of siRNA within micelleplex structure. For TEM size and morphology measurements, micelleplexes were made, as described above in a total volume of 20 μL in 5% glucose. TEM Samples were added dropwise to a copper-coated grid and imaged with a JEM 2010 transmission electron microscope (JEOL, Tokyo, Japan).

5.2.6 Fluorescent Correlation Spectroscopy. Micelleplex stability in serum was analyzed by fluorescent correlation spectroscopy (FCS) on a two photon Miatai spectraphysics Zeiss axiovert 200 inverted microscope platform (Oberkochen, Germany) using 100 femtosecond excitation, 80 megahertz laser at 780 nm with a 488 nm filter. The FCS protocol and analysis method was adapted based on a previously published approach. (193, 238) Micelleplexes were made in 10 mM HEPES buffer containing 1.6 μM AlexaFluor-488 labeled siRNA as described above. Within an 8 chamber slide (Nunc, Fisher Scientific, Waltham, MA, USA), serum, free AlexaFluor-488, and AlexaFluor-488 containing micelleplexes were made as described earlier. Micelleplexes were made at various N/P ratios (5, 10, 15) and analyzed with 10% and 90% FBS for 85 minutes each. Data points were collected every 1/100 of a second using a correlator from ISS (Champaign, IL, USA). In the graphed results, each data point represents the average of 500 seconds. Samples were normalized to 0-100% free siRNA where free serum represents the baseline, 0% fluorescence, while free siRNA represents 100% fluorescence. The data were analyzed using GraphPad Prism 5.0 software.

5.2.7 Circular Dichroism. Circular dichroism was performed on each micelleplex formulation to gain insight on the siRNA complexation and condensation behavior. For analysis, 2 nmol of siRNA within 100 µL of 10 mM HEPES buffer solution was mixed with 100 µL of each polymer solution at variable N/P ratios (N/P 1, 3, 5, 7, 10, 15, and 20). Samples were incubated for 20 minutes, followed by a 1:1 dilution with 10 mM HEPES buffer at pH 7.4. Following dilution, the samples were pipetted into a 0.2 cm quartz cuvette and analyzed on a Jasco J-1500 CD Spectrometer (Easton, MD, USA). Five scans were collected for each sample at 20 ˚C at 200 nm/min between 200-320 nm at a response time of 1 s and bandwidth/data pitch of 1 nm.(191)

5.2.8 Tensiometry. Critical micelle concentration (CMC) of each polymer was recorded on a KSV tensiometer while following and adapting a previous approach.(239) Samples were diluted at various concentrations (0.01-2 mg/mL) with water and loaded into a 0.55 mm gauge needle. Once the tip of the needle was placed within the center of the screen, the plunger was depressed until a full drop of the sample was formed. Data collection occurred at 25 ˚C and automated software (KSV 2001) analyzed the formation of the droplet for the surface tension. Results were recorded and analyzed in GraphPad Prism 5.0. Theoretic hydrophilic-lipophilic balance (HLB) values were calculated according to Griffin's method.(240) Since all polymers are highly hydrophilic, their ionic nature was not further taken into consideration but the HLB values were solely calculated to assess the difference in hydrophobic content.

5.2.9 Luciferase Knockdown. SKOV-3/LUC cells stably expressing luciferase were used in this experiment. In 24 well plates, 60,000 SKOV-3/LUC cells were seeded per well and incubated overnight at 37 °C and 5% CO_2. Micelleplexes of the targeted polymer were made, as described previously with 50 pmol of luciferase targeted siRNA. SKOV-3/LUC cells were incubated at 37 °C and 5% CO_2. After predetermined time points (24 h, 48 h, 72 h), cells were washed twice with

200 μL of PBS and treated with 300 μL of lysis buffer (Cell Culture Lysis Reagent, CCLR, Promega, Madison, WI, USA). Afterwards, each well was scraped with a pipette to effectively dislodge cell debris from the bottom of the well. The plate was then rocked at room temperature for 5 minutes. Cell lysates were pipetted out of the well plate and transferred to 0.5 mL Eppendorf tubes and placed on ice. Each tube was vortexed for 10-15 seconds and then centrifuged at 12,000 g for 2 minutes at 4 °C. The supernatant was collected, and 20 μL of each sample was added to a white 96-well plate to be analyzed for luminescence using a Synergy 2 microplate reader (BioTek Instruments, Winooski, VT, USA). Each well was injected with 100 μL of luciferase assay reagent containing 10 mM luciferin (Sigma-Aldrich, St. Louis, MO, USA) by the plate reader immediately before the measurement. Samples were measured in triplicate and analyzed with a two-way ANOVA using GraphPad Prism 5.0 software representing average values and standard deviations.

5.3 RESULTS AND DISCUSSION

Several tri-block copolymer consisting of polyethyleneimine-graft-polycaprolactone-block-poly(ethylene glycol) copolymers were previously synthesized and descriptions along with basic characterizations have been previously published. (48) The previously published results showed the presence of folic acid did not cause any notable changes to the hydrodynamic diameter of the micelles, while the zeta potential with the folic acid made the micelles slightly more neutral than their non-targeted counterpart.(48) This result was also observed with variations of this triblock copolymer, as demonstrated by Liu et al. as well as other with other folic acid modified delivery systems.(25, 241) Although size and zeta potential can by themselves have an effect on the drug delivery capability of nanoparticles, this study takes a closer look at additional biophysical properties of these targeted, folic acid decorated micelleplexes, and their non-targeted counterparts. To begin, TEM images were taken of both targeted and non-targeted micelles as

shown in Figure 5.1 to confirm sizes, micelle structure formation, and shape and were consistent with previous results.(48) No noticeable differences were found between any of the triblock formulations when complexed with siRNA.

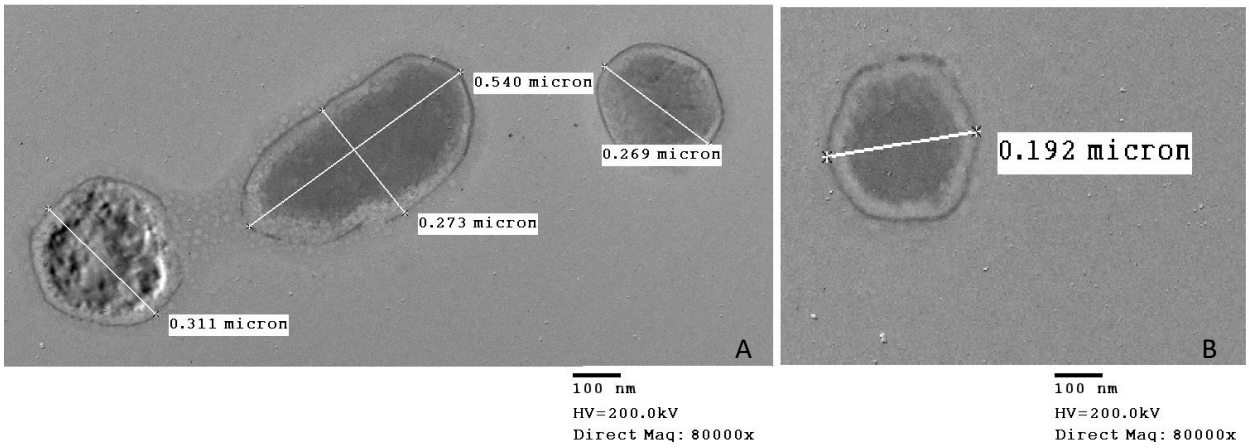

Figure 5.1: Characterizing Nanoparticle Size and Morphology. Micelle size and morphology was tested at N/P 5, with 40 pmol of EGFP siRNA by TEM. TEM samples were fixed on a grid for imaging. TEM images of null folate (A) and targeted micelleplexes (B) are shown above.

Once the micellar structure was confirmed, the siRNA binding properties within the micelleplexes were investigated with and without folic acid conjugated to the terminal end of the triblock co-polymer. In order to assess and characterize different conjugates' ability to condense siRNA, circular dichroism was performed. CD analysis can distinguish secondary and tertiary structure conformational changes within the siRNA backbone when it is electrostatically complexed within the micelleplex.(191, 233, 242) Changes in the chemical composition of the conjugates could theoretically change siRNA complexation and condensation behavior. At each N/P ratio, all CD spectra obtained from each conjugate at 264 nm showed a red shift, as well as an increase in the Cotton effect compared to free siRNA, without any noticeable change in the polarization degree after N/P 1. Similarly, a decrease in the polarization profile of free siRNA was observed at each polymer and N/P ratio at 210 nm. These were unlike the results obtained by Merkel et al. and O'Mahony et al. where they experienced a decrease in the cotton effect when

siRNA was electrostatically condensed within the polyplexes.(191, 242) However, the complexed siRNA within micelleplexes still contained the notable positive band at 260 nm and a negative band at 210 nm. This is indicative of the A-form of the molecule that is needed to be loaded into the RISC complex for mRNA degradation.(242) Therefore, we can conclude that every conjugate's PEI block was able to interact and complex with the siRNA backbone which is reflected in the change of the optical profile. Due to the similarity of optical profiles between the unmodified PEI and each triblock micelleplexes, we can deduce that the complexation of siRNA and change in its base stacking is a result of electrostatic interactions between PEI and the phosphates within the siRNA backbone which was not affected by the PEG or PCL blocks. Based on the CD results described here, the attachment of PCL-PEG or PCL-PEG-FOL did not seem to alter the siRNA interaction with PEI or the backbone of the molecule within the micelleplexes.

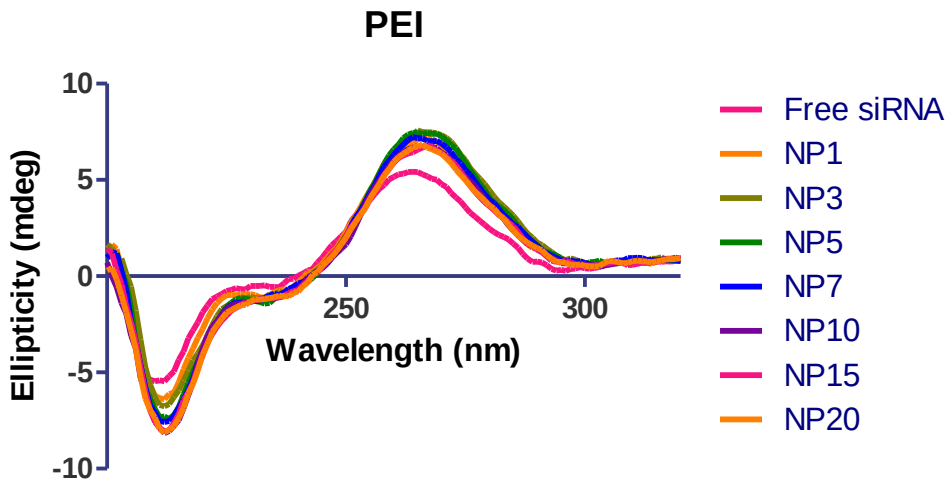

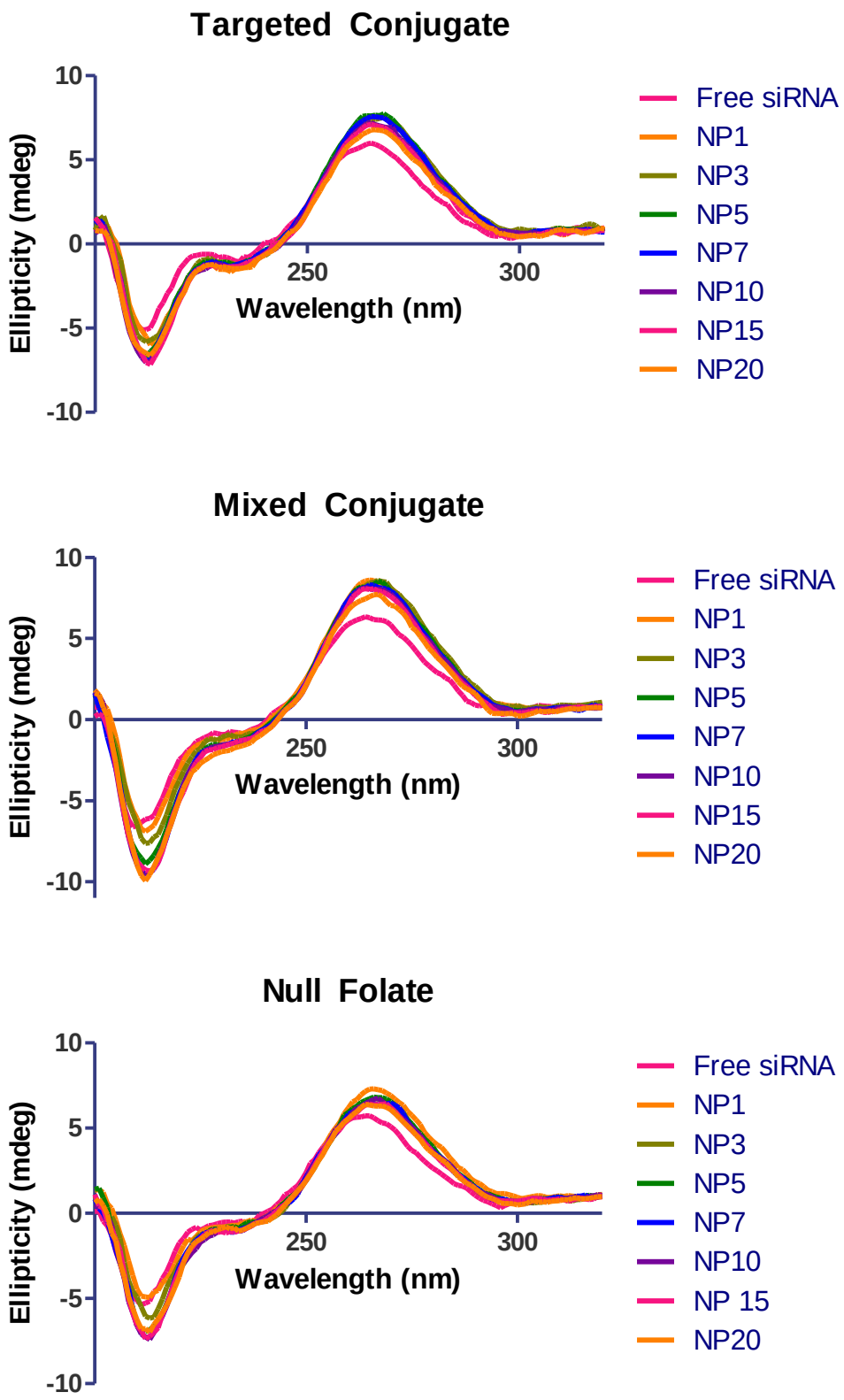

Figure 5.2: Circular Dichroism of Micelleplexes. Circular dichroism spectra of siRNA condensed within increasing polymer concentration in 10 mM HEPES buffer at pH 7.4

To build upon the studies previously published, further testing of micellar formations was carried out by tensiometry to determine the critical micelle concentration (CMC). Due to the amphiphilic nature of the triblock co-polymers, they have a thermodynamic driving force to create micelles. When increasing concentrations of amphiphilic polymers are added into an aqueous solution, the polymer chains start to aggregate into an organized structure with their hydrophobic polymer chains oriented towards the core of the micelle when the CMC is reached.(243, 244) In addition to the electrostatic interactions that occur with PEI, this process also aids in the protection and encapsulation of nucleic acids at the interface of the inner core and outer corona layer of the micelle for gene delivery. High CMC values indicate that the carrier will easily disassemble before it delivers the payload. Generally, micelles with high CMCs immediately dissociate more readily and their payload is prematurely released when they are injected into the body due to the dilution in the blood. As shown in Table 1, the CMC values of three conjugates were obtained via tensiometry across a broad range of dilutions. Interestingly, the targeted conjugate, as well as the non-targeted conjugate had very similar CMC, which were 23 µg/mL and 16 µg/mL respectively. The CMC values for these two tri-block copolymers, with and without folic acid modification, are greater than those described by Zheng et al. who reported values ranging between 62-512 µg/L for very similar copolymers.(181) Although they used a shorter hydrophobic chain, their polymers displayed lower CMCs as the grafting degree of the hydrophobic chain increased. In comparison with the targeted and non-targeted polymers, the mixed targeted conjugate in the panel investigated here had a 5 fold higher CMC at 105 µg/mL. Based on the polymers' statistical PEG-PCL grafting degrees, the hydrophilic content of the mixed conjugate was greater than that of the other two polymers, as reflected in its high theoretical HLB value in Table 1. As seen in previous studies, the grafting degree of PEG-PCL is lower than that of the targeted and non-targeted conjugates.

Therefore, overall, the PCL content decreased in the mixed conjugate. With a greater hydrophilicity, and decreased amphilicity of the conjugate, its solubility in water is higher and the thermodynamic driving force for forming micelles only comes into play at a higher concentration. The higher hydrophilicity of the mixed conjugate would be one explanation for its higher CMC value. However, it should also be noted that the mixed conjugate has a fifteen-fold higher folic acid concentrations than the targeted conjugate.(48) As described in previous studies, increased amounts of folic acid, as present in the mixed conjugate, have been shown to lead to instability or aggregation of micelles. (245) Since the presence of folic acid in the targeted conjugate did not strongly affect the CMC values, it appears that an optimal folic acid was obtained here which could help achieve a targeting effect without affecting micelle formation and stability. This CMC analysis suggests that the addition of a targeting ligand, such as folic acid, can have an effect on the CMC of the resultant micelles.

Polymer	CMC (mg/mL)	Theoretical HLB Values
Targeted Conjugate	0.023	16.67
Mixed Conjugate	0.105	19.61
Null Folate	0.016	18.18

Table 5.1: Critical Micelle Concentration and Theoretical HLB value. Critical micelle concentration (CMC) and calculated Hydrophilic-Lipophilic-Balance (HLB) ratio of each polymer in water was measured by tensiometry.

Once the micelles were formed, their stability in the presence of 10% serum (mimicking *in-vitro* conditions) and 90% serum (mimicking *in-vivo* conditions) was investigated with fluorescence correlation spectroscopy (FCS). The release of the encapsulated drug, in this case AlexaFluor-488 labeled siRNA, was monitored over time and results are depicted in Figure 5.3. The siRNA release was measured for each micelleplex over the course of 90 minutes, with

measurements taken every 1/100 of a second for multiple N/P ratios. The release of siRNA over time did not increase for any of the conjugates in 10% serum; however as the N/P ratio increased from 5 to 15, greater stability and better condensation of the siRNA micelleplexes was observed at any given time point. Each conjugate, with the exception of the targeted conjugate at N/P 5, released approximately 5-15% of the total siRNA loaded into the system. However, with 90% serum in the system, the targeted and mixed micelleplexes showed a lower ability to retain siRNA. Compared to the unmodified PEI and the mixed conjugate micelleplexes, the targeted and null folate micelleplexes displayed a greater ability to protect the siRNA from release. The mixed conjugate micelleplexes appeared to exhibit poorer siRNA retention than any other micelleplex. This observation could be related to the CMC value being greater for the mixed conjugate than the others. It is worth noting that the null folate non-targeted micelleplexes at 90% serum exhibited the best siRNA retention profiles across all N/P ratios with 15% release at N/P 5 and no measurable release at N/P 15. This creates a trend where increasing folic acid attached to the surface of the micelleplexes worsens the siRNA retention profiles. Therefore, as more folic acid attached disrupts the micelleplex formation and stability, these micelleplexes are more prone to siRNA release when serum is present in higher concentrations. Based on the CMC and FCS results, it becomes obvious that greater folic acid amounts on the surface of the micelles will not aid in the receptor targeting, but instead can become detrimental to the micelle stability in circulation and payload retention. This result may be more noticeable *in vivo* where higher serum concentrations are present and where the dilution of the micelleplexes into the bloodstream may cause the payload to be prematurely released.

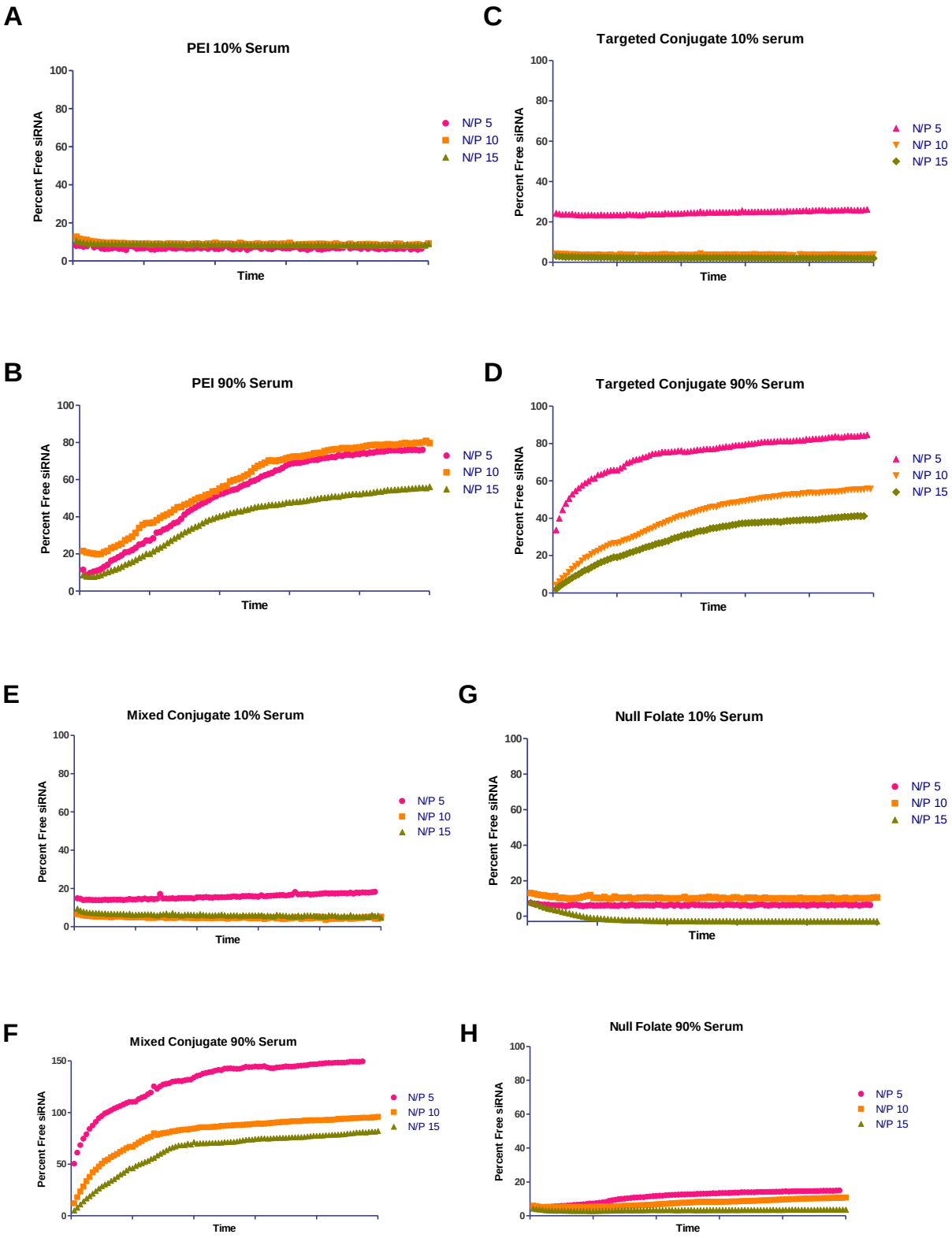

Figure 5.3: Fluorescent Correlation Spectroscopy of Micelleplexes. The stability of

mixelleplexes was tested in 10 and 90% FBS in 10 mM HEPES for 80 minutes. The siRNA complexes of each conjugate were analyzed at N/P ratios 5, 10, and 15.

After comprehensive biophysical characteristics of each micelleplex formulation, their efficacy, both in terms of siRNA uptake and protein knockdown, was evaluated *in vitro* for correlation with biophysical parameters. Flow cytometry uptake results of AF488 siRNA are presented in Figure 5.4. As shown, free siRNA cannot enter the cell very efficiently due to it being negatively charged and hydrophilic.(16, 56) However, when electrostatically packaged inside the micelleplexes, efficient siRNA delivery was achieved. Figure 5.4 demonstrates that the conjugates perform similarly as the unmodified PEI, confirming previous work.(48) However, the biophysical characterization offered above can help further explain these *in vitro* results. It is worth noting that the benefit of FRα targeting and receptor mediated uptake becomes more prominent at later time points beyond 4 hours.(48) At time points beyond 4 hours, the targeted micelleplexes outperform the null folate micelleplexes.(48) The significantly decreased uptake obtained after transfection with the mixed conjugate could be related to the increased folic acid concentration on the surface of the micelleplexes. Studies performed by Reddy et al and Ciuchi et al. demonstrated that very little folic acid on the surface of liposomes is needed in order to achieve receptor targeting, namely 0.033 molar percent. Furthermore, if more folic acid is added to the surface, this can lead to dimer and timer forming between the folic acid ligands resulting in the inability of the ligands to bind to FRα and even to precipitation of the liposomes.(225, 226) Consequently, the decrease in siRNA uptake by the mixed conjugate's micelleplexes in comparison to the targeted micelleplexes can be explained.

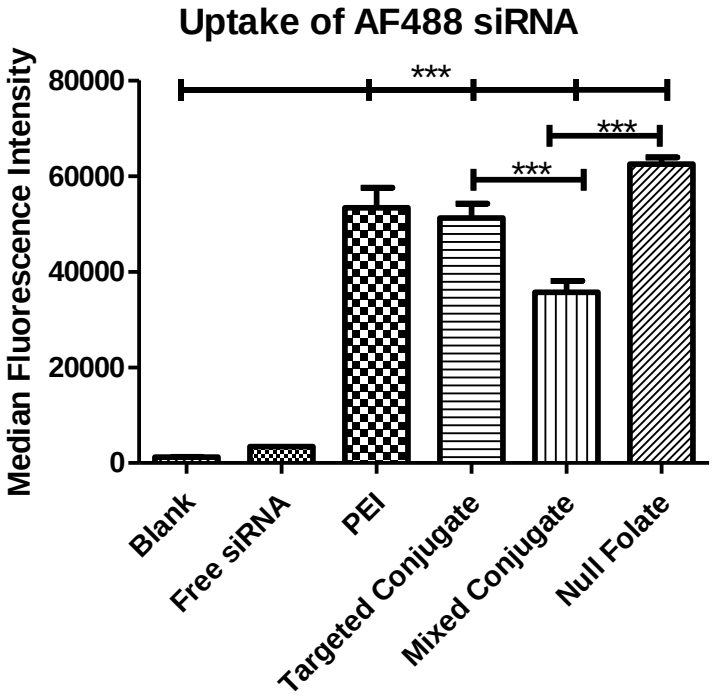

Figure 5.4: Alexa-fluor 488 siRNA uptake. siRNA uptake mediated by each polymer in SKOV-3 cells. Cells were transfected with 50 pmol of AF488 siRNA for 4 h and analyzed via flow cytometry. Results were analyzed by Prism. Samples were run in triplicates. Significance values were determined with a two-way ANOVA.*** $p<0.05$.

Once the micelleplexes are taken up into the cell, the siRNA needs to be released into the cytoplasm in order to achieve mRNA and subsequently protein knockdown. SKOV-3/LUC cells were transfected in order to evaluate protein knockdown over time and to demonstrate the micelleplexes' functionality *in vitro*. After time points of 72 and 96 hours, luciferase expression was analyzed. Due to the poor stability and uptake profiles of the mixed conjugate micelleplexes, they were not tested *in vitro* for luciferase gene knockdown. The targeted micelleplexes achieved a greater knockdown than the null folate micelleplexes at each time point. After 72 hours, the targeted micelleplexes achieved greater than 65% protein knockdown while the non-targeted null folate micelleplexes, achieved a maximum of 45% knockdown. Luciferase knockdown results with

the siRNA containing micelleplexes were comparable to knockdown described by Meyer et al. who achieved about 60-80% luciferase knockdown utilizing a PEGylated polycation to deliver siRNA. (246) Due to the micelleplexes being amphiphilic, they can efficiently enter cells (Figure 5.4) and be released from the endosome.(181) Therefore, we expected knockdown to occur with or without the targeting ligand. With this in mind, it is likely that there is an optimal concentration of folic acid that can be added to the micelleplexes to achieve a targeting benefit without significantly affecting their biophysical properties in a deleterious aspect.

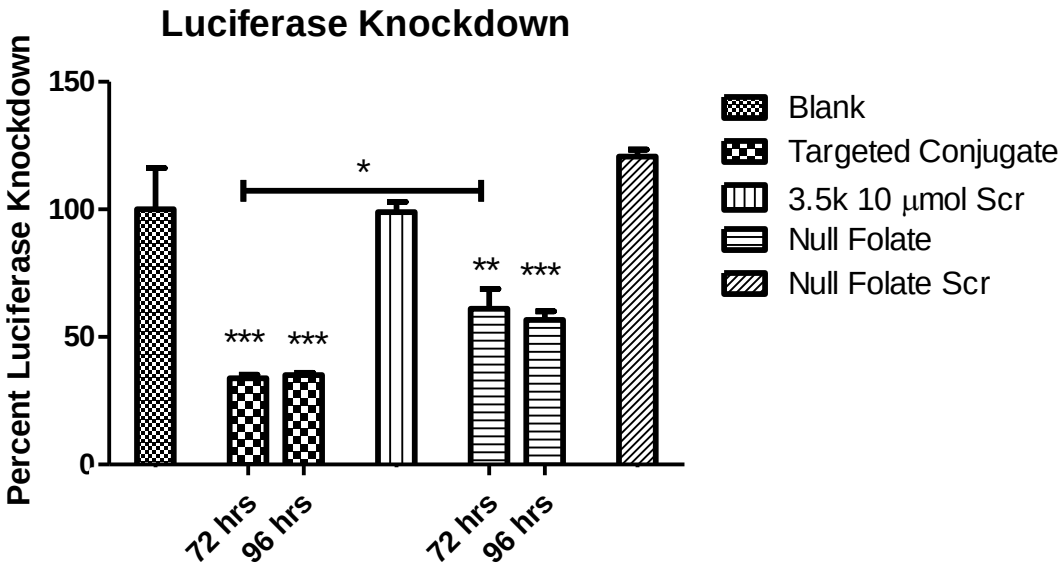

Figure 5.5: Luciferase Knockdown Assay. Knock down of luciferase in SKOV-3/LUC cells by 3.5k 10 μmol conjugate with 100 pmol of siRNA. Cells were transfected for 72 and 96 hours and harvested for a luciferase assay. Samples were run in triplicates. Significance values were determined with a two-way ANOVA. * $p<0.05$, ** $p<0.01$, *** $p<0.001$ compared to non-treated cells.

5.4 SUMMARY AND CONCLUSION

Lately, there has been an increased focus on personalized therapies in the clinic. In this regard, therapeutic nanotechnology has taken the approach of attaching targeting ligands onto nanoparticles to target disease specific cells by attaching substrates such as antibodies, small molecules, or proteins.(21, 231, 247, 248) These ligands can be used to target cell surface receptors such as integrin receptors, transferrin receptor, HER2 receptors, or folate receptors which are the focus of the targeted micelleplexes covered here. (19, 25, 30, 48) However, most manuscripts attempt to prove active targeting to the cells in a direct comparison between nanoparticles with and without the targeting ligand. Multiple studies have demonstrated that basic characteristics of nanoparticles such as size, shape, charge, and other physical or chemical characteristics have an impact on payload delivery.(23, 229, 249-254) Here, several biophysical characteristics of siRNA micelleplexes made with PEI-PLC-PEG triblock co-polymers with and without folic acid were analyzed to determine whether the addition of folic acid changes the nature of these micelleplexes. Size and morphology measurements by TEM analysis revealed no noticeable changes between micelleplexes with or without folic acid, but the addition of folic acid tended to decrease the zeta potential of the micelleplexes. Likewise, CD spectroscopy demonstrated that there was no difference in the ability to interact and condense siRNA regardless of the folic acid concentration on the surface of the particles. Each polymer was able to condense siRNA without changing the A form of the nucleic acid backbone, as shown in Figure 5.2. However, when higher concentrations of folic acid were present on the surface of the micelleplexes, a 15-fold increase in the CMC values was observed. This could be attributed to higher folic acid concentrations changing the hydrophilic corona of the micelles and disrupting the micelle formation. Instability problems can cause premature payload release or complete micelle disassociation into its monomer units when injected

into the bloodstream. These concerns were emphasized by the FCS measurements which addressed siRNA retention in the presence of serum. At low serum concentrations, mimicking *in vitro* concentrations, siRNA release did not increase over time (Figure 5.3). However, at 90% serum concentration, significant siRNA release was observed. Micelleplexes without folic acid displayed releases of 0-15%, decreasing as the N/P ratio increased. For the targeted micelleplexes, the more folic acid was present, the less stable the siRNA micelleplexes were over time. The targeted micelleplexes released 35-80% of the loaded siRNA, but increased stability was achieved as the N/P ratio increased. However, the mixed conjugate micelleplexes released 100% of their siRNA load at N/P 5 and 10, and 80% at N/P 15. Interestingly, the targeted and null folate micelleplexes outperformed unmodified PEI at each N/P ratio regarding stability. Overall, FCS data demonstrates that there is optimal folic acid decoration which can be achieved and allows for a targeting advantage, while not negatively affecting payload delivery. Overall, the presence of folic acid on the surface of micelleplexes for siRNA retention, while in the presence of serum, has a negative effect on stability. Lastly, siRNA uptake and protein knockdown was verified to show efficacy *in vitro* in Figures 5.4 and 5.5. Previously published results, in combination with what is shown here, demonstrate that FRα targeting is achieved and at time points beyond 4 hours.(48) In conclusion, the presence of folic acid changes many biophysical characteristics of self-assembled micelleplexes. Therefore, the comparison of non-targeted to targeted micelleplexes to determine receptor targeting efficiency may not be the most precise way to assess targeting efficacy since micelles can undergo drastic changes in their biophysical properties after targeting ligands are coupled.

CHAPTER 6 – INDIUM-LABELING OF SIRNA FOR SMALL ANIMAL SPECT IMAGING

Please note that this chapter, in its entirety, has been published in Imaging: Materials and protocols. The authors include myself and Dr. Olivia Merkel. I am the first author and wihtin this book chapter I performed the experimental protocol and wrote the chapter.

S. Jones, OM. Merkel. "Indium-labeling of siRNA for small animal SPECT imaging". *Methods in Molecular Biology (Springer **2016**), RNA lmaging: Methods and protocols, 1372, 79-88.*

6.1 Introduction

Since the Nobel Prize in physiology was awarded in 2006 to Andrew Fire and Greg Mello for their work in RNA interference (RNAi), there has been an increase in the development of RNAi as a therapeutic tool to transiently knock down specific proteins. Unfortunately, when it is delivered *in vivo*, naked small interfering RNA (siRNA) is taken up very poorly into the cell due to its molecular make up.(173, 174, 178, 255) To improve its uptake and specificity, siRNA can for example be packaged inside nanoparticles. Nanoparticle delivery offers several benefits such as increased stability, longer circulation time, capability to package multiple payloads, and specific targeting to tumor sites. (54, 170)

The most common routes of nanoparticle administration for therapeutic use are intravenous, transdermal, pulmonary administration, and intraocular.(256-258) For cancer therapy, intravenous delivery of the nanoparticles is most ideal due to the ability of the nanoparticles to inherently preferentially reach the tumors directly from the bloodstream due to the enhanced permeation and retention (EPR) effect.(185) However, when nanoparticles are administered intravenously, several obstacles need to be overcome. Among those obstacles are

the circulation profile and deposition of the nanoparticles. Both of those are key components to the success of any treatment.

In order to assess the efficacy of the nanoparticle deposition in the organ or tissue of interest, single photon emission computed tomography (SPECT) imaging can be used. SPECT imaging is often employed to detect radioactive species within the body.(259) More specifically, for siRNA delivery, this can be utilized to trace where radioactive siRNA travels throughout the bloodstream and where specifically it deposits inside the body. This approach provides useful information about the obstacles that are needed to be overcome for intravenous delivery. More specifically, SPECT imaging can illustrate whether the siRNA loaded nanoparticles are degraded in circulation before reaching the tumor site, as well as its biodistribution.(260, 261) Due to the need to overcome these hurdles for a successful treatment, siRNA imaging techniques are needed. This chapter outlines the technique to label siRNA with a DTPA chelator. Once the siRNA is sufficiently labeled with DTPA, it can be reacted with indium and annealed in order to become radioactive. Once the indium has been chelated to the DTPA, the siRNA can then be packaged inside a nanoparticle or other nanocarrier and imaged with a SPECT scanner.

6.2 Materials

6.2.1 siRNA Formulation

Due to their increased stability, high activity, and ability to be covalently modified, 2'-O-methylated 25/27mer DsiRNA targeted EGFP(262) from Integrated DNA Technologies (Leuven, Belgium) was used and is recommended for use. For coupling of DTPA, amine-labeled siRNA is recommended. Here, we used a duplex with an amino-hexyl modification at the 5-prime of the antisense strand.

1. siEGFP: sense: 5’-pACCCUGAAGUUCAUCUGCACCACdCdG, antisense: 3´-mAmCmUGmGGmACmUUmCAmAGmUAmGAmCGUGGUGGC-$C_6H_{12}NH_2$

6.2.2 Covalent modification of siRNA with pBn-SCN-Bn-DTPA

1. siEGFP - seen above.
2. pBn-SCN-Bn-DTPA (Macrocyclics).
3. 0.1M $NaHCO_3$ in DEPC water – filtered through a 0.22 µm filter before use.
4. 2M NaOAc in DEPC water – filtered through a 0.22 µm filter before use.
5. Dried DMSO (about three mL).
6. 0.22 µm filter.
7. 2 mL centrifuge tube.
8. Metal spatula wrapped in parafilm – Used to weigh out pBn-SCN-Bn-DTPA (*see* **Note 1**).
9. Aluminum foil.
10. Vortex.

6.2.3 Precipitation of the siRNA-DTPA complex

1. 2M NaOAc in RNase free water – filtered through a 0.22 µm filter before use.
2. Absolute ethanol - filtered through a 0.22 µm filter before use.
3. 15 mL conical tube.

6.2.4 Isolation of the siRNA-DTPA complex

1. Ultracentrifuge (*see* **Note 6**).
2. Lysis Buffer from Absolutely RNA miRNA Kit (Agilent).
3. 2M NaOAc in RNase free water – filtered through a 0.22 µm filter before use.
4. Absolute ethanol - filtered through a 0.22 µm filter before use.
5. 5 RNeasy Midi Kit (10) columns (Qiagen).

6.2.5 siRNA-DTPA Purification

1. Centrifuge.
2. Low salt buffer from the Absolutely RNA miRNA Kit (Agilent).
3. RNase free water.
4. Sterile 2 mL collection centrifuge tubes.

6.2.6 siRNA Concentration Measurement

1. Nanodrop.
2. RNase free water.
3. 0.5 mL tubes.
4. Parafilm.
5. Dry heat bath set to 94ºC.
6. Timer.

6.2.7 DTPA Concentration Measurement

1. Stock solution of the yttrium(III)-arsenazo III complex containing 5 μM arsenazo(III) (Chem-Impex INT'L INC.), and 1.6 μM yttrium(III) chloride (Acros Organics) in a 0.15 M NaOAc buffer at pH 4.
2. Stock soltuion of 0.123 mM DTPA dissolved in DI-H_2O with 3 molar equivalents of NaOH (*see* **Note 2**).
3. UV-Vis spectrophotometer.
4. UV-Vis disposable cuvette.

6.2.8 Indium Labeling

1. Radioactive Indium(III) chloride (Covidien, Mansfield, MA).
2. GE Healthcare Disposable PD-10 Desalting Columns.

3. RNase free water.
4. Scintillation vials (make and model to fit gamma counter).
5. Gamma counter (e.g. Packard 5005).
6. Nanodrop.

6.2.9 Animal Imaging

1. Mice, e.g. 6 week old balb/c mice.
2. Sterile Insulin Syringes.
3. Sterile siRNA formulation, e.g. nanoparticles.
4. Mouse anesthesia.
5. SPECT imaging device and mouse cradle, e.g. Siemens E.CAM with custom-made collimator.

6.3 Methods

6.3.1 React siRNA with pBn-SCN-DTPA:

1. Weigh out 5.11 mg of Double Stranded siRNA in a 2 mL centrifuge tube and dissolve it in 100 uL of RNase free water (*see* **Note 3**).
2. To the 2 mL tube, add 100 µL of filtered 0.1M $NaHCO_3$.
3. Next, weigh out 9.76 mg of pBn-SCN-Bn-DTPA and dissolve it in 540 µL of dry DMSO (*see* **Note 1 and 4**).
4. Add the 540 µL of the DTPA to siRNA mixture. The new total volume should be 740 µL (*see* **Note 5**).
5. Wrap the solution in tin foil, vortex thoroughly, and incubate for 6 hours. Agitate the solution every 30 minutes.

6.3.2 Precipitation of the siRNA-DTPA complex

1. Add 74 µL of filtered 2 M Na-acetate to the mixture (10% of the total amount of mixture).
2. Transfer the mixture to a 15 mL conical tube.
3. Add filtered absolute ethanol so that the final concentration is 80% v/v.
4. Freeze solution overnight at -80ºC.

6.3.3 Isolation of the siRNA-DTPA complex

1. Centrifuge the sample for 30 minutes at 12,000g in an ultracentrifuge (*see* **Note 6**).
2. Discard the supernatant.
3. Add 2.5 mL of Lysis Buffer from "Absolutely RNA miRNA Kit" (Agilent).
4. Vortex the solution.
5. Add 250 µL of filtered 2M Na-Acetate.
6. Add 7.25 mL of filtered absolute ethanol for a total of 10mL (*see* **Note 7**).
7. Vortex the solution and equally distribute the 10 mL onto 5 RNeasy Midi Kit (10) Qiagen Columns (see **Note 8**).

6.3.4 siRNA-DTPA Purification

1. Centrifuge the columns at 4,500g for 5 minutes, discard the flow through.
2. To each column, add 200 µL of the low salt buffer from the Absolutely RNA miRNA Kit (Agilent).
3. Centrifuge the solution at 4,500g for 2 minutes, discard the flow through.
4. Repeat steps 2 and 3.
5. To dry the column, spin them down at 5,000g for 5 minutes.
6. Transfer the columns to a new collection tube and add 200 µL of 60ºC hot RNase free water.
7. Centrifuge the solution at 5,000g for 5 minutes to collect the purified siRNA-DTPA.

8. Add 100 µL of 60ºC hot RNase free water and centrifuge at 5,000g for 5 minutes.
9. Combine the flow through from all of the columns into one sterile 2 mL tube.

6.3.5 siRNA Concentration Measurement

1. Measure the siRNA concentration on a nanodrop (Thermo Scientific - Nanodrop 2000c). Use RNase free water as your blank.
2. Under the hood, dilute the siRNA to a desired concentration and aliquot into 0.5 mL sterile tubes (*see* **Note 9**).
3. Filter the siRNA-DTPA solution to make it sterile.
4. Parafilm each tube and anneal the siRNA at 94ºC for exactly 2 minutes.
5. Let the samples cool down to room temperature.
6. Freeze the samples and keep frozen until needed.

6.3.6 DTPA Concentration Measurement

1. Using a UV-Vis spectrophotometer (Cary – 50 Bio), you will create the standard curve for DTPA concentrations.
2. Pipette 3 mL of the Y(III)-arsenazo III complex stock solution into a cuvette and read (652 nM) this as the blank.
3. Add 5 µL of the stock DTPA solution to the cuvette, gently mix, and read the solution again (*see* **Note 10**).
4. Add another 5 µL of the stock DTPA solution, read, and repeat.
5. Do this until you have generated enough points for your standard curve.
6. Each new data point will have an additional 5 µL added into the cuvette.

7. Once all the standards have been made and read on the spectrophotometer, discard the solution inside the cuvette and put 3 mL of fresh Y(III)-arsenazo III complex stock solution into the cuvette (*see* **Note 11**).
8. Add 5 µL of your siRNA-DTPA sample into the 3 mL and take the measurement.
9. Plot the standard curve for the DTPA concentrations versus absorbance and insert a linear line of best fit.
10. Using the equation yielded from the line of best fit, plut the absorbance value obtained from your sample measurement and plug that into the Y-value of the equation in order to solve for X.
11. The X-value obtained will be the concentration of DTPA in your sample.
12. Now that the DTPA and siRNA concenctations have been found for the siRNA-DTPA mixture, figure out the molar amounts of the siRNA and DTPA within your sample. From here, you can determine the molar equivalency of the siRNA and DTPA (*see* **Note 12**).

6.3.7 Indium Labeling and Purification

1. React radioactive $^{111}InCl_3$ with siRNA. In the example shown below, 116.9 MBq $^{111}InCl_3$ were reacted with 15 nmol siRNA. Incubate for 30 min at room termperature.
2. Equilibrate a PD-10 column with Rnase free water by washing it with 25 ml.
3. Prepare 24 scintillation vials in a rack and label them from 1-24.
4. Place vial 1 underneath the PD-10 column and start adding the siRNA-Indium mixture to the column slowly.
5. Collect 13 drops in the first vial as fraction 1 and then move on to the next vial. Collect 13 drops per fraction. Once the complete volume of the siRNA-Indium mixture is applied to the column, add Rnase free water. Collect 24 fractions.

6. Close the scintillation vial and measure the counts per minute (CPM) in every vial using a gamma counter.
7. Plot the CPM versus the fraction number.
8. Determine the siRNA concentration in the peak fraction using a Nanodrop (**Note 13**).

6.3.8 Animal Imaging

1. Prepare the siRNA formulation to be administered, e.g. nanoparticles.In the example below, micelles of polyethyleneimine-graft-polycaprolactone-block-poly(ethylene glycol) were prepared with 2 nmol siRNA per animal which was equivalent to approximately 3 MBq per animal.
2. Anesthetize the animals and administer the siRNA formulation. In the example below, injection to the tail vein was chosen.
3. Place the animals, one after the other, in the cradle and start the 360º imaging program (**Note 14**).

6.4 Notes

1. Wrap the metal spatula in parafilm so the DTPA does not complex to the metal ions from the spatula.
2. You should first dissolve the DTPA in DMSO before diluting in the DI-H_2O with NaOH. Make sure the DMSO is at least diluted out by a factor of 1:100.
3. Our siRNA had a MW of 17950.36 g/mol. Therefore we use 0.285 µmoles of siRNA.
4. Total pBn-SCN-DTPA (MW=649.9 g/mol) is 15.02 µmoles.
5. The solution turned cloudy upon the addition of the DTPA to the siRNA solution.
6. You should get a nice visible white pellet at the bottom of the 15 mL conical tube. A regular centrifuge that reaches a speed of 12,000g may as well be used.

7. Upon addition of the ethanol, the solution should turn slightly cloudy again.
8. You should put roughly 2 mL into each column due to the fact that each column can only retain 1 mg RNA and a limited volume. If you add too much, you may lose some during the purification steps.
9. To make calculations easier in the future, dilute the siRNA to either 100 mM or 50 mM. Aliquot the samples into small portions to prevent several freeze-thaw cycles.
10. Mix the samples by gently pipetting up and down within the cuvette. Be careful not to create any bubbles.
11. Make sure you rinse out the cuvette very well. When you read the fresh 3 mL of the complex solution, verify that the values are in line with the previous measurements.
12. Since each siRNA strand has only 1 amine group for DTPA to complex to, if performed correctly, your ratio should be approximately a 1:1 molar equivalence of DTPA and siRNA. If the ratio of DTPA per siRNA is higher than 1:1, residual free DTPA was not removed during the purification.
13. It may be necessary to combine 2 or more peak fractions based on the CPM values and RNA concentrations. If free DTPA is present in the siRNA solution when it is radiolabeled, a second small peak will appear around fraction 12, and free Indium appears around fraction 20.
14. The imaging procedure can be repeated at any given time. The half-life of ^{111}Indium is 2.6 days, and a significant amount of siRNA is typically excreted renally or even hepatically. Therefore, imaging at time points later than 48 hours can become challenging.

6.5 Conclusion

Within this protocol, a detailed procedure was dicussed to demonstrate an effective way to radiolabel siRNA with radioactive In-111. Furthermore, a step-by-step guide to perform the purification and analysis of the assay is entailed. This technique provides a facile method to trace siRNA distribution *in vivo* which is administered in siRNA therapeutics.(25, 191) Due to the nature of free siRNA being easily degraded in circulation and therefore usually requiring a carrier to protect it, it is necessary to label the siRNA molecule itself rather than the carrier. The caveat with this approach is that the signal acquired of In-111 may not reflect intact or active siRNA. Therefore, it is imperative to include other experimental parameters to ensure biological activity.

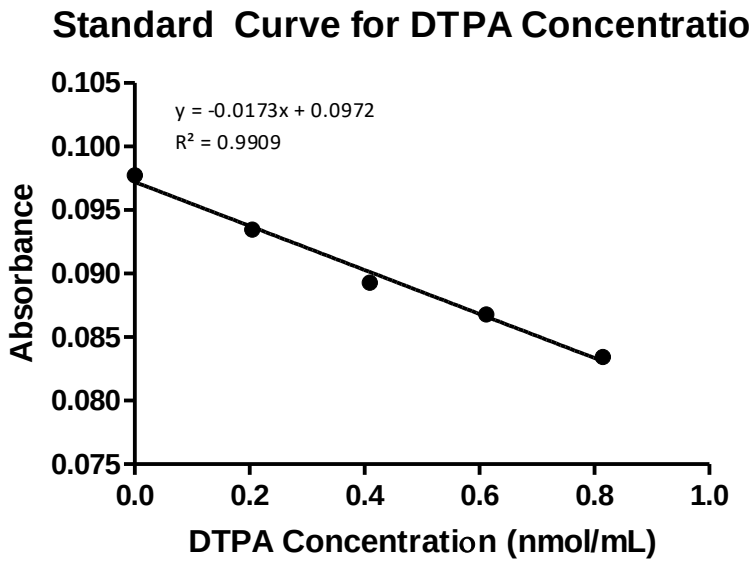

Figure 6.1 Scatter plot obtained from creating the standard curve of the DTPA concentrations. As seen below, the amount of DTPA added to the cuvette is on the X-axis, and Absorbance at 652 nm is on the Y-axis. From here, concentration of the DTPA inside the siRNA-DTPA mixture can be obtained.

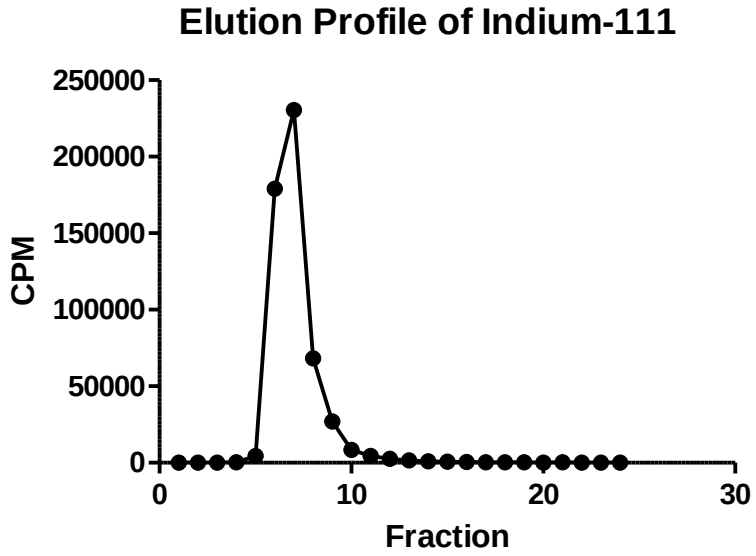

Figure 6.2: Scatter plot obtained from purifying and eluting ^{111}Indium-labeled siRNA over a PD-10 column. The radioactivity as measured in counts per minute (CPM) are shown on the Y-axis as a function of the fraction eluted on the X-axis. A clear peak is shown in fraction 7.

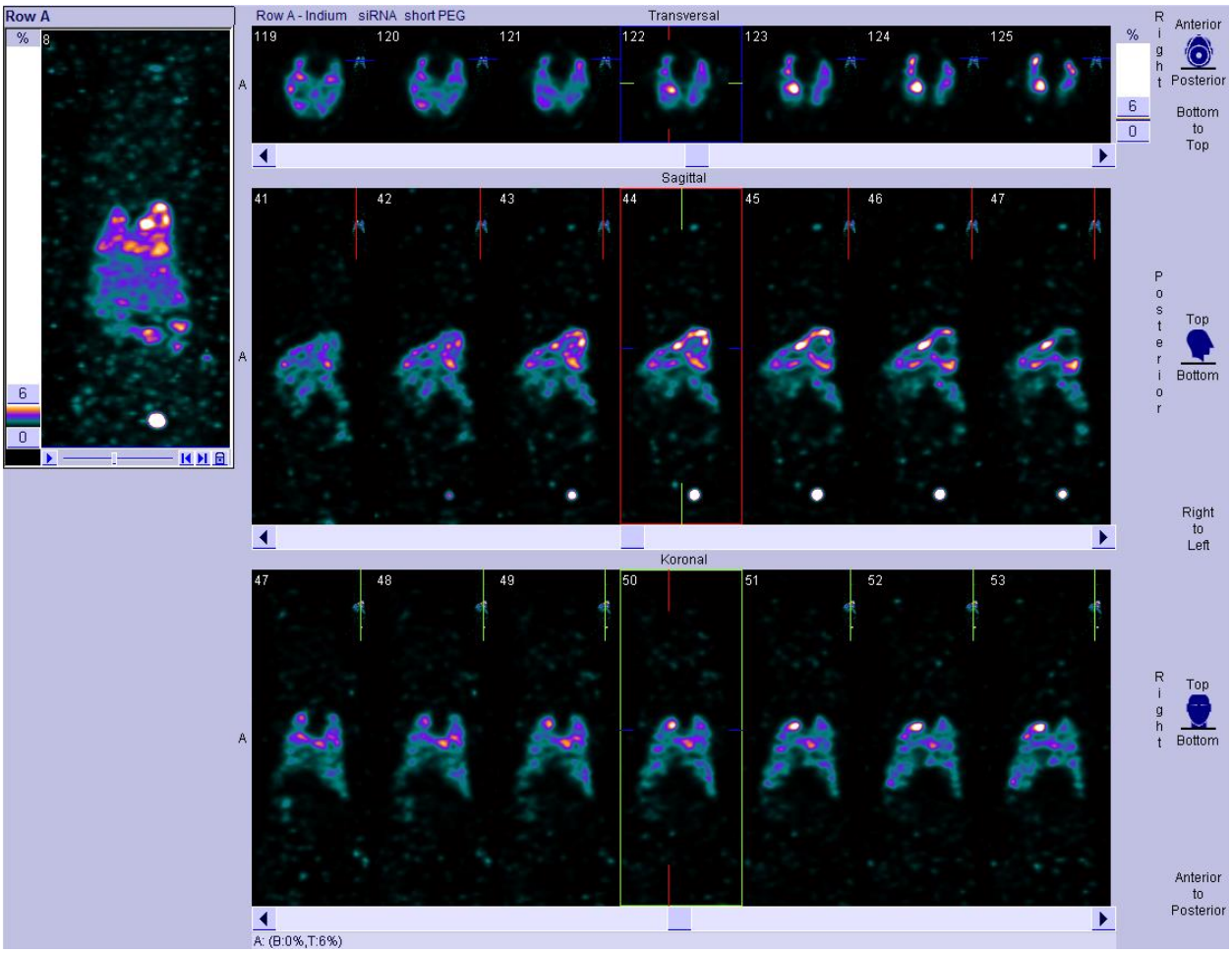

Figure 6.3: SPECT images of a 6 week-old balb/c mouse i.v. injected with 2.9 MBq ^{111}Indium-labeled siRNA formulated as micelles 2 h after injection. The formulation was obtained with a polymer carrying a short, 500 Da, PEG chain which is the reason for the accumulation of the micelles in the lung. Deposition in the liver and excretion through the kidneys into the bladder can be observed as well.

CHAPTER 7 – SPECT/CT AND BIOLUMENESENCE IMAGING OF FOLATE RECEPTOR ALPHA TUMOR TARGETING WITHIN AN ORTHOTOPIC OVARAIN CANCER MODEL

7.1 INTRODUCTION

Ovarian cancer remains one of the deadliest gynecological malignancies to date. With current treatment options, 65% of all women who are diagnosed will eventually succumb to the disease.(263, 264) A primary reason as to why patients have low survival rates is that a majority of patients are diagnosed at an advanced stage. The disease progression of ovarian cancer, if left untreated, produces aggressive and wide-spread metastatic lesions throughout the peritoneal cavity.(64) These metastatic lesions become deadly to patients by compressing and compromising vital organs. Primary treatments for these patients often include tumor de-bulking, along with a combinational chemotherapy regimen of a platinum and taxane agents.(263, 265) Unfortunately, with already wide-spread metastatic lesions, resistance and reoccurrence of the disease commonly complicates outcomes.(48, 211, 266) Resistance mechanisms often include an increase in anti-apoptotic proteins, increase activity of drug efflux pumps, or altered drug targets.(101, 118, 122, 123, 132, 153, 267, 268) If patients experience chemoresistance, treatment options become considerably limited.

The American Cancer Society, along with Endocyte estimates that over 85% of ovarian cancer patients have an overexpression of folate receptor alpha (FRα).(32, 33) Folate receptor is expressed in four distinct isoforms: alpha, beta, gamma, and delta.(39, 40, 163) Both alpha and beta isoforms are cell surface receptors that are glycosylphosphatidylinositol-anchored (GPI) and linked to the membrane.(163) FRα and FRβ have a very select expression profiles. FRα is expressed on the proximal side of the tubules of the kidneys, spleen, and certain lung tissues, as well as a variety of cancers.(32, 33, 70, 71, 241) Additionally, FRβ is mainly expressed on

activated macrophages. Both receptors express high affinities for folic acid (K_d = 1-10 nM). Therefore, folate receptors have been exploited by researchers to deliver a targeted payload to specific cells of interest by linking a targeting moiety of folic acid to either a drug itself or a delivery vehicle. This approach has been implemented for treating a variety of cancers and autoimmune diseases.(5, 209, 212, 221, 225) Accordingly, nanomedicine researchers have utilized this approach to selectively deliver a nanoformulated payload to target cells, while decreasing off target toxicity caused by uptake of the payload into healthy cells.

One type of payload that researchers have been utilizing in a targeted delivery approach is small interfering RNA (siRNA). siRNA has shown promising potential in treating diseases, such as cancer, by silencing genes that give rise to a diseased phenotype Here, we added a folic acid targeting ligand to the surface of the nanocarriers to take advantage of the FRα overexpression within our xenograft mouse model and to skew tissue distribution toward the tumor. To deliver the siRNA, triblock copolymers were utilized containing polyethyleneimine (PEI) to electrostatically condense and protect the siRNA. PEI has been documented to be an efficient carrier and transfection reagent. The polymers here were modified with a polyethylene glycol (PEG) chain to increase biocompatibility and circulation profiles, increase the stealth-like character of the nanocarriers to avoid macrophage detection and to decrease the interaction with serum proteins.(191, 221) Lastly, a polycaprolactone (PCL) block was added in the middle as a linker between PEI and PEG to increase the hydrophobic content of the polymer, drive micelle formation, and to aid in cleaving the polymer chains and releasing the siRNA once inside the cell due to its susceptibility to hydrolytic degradation.(25, 269) Previous work performed with PEI-PCL-PEG, or PPP, polymers has shown their ability to deliver siRNA *in vitro* to FRα overexpressing cells, achieve a sustained protein knockdown, and display long-circulation profiles *in vivo*.(25, 48, 180,

181, 183, 217) Here, we used modified architectures of the polymer and their block ratios in order to display their efficacy *in vivo* and ultimately show their ability to mediate gene silencing *in vivo*. Furthermore, we compared the FRα targeted and non-targeted formulations in a SKOV-3/LUC FRα overexpressing cell line employed within a murine orthotopic xenograft model of ovarian cancer.

7.2 MATERIALS AND METHODS

7.2.1 Materials: Hetero-bifunctional poly(ethylene glycol) (3.5 kDa), as well as methyl terminated monofunctional poly(ethylene glycol) (5 kDa) was purchased from JenKem Technologies (Plano, TX, USA) and chemically modified based on previously published protocols.(48) Hyper-branched polyethylenimine (*hy*-PEI, 25 kDa) was purchased from BASF (Ludwigshafen, Germany). Dicer substrate double-stranded siRNA (DsiRNA) targeting the Enhanced Green Fluorescent Protein gene (EGFP siRNA, 25/27), Firefly Luciferase (luc), Negative Control (scr), as well as Alexa Fluor-488 labeled siRNA were purchased from Integrated DNA Technologies (IDT, Coralville, IA, USA). Folic acid depleted Dulbecco's Modified Eagle's Medium (10x) for cell culture, phosphate buffered saline (PBS), heat-inactivated fetal bovine serum (FBS), D-(+)-glucose, and sodium bicarbonate were purchased from Sigma-Aldrich (St. Louis, MO, USA). The chelator pBn-SCN-Bn-DTPA was purchased from Macrocyclics (Plano, TX, USA) while arsenazo(III) was purchased from Chem-Impex INT'L INC (Wood Dale, IL, USA), and yttrium(III) chloride was obtained from Acros Organics (Geel, Belgium).

7.2.2 Cell Culture: The SKOV-3 SKOV-3/LUC human ovarian cancer cell line was obtained from ATTC (LG Promochem, Wesel, Germany). The SKOV-3/LUC cell line was engineered by stably transfecting the parental SKOV-3 cell line to stably express the reporter gene luciferase as previously published.(188) SKOV-3 and SKOV-3/LUC ovarian cancer cells were cultured in

folate-free DMEM cell culture medium (Sigma-Aldrich) supplemented with 0.584 gm/L of L-glutamine, 3.7 gm/L sodium bicarbonate, 10% fetal bovine serum (Thermo Scientific Hyclone), and 1% penicillin/streptomycin at 37 °C and 5% CO_2. Cells were grown in 75 and 175 cm^2 cell culture flasks (Thermo Scientific) and passaged every 2-3 days when they had reached confluency.

7.2.3 Preparation of PEI-g-PCL-b-PEG-Fol Micelleplexes*:* Each polymer was dissolved in water to yield a 1 mg/mL concentration based on the 25 kDa PEI content. Concentrations were tested with a copper assay, as described before.(48) Once dissolved, samples were filtered through a 0.22 μm filter for sterilization. Subsequently, micelleplexes were prepared for both *in vitro* and *in vivo* work by mixing polymer and siRNA solutions together based on a previously published protocol.(48)

7.2.4 In-111 siRNA Radiolabeling and Purification: To investigate *in vitro* cellular uptake and *in vivo* pharmacokinetics and biodistribution, indium-111 labeled siRNA was synthesized based upon a previously published protocol.(270) Briefly, siRNA modified with an amine functional group on the 5' end was labeled with the chelator, p-SCN-Bn-DTPA. After purification, it was incubated with ^{111}InCl3 for 30 minutes. Afterwards, the mixture was run though a PD-10 size exclusion column in order to separate free In-111 fractions from siRNA-DTPA-In-111 fractions. In-111 bound to siRNA was verified through gamma scintillation counting and UV absorption detection at 260 nm. If needed, peak fractions were combined for *in vivo* studies.

7.2.5 Cellular Uptake of Micelleplexes by Gamma Counting: In 24-well plates (Corning Incorporated, Corning, NY), 60,000 SKOV-3 cells were incubated over night at 37 °C and 5% CO_2. In each well, freshly made micelleplexes containing 50 pmol of siRNA-DTPA-In-111 were added. Negative controls consisted of blank/untreated cells, while positive control cells were treated with siRNA containing lipoplexes made with lipofectamine (Life Technologies, Carlsbad,

CA, USA) and polyplexes made with unmodified *hy*-PEI. Cells were transfected for 4 hours at 37 °C and in the presence of 5% CO_2. Cells were washed twice with 1X PBS + 2 mM EDTA, trypsinized and spun down at 350 g for 5 min. After centrifugation, the cells were re-suspended in 1X PBS + 2 mM EDTA buffer and analyzed via Packard Tricarb 2910TR liquid scintillation counter (PerkinElmer, Waltham, MA). Samples were all run in triplicate and analysis of the data was performed by GraphPad Prism 5.0 software for calculating mean values and standard deviations.

7.2.6 Albumin Binding Assay: An albumin binding assay was performed to detect and mimic plasma protein affinities with siRNA and siRNA containing micelleplexes. Procedures utilized here followed a previously published protocol.(193, 271) To assess albumin binding, a concentrated stock of albumin was made in PBS at 450 mg/mL containing 0.005% v/v Tween 80. Further dilutions of the stock albumin were made in DMEM medium. Micelleplexes containing In111-DTPA-siRNA were formed and incubated with 45 mg/mL, 4.5 mg/mL, 0 mg/mL albumin (DMEM media) for 1 hour at 37 ˚C. After incubation, solutions were transferred to 30,000 MWCO spin columns and centrifuged at 735 g for 15 minutes at room temperature. Following centrifugation, the flow through was discarded and the remaining aliquot was analyzed for siRNA content using gamma scintillation counting.

7.2.7 Confocal Scanning Laser Microscopy (CLSM)*:* SKOV-3 cells were seeded in a Permanox 8 chamber slide (Nunc, Fisher Scientific, Waltham, MA, USA) at a density of 25,000 cells in 300 μL and incubated over-night at 37 °C and in the presence of 5% CO_2. Micelleplexes were made as described above using 40 pmol of AF-488 labeled siRNA. After incubating the cells with the micelleplexes for 4 hours, the supernatant was decanted and cells washed with 300 μL of PBS for 2-3 minutes. Afterwards, cells were fixed with 4% paraformaldehyde solution in PBS for 20

minutes at room temperature. Cells were then washed twice with 300 μL of PBS for 2-3 minutes followed by DAPI nuclear staining at a concentration of 175 ng/mL (Life Technologies, Carlsbad, CA, USA) for 20 minutes at room temperature while shaking. Cells were then washed twice with 300 μL of PBS. The chambers were removed, the slides were blotted to remove any excess wash solution with a Kimwipe, and Fluorsave (CalBiochem, San Diego, CA, USA) was added to the slide and coverslips mounted over the samples. The samples were incubated for at least 1-2 hours in the dark to let the coverslip adhere to the chamber slide. For excitation of AF488, an excitation wavelength of 490 nm was used while emission was detected with a spectral detector at 525 nm. DAPI staining was excited with a UV laser that had an excitation wavelength of 364 nm, and emission was detected at 385 nm. Images were recorded using a Zeiss LSM 780 confocal microscope and overlaid with brightfield light to gain information about cellular structures.

7.2.8 *In Vivo* Pharmacokinetics, Biodistribution, and SPECT Imaging: All animal experiments were approved by a Wayne State University Institutional Animal Care and Use Committee. For *in vivo* experiments, 6-week-old female nude mice were purchased from Charles River Laboratories and injected with 6 million SKOV-3/LUC cells intraperitoneally based on previously established protocols (272-274). Mice were monitored and tumor growth was observed with bioluminescence imaging using a Bruker Carestream In-Vivo Extreme (Billerica, MA, USA) for 6 weeks before use. At four weeks post injection, the mice were placed on a folic acid-deficient diet (Envigo RMS, Indianapolis, USA) in order to reduce their serum folate to a level near that of human serum and to increase the folate receptor alpha status of the cancer cells.(271) On the day of the experiments, mice were injected intraperitoneally (I.P.) or intravenously (I.V.) with targeted or non-targeted micelleplexes containing 35 μg of siRNA-DTPA-In-111. After dosing, 25 μL of blood were drawn retro-orbitally from the mice's right eyes at 1, 3, 5, 15, 30, 60, and 120 min and analyzed by gamma

counting for the presence of In111-DTPA-siRNA. SPECT/CT scans were taken on a Siemens Inveon SPECT/CT (Siemens, Erlangen, Germany) at 4 hours and 24 hours post-injection. After the second scan, mice were sacrificed for organ harvesting to assess biodistribution of the siRNA. Once sacrificed, the liver, kidneys, lungs, brain, spleen, bowels, and tumors were dissected, weighed, and analyzed via gamma counting for the presence of In111-DTPA-siRNA. Results in counts per minute (CPM) of each tissue and blood sample were compared to a freshly made standard curve of In-111 and normalized to the injected dose. All biodistribution results are given as percent of the injected dose per gram of organ weight (%ID/g) while pharmacokinetic studies are represented by percent injected dose per mL of blood (%ID/mL).

7.2.9 Bioluminescence Imaging (BLI): Tumor growth and luciferase knockdown of animals were monitored on a Bruker Carestream In-Vivo Xtreme (Billerica, MA, USA). Tumor growth was monitored every 2 weeks until the 6-week time point. Animals designated to BLI studies were injected I.P. with 100 µL of a freshly prepared 15 mg/mL D-Luciferin (System Bioscience, San Francisco, USA) stock solution in PBS per 10 g of their body weight. After ten minutes, mice were treated with 3% isoflurane until sufficiently sedated. Maintenance isoflurane was used during imaging to keep the mice sedated. BLI images were taken with a three-minute exposure under high sensitivity and aperture of the lens set at an f-stop of 1.1. Simultaneously, X-ray images were taken under standard 1.2 second exposure. Images were transferred to ImageJ and region of interests (ROI) were drawn around the tumor and metastases to determine luciferase expression. Values were normalized to the day 0 luciferase expression and analysis was performed by GraphPad Prism 5.0 software.

7.3 RESULTS AND DISCUSSION

Previous *in vitro* studies performed in Chapter 4 with tri-block copolymers consisting of polyethylenimine-graft-polycaprolactone-block-poly(ethylene glycol) (PEI-*g*-PCL-*b*-PEG-FOL) with folic acid have demonstrated efficient siRNA delivery via folate receptor alpha (FRα) targeting and protein knockdown. Here, we focused on the *in vivo* performance of these micelleplexes by bioluminescence (BLI) and single-photon emission computed tomography (SPECT) imaging. In order to utilize SPECT imaging capabilities and to monitor siRNA tumor deposition and biodistribution, the siRNA needed to be labeled with Indium-111 (In-111).(270) To determine whether chelation of In-111 effected siRNA uptake profiles of the targeted and non-targeted micelleplexes, gamma scintillation experiments were performed and compared with CLSM results of fluorescently labeled siRNA as shown in Figures 7.1 and 7.2. After 4 hours post transfection, uptake profiles of both targeted and non-targeted micelleplexes were analyzed in comparison to lipofectamine and unmodified PEI. As shown in Figure 7.1, both micelleplexes delivered indium labeled siRNA just as effectively as the unmodified PEI but not as efficient as lipofectamine which was expected. Although uptake profiles of lipofectamine demonstrate greater siRNA delivery, protein knockdown was shown in Chapter 3 to be similar when compared to the targeted micelleplex.(48) Additionally, the tri-block copolymers were previously shown to be better biocompatible than lipofectamine.(48) Therefore, although the uptake profile of Lipofectamine seemingly demonstrates a greater payload delivery efficiency, the overall effect was offset by its toxicity.

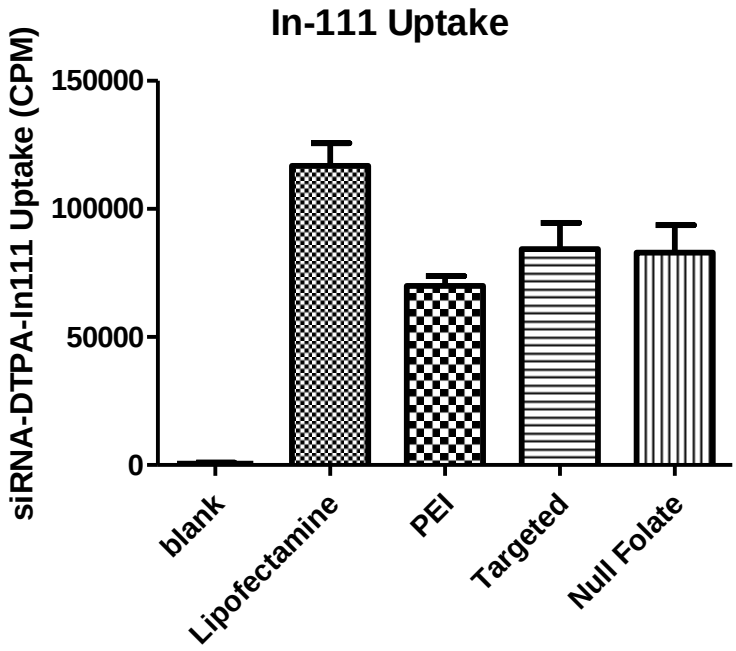

Figure 7.1: siRNA uptake studies using gamma scintillation counting. Uptake study over 4 hours with Indium-111 labeled siRNA for 4 hrs. Samples were run in triplicates and error bars represent the standard deviation.

To visualize siRNA delivery and internalization within the cell, CLSM images were taken of fluorescent siRNA delivered by different formulations, as shown in Figure 7.2. Figure 7.2 B clearly demonstrates that the targeted micelleplexes experience an apparent targeting advantage on cells which overexpress FRα. The FR-targeted micelleplexes seemingly coat the outside of the cell, utilizing FR-mediated endocytosis which would result in greater siRNA accumulation intracellularly over time. Conversely, null folate micelleplexes (Figure 7.2 C) do not undergo receptor-mediated endocytosis, but are taken up by adsorptive endocytosis. As described previously, these tri-block copolymers with folic acid were designed to encapsulate siRNA into micelleplexes in order to hijack the cells' normal receptor mediated endocytosis mechanisms, to escape the endosome, and to release siRNA into the cytoplasm.(48) Therefore, FRα targeted micelleplexes achieve a targeting advantage to deliver the siRNA over their non-targeted

counterparts, which can be visually depicted in Figures 7.2 B and C. It should be noted that these confocal images are not quantitative. Therefore, the total amount of siRNA shown in Figures 7.2 B and C may not be significantly different, as measured by flow cytometry. However, due to the different mechanisms of uptake between targeted and non-targeted micelleplexes, the subcellular distribution is different; which has been previously reported.(48, 245) The FRα targeted micelleplexes deliver siRNA more efficiently into the cytoplasm, where the non-targeted micelleplexes are entrapped within the endosomes.

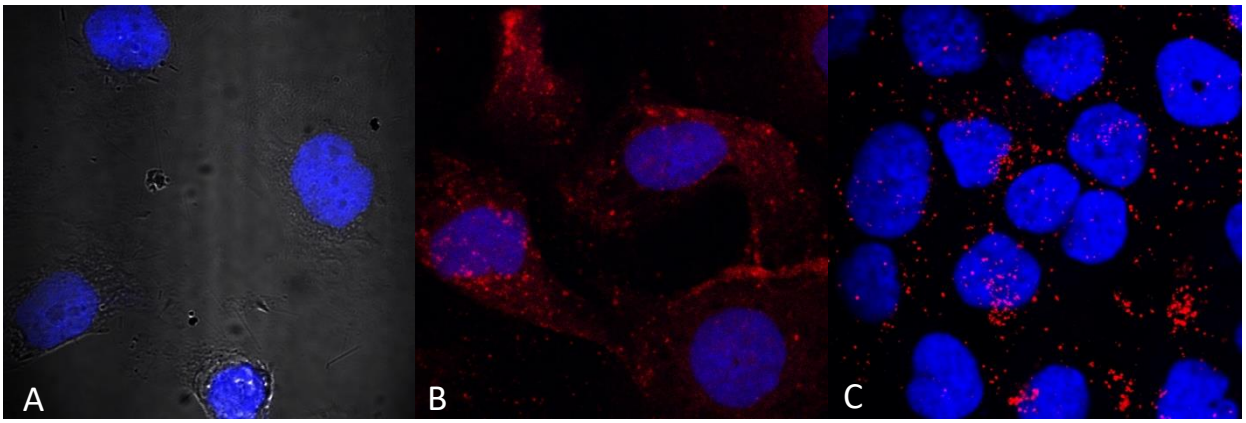

Figure 7.2: siRNA uptake studies using confocal laser scanning microscopy. Confocal images were taken of untreated cells (A), targeted micelleplexes (B), and null folate targeted conjugates (C).

As expected, due to its negative charge, hydrophilicity, and ease of degradation by nucleases in circulation, naked siRNA has poor ability for cellular uptake and a short half-life *in vivo*.(16, 193, 231) Modifications to the siRNA backbone such as C6 or 2'-O-(2-methoxyethyl) can increase the stability of siRNA for longer lasting circulation. Additionally, previous studies have demonstrated that positively charged polymers can electrostatically condense the siRNA and subsequently protect it from RNase degradation and competing ion displacement.(48, 183, 275) In order to investigate the potential for siRNA to be displaced and adsorbed by serum, an albumin binding assay was performed. In this assay, siRNA or siRNA-containing polyplexes are filtered,

whereas albumin bound siRNA or albumin bound micelleplexes are held back in the filtration device. As shown in Figure 7.3, albumin binding of the micelleplexes was observed at a low serum concentration (4.5 mg/mL) which mimics *in vitro* conditions and at a more physiologically relevant concentration of serum (45 mg/mL).(276) At both serum concentrations, both the targeted and non-targeted micelleplexes were filtered in a comparable manner with no statistical difference. In comparison, similar studies performed with PEI-PEG complexes, showed albumin binding of approximately 30% siRNA when incubated with low and physiologic concentrations of serum albumin.(193) Here, we show a 14% albumin binding of siRNA from the micelleplexes at 4.5 mg/mL serum, and 25% albumin binding at 45 mg/mL for both targeted and non-targeted micelleplexes. It should be noted, however, that although there is only 14% and 25% albumin binding at both serum concentrations, this may not accurately represent the amount of siRNA that will be bioavailable for knockdown. This is attributed to the possibility of both free siRNA and micelleplexes binding to the serum and therefore exceeding the pore size for filtration. However, the difference between results obtained with PEG-PEI polyplexes and the data obtained here for micelleplexes at low serum concentrations could be due to the charge difference between the two delivery systems. While the micelleplexes have only a slightly positive charge (around +5-10 mV), the polyplexes described earlier (Chapter 3) demonstrated zeta potentials at or above + 20 mV. With a decrease in the overall positive charge of the micelleplexes, there could be a subsequent decrease in the serum albumin binding.

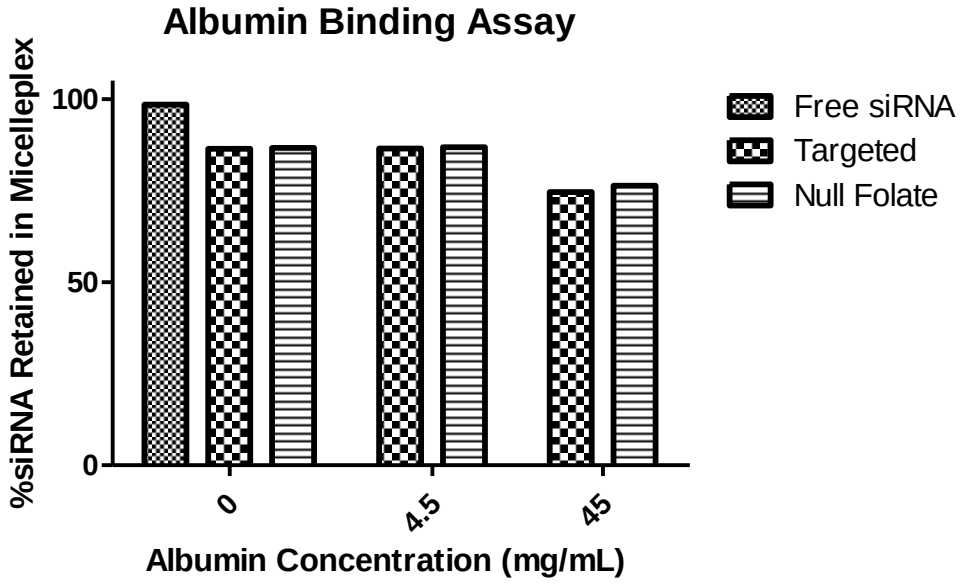

Figure 7.3: Albumin binding study. Assessment of indium-111 labeled siRNA binding to albumin at concentrations 4.5 and 45 mg/mL. Samples were run in triplicates.

Once stability and serum binding profiles were analyzed, *in vivo* pharmacokinetics of both targeted and non-targeted micelleplexes formed with In-111 labeled siRNA were analyzed for both administration routes. Previous studies performed with free, non-formulated In-111 labeled siRNA showed an elimination half-life from the blood of approximately 15 minutes.(193) Here, I.V. injected targeted micelleplexes had alpha phase half-lives of 13.2 min for the targeted and 4.95 min for the non-targeted formulations. This reflects that the distribution between compartments was very fast in case of non-targeted micelleplexes, whereas targeted ones remained in the central compartment a bit longer. Accordingly, the beta elimination phase half-lives were clearly different with 117.8 min for the targeted and 22.31 min for the non-targeted formulation, explaining the overall lower bioavailability of the non-targeted micelleplexes. The bioavailability of the micelleplexes was analyzed through statistical determination of the area under the curve (AUC). Overall, both the targeted and non-targeted micelleplexes displayed much shorter circulation

profiles than in previous reports with similar tri-block copolymers.(25, 183, 193) For I.P. injected micelleplexes, the corresponding AUC for the targeted and non-targeted micelleplexes were 125.2 %ID min/mL and 157.4 %ID min/mL, respectively. This demonstrates the different absorption profiles as reflected in the difference of the t_{max} values. While t_{max} for the non-targeted micelleplexes was reached at 60 min, the absorption of the targeted micelleplexes from the peritoneum into the circulation was less quantitative and reached a maximum at a t_{max} of 15 min already. Afterwards, the targeted micelleplexes were slowly excreted, while absorption of the non-targeted micelleplexes lasted until 60 min post injection. Thus, the non-targeted formulation reached a greater bioavailability when injected I.P. Conversely, when injected I.V., targeted micelleplexes displayed a slightly better bioavailability with an AUC of 103.7 %ID min/mL versus 87.90 %ID min/mL for their non-targeted counterpart. Therefore, the AUC for I.P injected micelleplexes was about 1.25-1.5 times greater than after I.V injection. The decreased bioavailability of both micelleplexes, when compared to previously published data using similar polymers, reflects that the nanoparticles are cleared from circulation relatively quickly. One possible reason is simple excretion, but another explanation could as well be extravasation out of the blood stream and into target or non-target tissues, which was investigated in the biodistribution experiments. While free siRNA is likely cleaved by nucleases, adsorbed to proteins within the bloodstream, or taken up by the kidney for excretion, micelleplexes have the capabilities to protect and retain siRNA. This assumption is based on previously published data and results shown in Figures 7.3 and 7.4.(48) The short circulation half-lives of both the targeted and non-targeted micelleplexes are therefore most likely due to fast extravasation out of circulation and into organs when compared to free siRNA, which is only excreted. The half-lives of each micelleplex at each administration route were analyzed with a two-compartment PK model instead a one-compartment

model based on curve fitting. The two-compartment model yielded a R^2 values of 0.644 and 0.945 for the targeted and null-folate, respectively, while the R^2 values in the one-compartment models were 0.643 and 0.940. Since the micelleplexes show rapid accumulation in the liver, a two-compartment model seems more appropriate with the deeper compartment reflecting the accumulation in liver, spleen, and at early times points the tumor.

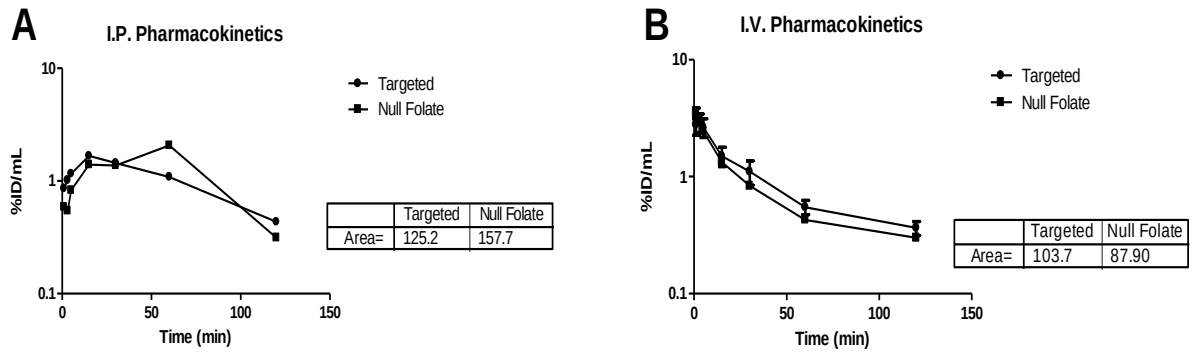

Figure 7.4: *In vivo* pharmacokinetic analysis of nude mice. Pharmacokinetic analysis of Indium-111 injected nude mice both intraperitoneally (n=6) (A) and intravenously (n=10) (B). Blood samples were collected retro-orbitally at 1, 3, 5, 15, 30, 60, and 120 minutes' post injection. Blood samples were analyzed via gamma scintillation counting. Error bars represent standard deviation of the mean.

Mice were sacrificed 24 hours post I.V or I.P injection of targeted or non-targeted micelleplexes, and their organs were harvested to determine the amount of siRNA taken up into the tumor and other main organs. The biodistribution results of both administration routes can be found in Figure 7.5. After I.P. injection, the two strongest signals were found within the kidneys (7.78 and 7.36 %ID/g, respectively) and the tumor (including all metastatic sites) (5.63 and 5.28 %ID/g, respectively) for both the targeted and non-targeted micelleplexes. These results demonstrate that with the used formulations, the targeting effect was minimal when the siRNA loaded micelleplexes were injected I.P. When micelleplexes were injected I.V., the first pass metabolism caused accumulation of the majority of the normalized injected dose per gram in the liver (38% for targeted and 53% for non-targeted), as expected. There was a slight improvement in the tumor uptake for the targeted versus non-targeted micelleplexes (3.4% and 2.4%,

respectively). However, the strong accumulation in the liver explains the rapid clearance of the micelleplexes from the circulation as described above. Unfortunately, this rapid deposition in a deep compartment interferes with circulation and deposition in the target tissue. In comparison, studies performed by Liu et al. demonstrated 17% ID/g tumor uptake with similar tri-block copolymers.(25) However, the micelleplexes used by Li et al. showed approximately 6-fold higher bioavailability and considerably slower deposition with approximately 8-fold less accumulation in the liver which allowed for slow but highly efficient tumor targeting. Additionally, the previously reported results were obtained in a subcutaneous ovarian cancer model. Here, we demonstrate tumor uptake in a more clinically relevant orthotopic ovarian cancer model. This model more accurately represents patient's disease and is more predicative of drug efficacy but unfortunately, in combination with the shorter circulation times of the formulations used here, did not reflect the same targeting efficacy. Similarly, studies performed with FRα targeted gold nanospheres or PEG coated gadolinium achieved 5.26% siRNA and 5% nanoparticle uptake in the tumor, respectively.(277, 278) Especially in case of the I.P. administration route, we found considerable siRNA uptake in the kidneys. This observation can be explained by siRNA preferentially accumulating inside the kidneys. Although FRα is expressed within the proximal tubules of the kidneys, and unavailable via access by the bloodstream, these data suggest that the uptake within the kidneys is likely due to siRNA renal accumulation rather than active FRα targeting.(71, 213, 279) Taken together, our findings demonstrate that tumor accumulation of our tri-block micelleplexes occurs mainly through passive targeting, potentially the EPR effect, rather than active tumor targeting. The potential role of the EPR effect was only observed after I.P. administration, however, whereas the tumors were not efficiently reached after I.V. injections due to the short circulation times of the nanoparticles. This observation reinforces the idea that the EPR

effect may not play an important role in nanoparticle delivery in a clinical setting.(13, 280, 281) Compared to the results reported by Liu et al., this FRα delivery system has a greater amount of off-target uptake, especially in the liver. This could be a result of the FRα micelleplexes bearing a greater grafting degree and thus more folic acid on their surface, resulting in a higher valency.(25, 48) These data can likely be explained by the observation that targeted particles with higher valency display a greater degree of off-target binding *in vivo*.(28)

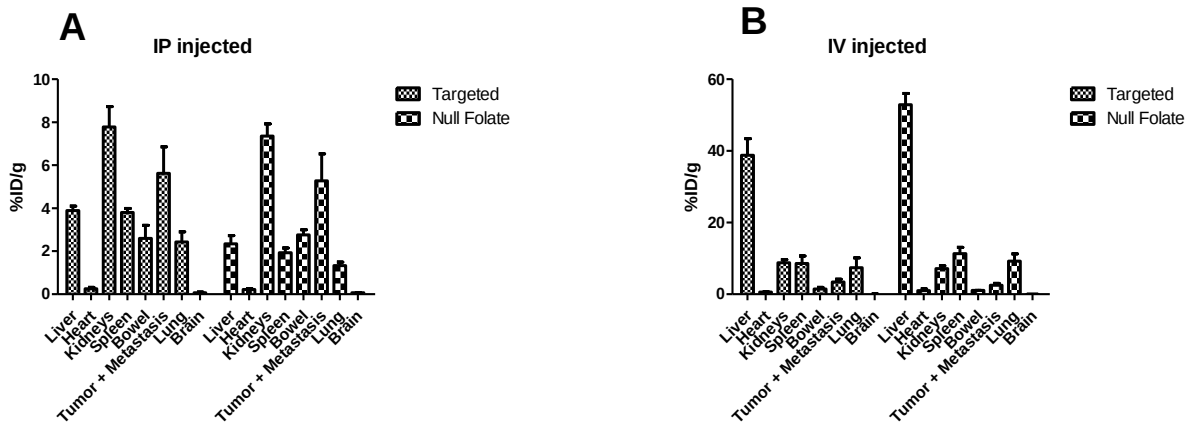

Figure 7.5: *In vivo* biodistribution analysis of nude mice. Biodistribution analysis of Indium-111 injected nude mice both intraperitoneally (A) and intravenously (B). Animals were sacrificed and organs were harvested 24 hours post injection and read under gamma scintillation counting.

SPECT/CT images of the targeted micelleplexes were taken 4 hours and 24 hours post I.P injection. Those images are shown in Figure 7.6 A and B in all three anatomical planes. At 4 hours, there was a surprising amount of localization within the primary tumor which could be due to an initial effect of receptor-ligand interaction between the micelleplexes and the tumor cells. The two additional signals in the coronal plane can be surely assigned to the kidneys, reflecting the biodistribution results. Many metastatic lesions in ovarian cancer patients occur within the peritoneum.(64) Likewise, many of the smaller metastatic tumors in the mice developed all around the liver and on the caudal side of the diaphragm. As shown in the saggital plane image in Figure

7.6 A, siRNA uptake was achieved within these metastatic lesions. Scans taken at the 24-hour time point did not show significant retention of the siRNA within the primary tumor at this later time point. Instead, the coronal plane image shows a strong signal in the liver which in this plane covers the kidneys. In the saggital plane image, siRNA uptake in the kidneys, and possibly in the metastatic lesions within the peritoneum located adjacent to the liver and diaphragm, can be found. This result demonstrates that targeting effects of the micelleplexes were washed out after 24 hours, leading to excretion via the kidneys and emphasizes the lack of impact of the EPR effect on short circulating nanoparticles which was no longer observed at the 24 h time point.(13, 280, 281) Using an orthotopic model which is closer to a clinical representation and function of the disease state, we were able to better understand the fate of our micelleplexes. Overall, the SPECT/CT images display nicely that siRNA is taken up by the primary and secondary tumors, and that potentially, if sacrificed at an earlier time point, there may be an enhanced tumor targeting effect of siRNA localized within the tumor that was washed out at 24 h post injection. Considering that the circulation time of the micelleplexes used here was much shorter than described by Liu et al., an earlier t_{max} for tumor deposition is not unlikely.

Figure 7.6: *In vivo* SPECT/CT images. Biodistribution analysis of Indium-111 injected nude mice intraperitoneally at 4 hours post injection (A) and 24 hours post injection (B). From left to right: Transversal, coronal, saggital.

After pharmacokinetic, biodistribution, and tumor accumulation analysis, it was imperative to assess the efficacy of the siRNA that localized within the tumor for protein knockdown. As the animal model was based on injection of a luciferase expressing cell line, SKOV-3/LUC, it offered the ability of measuring firefly luciferase expression *in vivo*. Therefore, we were able to monitor tumor growth throughout the duration of the study, as well as luciferase knockdown by firefly luciferase directed siRNA. In our animal model, as well as clinically, FRα is significantly over-expressed in ovarian tumors.(70, 71, 163) For the knockdown experiments, we utilized firefly luciferase directed and scrambled siRNA to determine RNAi effects. As shown in Figure 7.7, we analyzed luciferase knockdown over 72 hours after a single injection of 35 µg of siRNA. After 48

hours, the micelleplexes containing luciferase directed siRNA showed an impressive 62% knockdown. Conversely, the scrambled siRNA did not show any knockdown, but rather a drastic increase in luciferase signal was measured, which was related to tumor growth. After 72 hours, we saw a stark increase in the initially knocked down gene expression, signaling the end of the transient knockdown. This observation was consistent with our previous data in Chapter 3 for protein knockdown *in vitro* displaying the most efficient protein knockdown at 48 hours post transfection.(48) Interestingly, the mice treated with scrambled siRNA displayed a decrease in the overall luciferase signal after 48 hours. This could be due to necrotic tissue within the already advanced tumors. Advanced ovarian cancers are known to grow rapidly with a very aggressive disease progression.(64) This *in vivo* trend was promising due to the greater than 60% knockdown of luciferase expression. In comparison, Bartlett et al., Gutbier et al., and Klein et al. all achieved approximately a 50% *in vivo* knockdown with siRNA containing nanoparticles.(282-284) On the contrary, Hobel et al. demonstrated that 0.1% of the total injected siRNA that reach the tumor was capable of VEGF downregulation.(285) The knockdown is visualized in Figure 7.8 A-F which are representative images of the bioluminescence recordings at time points 0, 48, and 72 hours post injection. Animals treated with luciferase directed siRNA are shown in A-C, while animals treated with scrambled siRNA treatment can be found in D-F. Here, it is obvious that luciferase protein knockdown occurs after 24 and 48 hours, as shown in Figures 7.8 A and B, but then luciferase expression increases at the 72-hour time point (8 C). Similarly, we can visually appreciate the increase in signal after the treatment with scrambled siRNA between Figures 7.8 D and E. Overall, our *in vivo* bioluminescence imaging data analysis shows a strong trend which indicates that folate decorated micelleplexes can efficiently knock down luciferase expression by more than 60% in an orthotopic xenograft mouse model of ovarian cancer. Unfortunately, humane endpoints were

reached after 72 h which in this particular model involves ascites and serious weight loss. Therefore, a second dose was not administered.

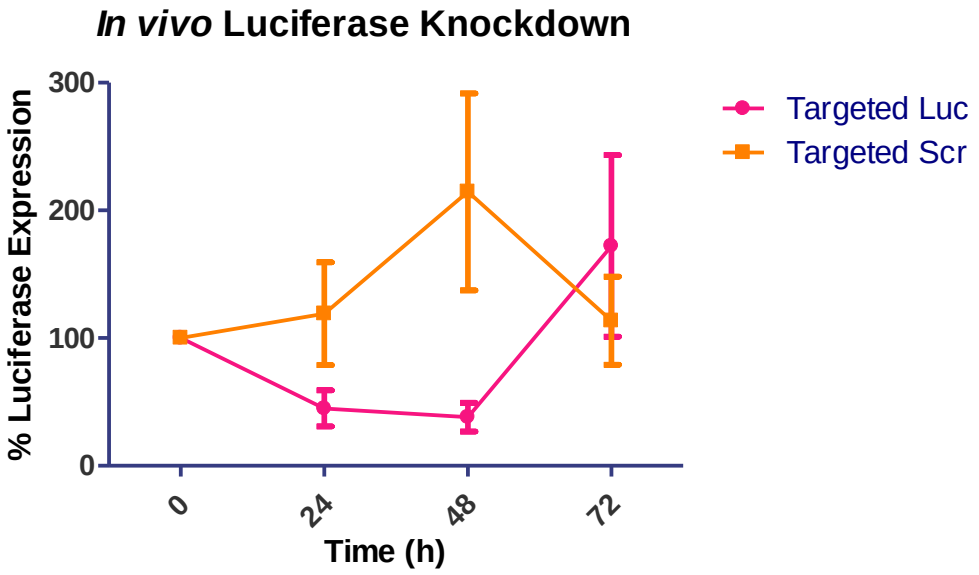

Figure 7.7: In Vivo Bioluminescence luciferase knockdown. Luciferase knockdown *in vivo* after injection of luciferase siRNA containing FRα targeted micelleplexes (n=6) and scramble siRNA containing FRα targeted micelleplexes (n=4). Error bars represent SEM.

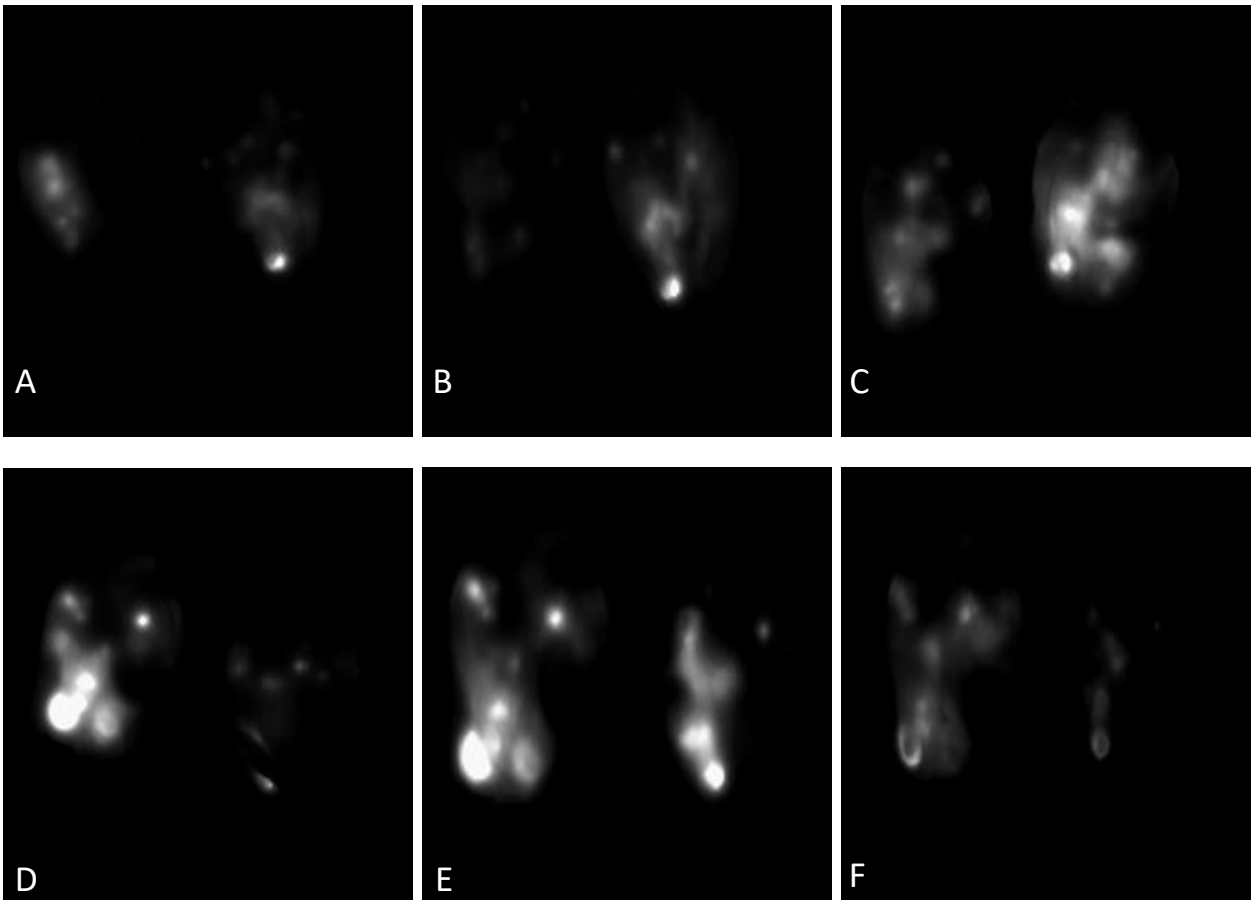

Figure 7.8: *In vivo* Bioluminescence luciferase imaging. Bioluminescence images of luciferase knockdown *in vivo* after injection of luciferase siRNA containing FRα targeted micelleplexes (A-C) and scramble siRNA containing FRα targeted micelleplexes (D-F). Timepoints displayed here are 0 hours (A, D), 48 hours (B, E), and 72 hours (C, F).

7.4 SUMMARY AND CONCLUSION

Ovarian cancer is the leading gynecologic malignancy and results in a significantly high case-to-fatality ratio.(64) Three out of every four patients are diagnosed at an advanced stage. Here, we assessed the *in vivo* functionality of FRα-targeted and non-targeted tri-block copolymers containing siRNA within a SKOV-3 murine orthotopic xenograft ovarian cancer model. Initial assessment of these micelleplexes needed to evaluate whether indium-labeling of siRNA altered the uptake profiles of the micelleplexes from previously reported results. Figures 7.1 and 7.2 demonstrate that these micelleplexes can efficiently deliver siRNA to the cells, *in vitro*.

Furthermore, the rational design for this delivery vector was to utilize and hijack the cells' natural FRα-mediated endocytosis mechanism for siRNA delivery. Therefore, theoretically, the targeted micelleplexes would have a targeting benefit over the non-targeted micelleplexes due to the high receptor expression within SKOV-3 cells. However, as demonstrated here, both micelleplexes can efficiently deliver siRNA to the cell and ultimately were taken up into the tumor in this orthotopic model, as shown in Figures 7.1, 7.2, and 7.5.

Stability testing of each micelleplex using low and high concentration levels of serum displayed acceptable siRNA retention within the micelleplex. After 1 hour of incubation, at serum levels mimicking *in vivo* conditions, 25% of the siRNA diffused out of the micelleplex. *In vivo* pharmacokinetic analysis of both targeted and non-targeted micelleplexes was assessed after both I.V and I.P administration. Overall, the AUC for I.P injected micelleplexes were about 1.25-1.5 times greater than the I.V injected ones. Interestingly, the non-targeted formulation had a greater bioavailability than the targeted formulations in I.P. injected mice, but showed smaller AUCs when injected I.V. Based on the stability and pharmacokinetic analysis here and in previously published work, micelleplexes based on the tri-block copolymers described here are expected to be relatively stable *in vivo* and to remain intact before reaching major organs.

In addition to the pharmacokinetic analysis, general biodistribution, tumor uptake, and luciferase protein knockdown was assessed. When injected I.P., the two strongest signals of biodistribution occurred within the kidneys (7.78 %ID/g for targeted and 7.36 %ID/g for non-targeted micelleplexes) and tumors (5.63 %ID/g targeted and 5.28 %ID/g non-targeted micelleplexes). Due to the primary tumor and metastatic lesions being spread throughout the peritoneal cavity, passive targeting of both micelleplexes may be a probable cause for decreasing any observable receptor targeting effect achieved by local I.P. injection in tumor tissue. However,

due to the lack of micelleplexes reaching the tumor site after I.V. injection, the EPR effect likely has little impact within this clinically relevant model. Liver uptake was minimal compared to the kidneys and tumors when injected I.P., but still showed 1.5 times higher uptake for targeted than non-targeted micelleplexes. Conversely, when injected I.V., a noticeable difference between both formulations was observed regarding uptake in the liver. Targeted and non-targeted micelleplexes accumulated with 39 and 53 %ID/g, respectively. Tumor uptake was also affected, dropping to 3.4 and 2.4 %ID/g for targeted and non-targeted micelleplexes. However, due to the wash-out of the micelleplexes seen in the SPECT/CT images after the strong tumor uptake of the targeted micelleplexes after 4 hours, leading to a diffuse uptake after 24 hours, a greater overall uptake and targeting benefit would likely have been observed at earlier time points. This decrease in overall uptake was expected because I.V. injected nanoparticles have to extravasate out of the blood vessel in order to be taken up by tumor tissue where targeting ligands will then aid in the process of intracellular delivery. SPECT/CT images displayed tumor uptake for targeted micelleplexes 4 hours post injection but reduced signals in primary tumors at 24 hours post injection. Negligible uptake was seen in the brain and heart for either micelleplex with any injection route.

As the most successful tumor deposition was achieved after I.P injection of targeted micelleplexes, we chose to utilize BLI to assess pharmacologic effects of siRNA delivery, measured by luciferase knockdown. After a single injection of 35 µg of siRNA formulated in targeted micelleplexes, an impressive 62% knockdown of luciferase was measured 48 hours after injection. However, after 72 hours, the transient knockdown ended and a sharp increase in the luciferase activity was noted. Tumors treated with targeted micelleplexes containing scrambled siRNA displayed a steady increase in luciferase expression after injection.

Overall, these tri-block copolymers displayed effective siRNA delivery profiles *in vitro* and suitable siRNA retention in the presence of high serum concentrations. *In vivo*, these siRNA containing micelleplexes achieved 5-6% tumor uptake in a SKOV-3 murine ovarian cancer orthotopic xenograft model when injected I.P which yielded a 62% luciferase knockdown. Therefore, this platform of amphiphilic tri-block copolymers provides a promising option for *in vivo* siRNA delivery and gene knockdown in ovarian cancers.

CHAPTER 8 – CONCLUSIONS

This goal of this dissertation was to successfully synthesize a tri-block copolymer that could effectively deliver siRNA in a targeted manner towards FRα. FRα-mediated drug delivery has promising therapeutic and imaging potential for treating auto-immune diseases and certain cancers. Within this dissertation, the siRNA delivery efficiency of PEI-*g*-PCL-*b*-PEG-Fol micelleplexes was demonstrated. Chapter 3 highlighted the FRα targeting efficiency and *in vitro* protein knockdown capabilities. Furthermore, chapter 3 provided an alternative mechanism to resensitize SKOV-3 ovarian cancer cells to paclitaxel treatment via TLR-4 knockdown. Following preliminary studies, the receptor targeting mechanism of PEI-PCL-PEG-Fol micelleplexes was explored further. Chapter 4 utilizes *in vitro* assays along with AFM techniques to study the effects of monovalent and multivalent receptor binding. Additionally, binding studies were performed with excess folic acid to revisit the concept of competition assays to prove or disprove receptor targeting. Further biophysical studies were performed on the targeted and non-targeted tri-block copolymers, which can be found in chapter 6. Overall, chapter 6 demonstrates that there is an optimal folic acid concentration to achieve FRα targeting while not disrupting key biophysical parameters of micelle formation and stability.

Lastly, *in vivo* efficacy was evaluated in an orthotopic xenograft mouse model in chapter 7. This model represents a more clinically relevant disease state when compared to patients. Within this model, siRNA delivery was observed within the primary tumor and metastatic lesions. However, both targeted and non-targeted micelleplexes effectively delivered siRNA suggesting that uptake was primarily due to passive targeting. Overall, these PEI-*g*-PCL-*b*-PEG-Fol micelleplexes provide a promising option for effective siRNA delivery and gene knockdown.

REFERENCES

1. Kim BYS, Rutka JT, Chan WCW. Nanomedicine. New England Journal of Medicine. 2010;363(25):2434-43.

2. Farokhzad OC, Langer R. Nanomedicine: Developing smarter therapeutic and diagnostic modalities. Advanced Drug Delivery Reviews. 2006;58(14):1456-9.

3. Anselmo AC, Mitragotri S. Nanoparticles in the clinic. Bioengineering & Translational Medicine. 2016;1(1):10-29.

4. Duncan R, Gaspar R. Nanomedicine(s) under the Microscope. Molecular Pharmaceutics. 2011;8(6):2101-41.

5. Lee RJ, Low PS. Delivery of liposomes into cultured KB cells via folate receptor-mediated endocytosis. J Biol Chem. 1994;269(5):3198-204.

6. Akbarzadeh A, Rezaei-Sadabady R, Davaran S, Joo SW, Zarghami N, Hanifehpour Y, et al. Liposome: classification, preparation, and applications. Nanoscale Research Letters. 2013;8(1):102.

7. Barenholz Y. Doxil(R)--the first FDA-approved nano-drug: lessons learned. J Control Release. 2012;160(2):117-34.

8. Wagner V, Dullaart A, Bock AK, Zweck A. The emerging nanomedicine landscape. Nature biotechnology. 2006;24(10):1211-7.

9. Riehemann K, Schneider SW, Luger TA, Godin B, Ferrari M, Fuchs H. Nanomedicine--challenge and perspectives. Angewandte Chemie (International ed in English). 2009;48(5):872-97.

10. Suk JS, Xu Q, Kim N, Hanes J, Ensign LM. PEGylation as a strategy for improving nanoparticle-based drug and gene delivery. Advanced Drug Delivery Reviews. 2016;99, Part A:28-51.

11. Safra T, Muggia F, Jeffers S, Tsao-Wei DD, Groshen S, Lyass O, et al. Pegylated liposomal doxorubicin (doxil): Reduced clinical cardiotoxicity in patients reaching or exceeding cumulative doses of 500 mg/m2. Annals of Oncology. 2000;11(8):1029-33.

12. O'Brien MER, Wigler N, Inbar M, Rosso R, Grischke E, Santoro A, et al. Reduced cardiotoxicity and comparable efficacy in a phase III trial of pegylated liposomal doxorubicin HCl (CAELYX™/Doxil®) versus conventional doxorubicin for first-line treatment of metastatic breast cancer. Annals of Oncology. 2004;15(3):440-9.

13. Greish K. Enhanced permeability and retention (EPR) effect for anticancer nanomedicine drug targeting. Methods in molecular biology (Clifton, NJ). 2010;624:25-37.

14. Maeda H, Wu J, Sawa T, Matsumura Y, Hori K. Tumor vascular permeability and the EPR effect in macromolecular therapeutics: a review. J Control Release. 2000;65(1-2):271-84.

15. Prabhakar U, Maeda H, Jain RK, Sevick-Muraca EM, Zamboni W, Farokhzad OC, et al. Challenges and key considerations of the enhanced permeability and retention (EPR) effect for nanomedicine drug delivery in oncology. Cancer Res. 2013;73(8):2412-7.

16. Wang J, Lu Z, Wientjes MG, Au JLS. Delivery of siRNA Therapeutics: Barriers and Carriers. The AAPS Journal. 2010;12(4):492-503.

17. Miele E, Spinelli GP, Miele E, Tomao F, Tomao S. Albumin-bound formulation of paclitaxel (Abraxane(®) ABI-007) in the treatment of breast cancer. Int J Nanomedicine. 2009;4:99-105.

18. Ma P. Paclitaxel Nano-Delivery Systems: A Comprehensive Review. 2013;4(2):1000164-.

19. Dou S, Yao YD, Yang XZ, Sun TM, Mao CQ, Song EW, et al. Anti-Her2 single-chain antibody mediated DNMTs-siRNA delivery for targeted breast cancer therapy. J Control Release. 2012;161(3):875-83.

20. Gu FX, Karnik R, Wang AZ, Alexis F, Levy-Nissenbaum E, Hong S, et al. Targeted nanoparticles for cancer therapy. Nano Today. 2007;2(3):14-21.

21. Sanna V, Nurra S, Pala N, Marceddu S, Pathania D, Neamati N, et al. Targeted Nanoparticles for the Delivery of Novel Bioactive Molecules to Pancreatic Cancer Cells. Journal of Medicinal Chemistry. 2016;59(11):5209-20.

22. Krais A, Wortmann L, Hermanns L, Feliu N, Vahter M, Stucky S, et al. Targeted uptake of folic acid-functionalized iron oxide nanoparticles by ovarian cancer cells in the presence but not in the absence of serum. Nanomedicine : nanotechnology, biology, and medicine. 2014;10(7):1421-31.

23. Cho K, Wang X, Nie S, Chen Z, Shin DM. Therapeutic Nanoparticles for Drug Delivery in Cancer. Clinical Cancer Research. 2008;14(5):1310-6.

24. Tortorella S, Karagiannis TC. Transferrin receptor-mediated endocytosis: a useful target for cancer therapy. The Journal of membrane biology. 2014;247(4):291-307.

25. Liu L, Zheng M, Librizzi D, Renette T, Merkel OM, Kissel T. Efficient and Tumor Targeted siRNA Delivery by Polyethylenimine-graft-polycaprolactone-block-poly(ethylene glycol)-folate (PEI-PCL-PEG-Fol). Mol Pharm. 2016;13(1):134-43.

26. Leamon CP. Folate-targeted drug strategies for the treatment of cancer. Curr Opin Investig Drugs. 2008;9(12):1277-86.

27. Das M, Mohanty C, Sahoo SK. Ligand-based targeted therapy for cancer tissue. Expert opinion on drug delivery. 2009;6(3):285-304.

28. Movahedi K, Schoonooghe S, Laoui D, Houbracken I, Waelput W, Breckpot K, et al. Nanobody-based targeting of the macrophage mannose receptor for effective in vivo imaging of tumor-associated macrophages. Cancer Res. 2012;72(16):4165-77.

29. Kelemen LE. The role of folate receptor alpha in cancer development, progression and treatment: cause, consequence or innocent bystander? International journal of cancer. 2006;119(2):243-50.

30. Xie Y, Kim NH, Nadithe V, Schalk D, Thakur A, Kilic A, et al. Targeted delivery of siRNA to activated T cells via transferrin-polyethylenimine (Tf-PEI) as a potential therapy of asthma. J Control Release. 2016;229:120-9.

31. Ragelle H, Colombo S, Pourcelle V, Vanvarenberg K, Vandermeulen G, Bouzin C, et al. Intracellular siRNA delivery dynamics of integrin-targeted, PEGylated chitosan-poly(ethylene imine) hybrid nanoparticles: A mechanistic insight. J Control Release. 2015;211:1-9.

32. Assaraf YG, Leamon CP, Reddy JA. The folate receptor as a rational therapeutic target for personalized cancer treatment. Drug resistance updates : reviews and commentaries in antimicrobial and anticancer chemotherapy. 2014;17(4-6):89-95.

33. Campbell IG, Jones TA, Foulkes WD, Trowsdale J. Folate-binding protein is a marker for ovarian cancer. Cancer Res. 1991;51(19):5329-38.

34. Rijnboutt S, Jansen G, Posthuma G, Hynes JB, Schornagel JH, Strous GJ. Endocytosis of GPI-linked membrane folate receptor-alpha. The Journal of cell biology. 1996;132(1):35-47.

35. Antony AC. Folate receptors. Annual review of nutrition. 1996;16:501-21.

36. Smart EJ, Mineo C, Anderson RG. Clustered folate receptors deliver 5-methyltetrahydrofolate to cytoplasm of MA104 cells. The Journal of cell biology. 1996;134(5):1169-77.

37. Lu Y, Low PS. Folate-mediated delivery of macromolecular anticancer therapeutic agents. Adv Drug Deliv Rev. 2002;54(5):675-93.

38. Sabharanjak S, Mayor S. Folate receptor endocytosis and trafficking. Advanced Drug Delivery Reviews. 2004;56(8):1099-109.

39. Wu M, Fan J, Gunning W, Ratnam M. Clustering of GPI-anchored folate receptor independent of both cross-linking and association with caveolin. The Journal of membrane biology. 1997;159(2):137-47.

40. Elnakat H, Ratnam M. Distribution, functionality and gene regulation of folate receptor isoforms: implications in targeted therapy. Adv Drug Deliv Rev. 2004;56(8):1067-84.

41. Stella B, Arpicco S, Peracchia MT, Desmaele D, Hoebeke J, Renoir M, et al. Design of folic acid-conjugated nanoparticles for drug targeting. Journal of pharmaceutical sciences. 2000;89(11):1452-64.

42. O'Shannessy DJ, Somers EB, Albone E, Cheng X, Park YC, Tomkowicz BE, et al. Characterization of the human folate receptor alpha via novel antibody-based probes. Oncotarget. 2011;2(12):1227-43.

43. Chen C, Ke J, Zhou XE, Yi W, Brunzelle JS, Li J, et al. Structural basis for molecular recognition of folic acid by folate receptors. Nature. 2013;500(7463):486-9.

44. O'Shannessy DJ, Somers EB, Wang L, Wang H, Hsu R. Expression of folate receptors alpha and beta in normal and cancerous gynecologic tissues: correlation of expression of the beta isoform with macrophage markers. J Ovarian Res. 2015;8.

45. Shen F, Wu M, Ross JF, Miller D, Ratnam M. Folate Receptor Type .gamma. Is Primarily a Secretory Protein Due to Lack of an Efficient Signal for Glycosylphosphatidylinositol Modification: Protein Characterization and Cell Type Specificity. Biochemistry. 1995;34(16):5660-5.

46. Shen F, Ross JF, Wang X, Ratnam M. Identification of a novel folate receptor, a truncated receptor, and receptor type .beta. in hematopoietic cells: cDNA cloning, expression, immunoreactivity, and tissue specificity. Biochemistry. 1994;33(5):1209-15.

47. Bianchi E, Doe B, Goulding D, Wright GJ. Juno is the egg Izumo receptor and is essential for mammalian fertilization. Nature. 2014;508(7497):483-7.

48. Jones SK, Lizzio V, Merkel OM. Folate Receptor Targeted Delivery of siRNA and Paclitaxel to Ovarian Cancer Cells via Folate Conjugated Triblock Copolymer to Overcome TLR4 Driven Chemotherapy Resistance. Biomacromolecules. 2016;17(1):76-87.

49. Fidler IJ. Tumor Heterogeneity and the Biology of Cancer Invasion and Metastasis. Cancer Research. 1978;38(9):2651-60.

50. Marusyk A, Polyak K. Tumor heterogeneity: Causes and consequences. Biochimica et Biophysica Acta (BBA) - Reviews on Cancer. 2010;1805(1):105-17.

51. Tang S, Yin Q, Zhang Z, Gu W, Chen L, Yu H, et al. Co-delivery of doxorubicin and RNA using pH-sensitive poly (beta-amino ester) nanoparticles for reversal of multidrug resistance of breast cancer. Biomaterials. 2014;35(23):6047-59.

52. Zhu C, Jung S, Luo S, Meng F, Zhu X, Park TG, et al. Co-delivery of siRNA and paclitaxel into cancer cells by biodegradable cationic micelles based on PDMAEMA-PCL-PDMAEMA triblock copolymers. Biomaterials. 2010;31(8):2408-16.

53. Tsouris V, Joo MK, Kim SH, Kwon IC, Won YY. Nano carriers that enable co-delivery of chemotherapy and RNAi agents for treatment of drug-resistant cancers. Biotechnol Adv. 2014;32(5):1037-50.

54. Akhtar S. Non-viral cancer gene therapy: Beyond delivery. Gene Therapy. 2006;13:739.

55. Zhang J, Li X, Huang L. Non-viral nanocarriers for siRNA delivery in breast cancer. J Control Release. 2014;190:440-50.

56. Xu C-f, Wang J. Delivery systems for siRNA drug development in cancer therapy. Asian Journal of Pharmaceutical Sciences. 2015;10(1):1-12.

57. Fire A, Xu S, Montgomery MK, Kostas SA, Driver SE, Mello CC. Potent and specific genetic interference by double-stranded RNA in Caenorhabditis elegans. Nature. 1998;391(6669):806-11.

58. Kim HJ, Kim A, Miyata K, Kataoka K. Recent progress in development of siRNA delivery vehicles for cancer therapy. Adv Drug Deliv Rev. 2016.

59. Juliano R, Bauman J, Kang H, Ming X. Biological barriers to therapy with antisense and siRNA oligonucleotides. Mol Pharm. 2009;6(3):686-95.

60. Dominska M, Dykxhoorn DM. Breaking down the barriers: siRNA delivery and endosome escape. Journal of Cell Science. 2010;123(8):1183-9.

61. Kang SH, Cho HJ, Shim G, Lee S, Kim SH, Choi HG, et al. Cationic liposomal co-delivery of small interfering RNA and a MEK inhibitor for enhanced anticancer efficacy. Pharm Res. 2011;28(12):3069-78.

62. De Smedt SC, Demeester J, Hennink WE. Cationic Polymer Based Gene Delivery Systems. Pharmaceutical Research. 2000;17(2):113-26.

63. Yu YH, Kim E, Park DE, Shim G, Lee S, Kim YB, et al. Cationic solid lipid nanoparticles for co-delivery of paclitaxel and siRNA. Eur J Pharm Biopharm. 2012;80(2):268-73.

64. Lengyel E. Ovarian cancer development and metastasis. The American journal of pathology. 2010;177(3):1053-64.

65. Auersperg N, Wong A, Choi K, Kang S, Leung P. Ovarian surface epithelium: Biology, endocrinology, and pathology. Endocr Rev. 2001;22.

66. Siegel RL, Miller KD, Jemal A. Cancer statistics, 2016. CA: a cancer journal for clinicians. 2016;66(1):7-30.

67. Eisenkop SM, Spirtos NM. The clinical significance of occult macroscopically positive retroperitoneal nodes in patients with epithelial ovarian cancer. Gynecol Oncol. 2001;82(1):143-9.

68. Ledermann JA, Kristeleit RS. Optimal treatment for relapsing ovarian cancer. Ann Oncol. 2010;21 Suppl 7:vii218-22.

69. Services USDoHaH. What you need to know about Ovarian Cancer National Institute of Health2006 [1-47].

70. Markert S, Lassmann S, Gabriel B, Klar M, Werner M, Gitsch G, et al. Alpha-folate receptor expression in epithelial ovarian carcinoma and non-neoplastic ovarian tissue. Anticancer Res. 2008;28(6A):3567-72.

71. Parker N, Turk MJ, Westrick E, Lewis JD, Low PS, Leamon CP. Folate receptor expression in carcinomas and normal tissues determined by a quantitative radioligand binding assay. Analytical Biochemistry. 2005;338(2):284-93.

72. van Dam GM, Themelis G, Crane LMA, Harlaar NJ, Pleijhuis RG, Kelder W, et al. Intraoperative tumor-specific fluorescence imaging in ovarian cancer by folate receptor-[alpha] targeting: first in-human results. Nat Med. 2011;17(10):1315-9.

73. King M-C, Marks JH, Mandell JB. Breast and Ovarian Cancer Risks Due to Inherited Mutations in BRCA1 and BRCA2. Science. 2003;302(5645):643-6.

74. Sourbier C. Ovarian cancer: emerging molecular-targeted therapies. Biologics. 2012;6:147-54.

75. Eliopoulos AG, Kerr DJ, Herod J, Hodgkins L, Krajewski S, Reed JC, et al. The control of apoptosis and drug resistance in ovarian cancer: influence of p53 and Bcl-2. Oncogene. 1995;11(7):1217-28.

76. Petty R, Evans A, Duncan I, Kurbacher C, Cree I. Drug resistance in ovarian cancer - the role of p53. Pathology oncology research : POR. 1998;4(2):97-102.

77. Flesken-Nikitin A, Choi KC, Eng JP, Shmidt EN, Nikitin AY. Induction of carcinogenesis by concurrent inactivation of p53 and Rb1 in the mouse ovarian surface epithelium. Cancer Res. 2003;63.

78. Hutson R, Ramsdale J, Wells M. p53 protein expression in putative precursor lesions of epithelial ovarian cancer. Histopathology. 1995;27.

79. Clark-Knowles KV, Garson K, Jonkers J, Vanderhyden BC. Conditional inactivation of Brca1 in the mouse ovarian surface epithelium results in an increase in preneoplastic changes. Exp Cell Res. 2007;313.

80. Vaidyanathan A, Sawers L, Gannon A-L, Chakravarty P, Scott AL, Bray SE, et al. ABCB1 (MDR1) induction defines a common resistance mechanism in paclitaxel- and olaparib-resistant ovarian cancer cells. Br J Cancer. 2016;115(4):431-41.

81. Johnatty SE, Beesley J, Gao B, Chen X, Lu Y, Law MH, et al. ABCB1 (MDR1) polymorphisms and ovarian cancer progression and survival: A comprehensive analysis from the Ovarian Cancer Association Consortium and The Cancer Genome Atlas. Gynecol Oncol. 2013;131(1):8-14.

82. Lu L, Katsaros D, Wiley A, Rigault de la Longrais IA, Puopolo M, Yu H. Expression of MDR1 in epithelial ovarian cancer and its association with disease progression. Oncology research. 2007;16(8):395-403.

83. Abbasi M, Lavasanifar A, Uludag H. Recent attempts at RNAi-mediated P-glycoprotein downregulation for reversal of multidrug resistance in cancer. Med Res Rev. 2013;33(1):33-53.

84. Iyer AK, Singh A, Ganta S, Amiji MM. Role of integrated cancer nanomedicine in overcoming drug resistance. Adv Drug Deliv Rev. 2013;65(13-14):1784-802.

85. Yu L, Wang Z. Difference in expression of Bcl-2 and Bcl-xl genes in cisplatin-sensitive and cisplatin-resistant human in ovarian cancer cell lines. Journal of Huazhong University of Science and Technology Medical sciences = Hua zhong ke ji da xue xue bao Yi xue Ying De wen ban = Huazhong keji daxue xuebao Yixue Yingdewen ban. 2004;24(2):151-3.

86. Hemmi H, Takeuchi O, Kawai T, Kaisho T, Sato S, Sanjo H, et al. A Toll-like receptor recognizes bacterial DNA. Nature. 2000;408(6813):740-5.

87. Takagi M. Toll-like Receptor

—A Potent Driving Force behind Rheumatoid Arthritis&mdash. Journal of Clinical and Experimental Hematopathology. 2011;51(2):77-92.

88. Wang AC, Su QB, Wu FX, Zhang XL, Liu PS. Role of TLR4 for paclitaxel chemotherapy in human epithelial ovarian cancer cells. Eur J Clin Invest. 2009;39(2):157-64.

89. Byrd-Leifer CA, Block EF, Takeda K, Akira S, Ding A. The role of MyD88 and TLR4 in the LPS-mimetic activity of Taxol. Eur J Immunol. 2001;31(8):2448-57.

90. Szajnik M, Szczepanski MJ, Czystowska M, Elishaev E, Mandapathil M, Nowak-Markwitz E, et al. TLR4 signaling induced by lipopolysaccharide or paclitaxel regulates tumor survival and chemoresistance in ovarian cancer. Oncogene. 2009;28(49):4353-63.

91. Coussens LM, Werb Z. Inflammation and cancer. Nature. 2002;420(6917):860-7.

92. Lin W-W, Karin M. A cytokine-mediated link between innate immunity, inflammation, and cancer. Journal of Clinical Investigation. 2007;117(5):1175-83.

93. Landskron G, De la Fuente M, Thuwajit P, Thuwajit C, Hermoso MA. Chronic Inflammation and Cytokines in the Tumor Microenvironment. Journal of Immunology Research. 2014;2014:19.

94. Kelly MG, Alvero AB, Chen R, Silasi DA, Abrahams VM, Chan S, et al. TLR-4 signaling promotes tumor growth and paclitaxel chemoresistance in ovarian cancer. Cancer Res. 2006;66(7):3859-68.

95. National Breast Cancer Foundation I. Breast Cancer Facts 2015 [Available from: http://www.nationalbreastcancer.org/breast-cancer-facts.

96. Society AC. Breast Cancer Survival Rates, by stage 2016 [Available from: http://www.cancer.org/cancer/breastcancer/detailedguide/breast-cancer-survival-by-stage.

97. Network MBC. Incidence and Incidence Rates 2016 [Available from: http://mbcn.org/education/category/incidence-and-incidence-rates.

98. Perspectives K. Treatments for Metastatic Breast Cancer 2016 [Available from: http://ww5.komen.org/BreastCancer/RecommendedTreatmentsforMetastaticBreastCancer.html.

99. O'Reilly EA, Gubbins L, Sharma S, Tully R, Guang MH, Weiner-Gorzel K, et al. The fate of chemoresistance in triple negative breast cancer (TNBC). BBA Clin. 2015;3:257-75.

100. Szakacs G, Paterson JK, Ludwig JA, Booth-Genthe C, Gottesman MM. Targeting multidrug resistance in cancer. Nat Rev Drug Discov. 2006;5(3):219-34.

101. Creixell M, Peppas NA. Co-delivery of siRNA and therapeutic agents using nanocarriers to overcome cancer resistance. Nano Today. 2012;7(4):367-79.

102. Yhee JY, Song S, Lee SJ, Park SG, Kim KS, Kim MG, et al. Cancer-targeted MDR-1 siRNA delivery using self-cross-linked glycol chitosan nanoparticles to overcome drug resistance. J Control Release. 2015;198:1-9.

103. Nieth C, Priebsch A, Stege A, Lage H. Modulation of the classical multidrug resistance (MDR) phenotype by RNA interference (RNAi). FEBS Lett. 2003;545(2-3):144-50.

104. Tseng YC, Mozumdar S, Huang L. Lipid-based systemic delivery of siRNA. Adv Drug Deliv Rev. 2009;61(9):721-31.

105. Gandhi NS, Tekade RK, Chougule MB. Nanocarrier mediated delivery of siRNA/miRNA in combination with chemotherapeutic agents for cancer therapy: current progress and advances. J Control Release. 2014;194:238-56.

106. Farrell D, Ptak K, Panaro NJ, Grodzinski P. Nanotechnology-based cancer therapeutics--promise and challenge--lessons learned through the NCI Alliance for Nanotechnology in Cancer. Pharm Res. 2011;28(2):273-8.

107. Andey T, Sudhakar G, Marepally S, Patel A, Banerjee R, Singh M. Lipid nanocarriers of a lipid-conjugated estrogenic derivative inhibit tumor growth and enhance cisplatin activity against triple-negative breast cancer: pharmacokinetic and efficacy evaluation. Mol Pharm. 2015;12(4):1105-20.

108. Wu Y, Zhang Y, Zhang W, Sun C, Wu J, Tang J. Reversing of multidrug resistance breast cancer by co-delivery of P-gp siRNA and doxorubicin via folic acid-modified core-shell nanomicelles. Colloids Surf B Biointerfaces. 2016;138:60-9.

109. Wong HL, Bendayan R, Rauth AM, Xue HY, Babakhanian K, Wu XY. A mechanistic study of enhanced doxorubicin uptake and retention in multidrug resistant breast cancer cells using a polymer-lipid hybrid nanoparticle system. J Pharmacol Exp Ther. 2006;317(3):1372-81.

110. He C, Hu Y, Yin L, Tang C, Yin C. Effects of particle size and surface charge on cellular uptake and biodistribution of polymeric nanoparticles. Biomaterials. 2010;31(13):3657-66.

111. Storm G, Belliot SO, Daemen T, Lasic DD. Surface modification of nanoparticles to oppose uptake by the mononuclear phagocyte system. Advanced Drug Delivery Reviews. 1995;17(1):31-48.

112. Jiang W, Kim BY, Rutka JT, Chan WC. Nanoparticle-mediated cellular response is size-dependent. Nature nanotechnology. 2008;3(3):145-50.

113. Lauweryns JM, Baert JH. Alveolar clearance and the role of the pulmonary lymphatics. The American review of respiratory disease. 1977;115(4):625-83.

114. Hilgenbrink AR, Low PS. Folate receptor-mediated drug targeting: from therapeutics to diagnostics. Journal of pharmaceutical sciences. 2005;94(10):2135-46.

115. Nelson AL. Antibody fragments: Hope and hype. mAbs. 2010;2(1):77-83.

116. Navarro G, Sawant RR, Biswas S, Essex S, Tros de Ilarduya C, Torchilin VP. P-glycoprotein silencing with siRNA delivered by DOPE-modified PEI overcomes doxorubicin resistance in breast cancer cells. Nanomedicine (Lond). 2012;7(1):65-78.

117. Essex S, Navarro G, Sabhachandani P, Chordia A, Trivedi M, Movassaghian S, et al. Phospholipid-modified PEI-based nanocarriers for in vivo siRNA therapeutics against multidrug-resistant tumors. Gene Ther. 2015;22(3):257-66.

118. Meng H, Mai WX, Zhang H, Xue M, Xia T, Lin S, et al. Codelivery of an optimal drug/siRNA combination using mesoporous silica nanoparticles to overcome drug resistance in breast cancer in vitro and in vivo. ACS Nano. 2013;7(2):994-1005.

119. Lin G, Zhu W, Yang L, Wu J, Lin B, Xu Y, et al. Delivery of siRNA by MRI-visible nanovehicles to overcome drug resistance in MCF-7/ADR human breast cancer cells. Biomaterials. 2014;35(35):9495-507.

120. Deng ZJ, Morton SW, Ben-Akiva E, Dreaden EC, Shopsowitz KE, Hammond PT. Layer-by-layer nanoparticles for systemic codelivery of an anticancer drug and siRNA for potential triple-negative breast cancer treatment. ACS Nano. 2013;7(11):9571-84.

121. Segovia N, Pont M, Oliva N, Ramos V, Borros S, Artzi N. Hydrogel doped with nanoparticles for local sustained release of siRNA in breast cancer. Advanced healthcare materials. 2015;4(2):271-80.

122. Huang Y, Anderle P, Bussey KJ, Barbacioru C, Shankavaram U, Dai Z, et al. Membrane transporters and channels: role of the transportome in cancer chemosensitivity and chemoresistance. Cancer Res. 2004;64(12):4294-301.

123. Huang Y, Sadee W. Membrane transporters and channels in chemoresistance and -sensitivity of tumor cells. Cancer Lett. 2006;239(2):168-82.

124. Wu H, Hait WN, Yang JM. Small interfering RNA-induced suppression of MDR1 (P-glycoprotein) restores sensitivity to multidrug-resistant cancer cells. Cancer Res. 2003;63(7):1515-9.

125. Donmez Y, Gunduz U. Reversal of multidrug resistance by small interfering RNA (siRNA) in doxorubicin-resistant MCF-7 breast cancer cells. Biomed Pharmacother. 2011;65(2):85-9.

126. Liang Z, Wu H, Xia J, Li Y, Zhang Y, Huang K, et al. Involvement of miR-326 in chemotherapy resistance of breast cancer through modulating expression of multidrug resistance-associated protein 1. Biochem Pharmacol. 2010;79(6):817-24.

127. Doyle L, Ross DD. Multidrug resistance mediated by the breast cancer resistance protein BCRP (ABCG2). Oncogene. 2003;22(47):7340-58.

128. Doyle LA, Yang W, Abruzzo LV, Krogmann T, Gao Y, Rishi AK, et al. A multidrug resistance transporter from human MCF-7 breast cancer cells. Proc Natl Acad Sci U S A. 1998;95(26):15665-70.

129. Ee PL, He X, Ross DD, Beck WT. Modulation of breast cancer resistance protein (BCRP/ABCG2) gene expression using RNA interference. Mol Cancer Ther. 2004;3(12):1577-83.

130. Salzano G, Riehle R, Navarro G, Perche F, De Rosa G, Torchilin VP. Polymeric micelles containing reversibly phospholipid-modified anti-survivin siRNA: a promising strategy to overcome drug resistance in cancer. Cancer Lett. 2014;343(2):224-31.

131. Akar U, Chaves-Reyez A, Barria M, Tari A, Sanguino A, Kondo Y, et al. Silencing of Bcl-2 expression by small interfering RNA induces autophagic cell death in MCF-7 breast cancer cells. Autophagy. 2008;4(5):669-79.

132. Li F, Sethi G. Targeting transcription factor NF-kappaB to overcome chemoresistance and radioresistance in cancer therapy. Biochim Biophys Acta. 2010;1805(2):167-80.

133. Liu H, Liu Y, Zhang JT. A new mechanism of drug resistance in breast cancer cells: fatty acid synthase overexpression-mediated palmitate overproduction. Mol Cancer Ther. 2008;7(2):263-70.

134. Gouaze V, Liu YY, Prickett CS, Yu JY, Giuliano AE, Cabot MC. Glucosylceramide synthase blockade down-regulates P-glycoprotein and resensitizes multidrug-resistant breast cancer cells to anticancer drugs. Cancer Res. 2005;65(9):3861-7.

135. Singel SM, Cornelius C, Zaganjor E, Batten K, Sarode VR, Buckley DL, et al. KIF14 promotes AKT phosphorylation and contributes to chemoresistance in triple-negative breast cancer. Neoplasia. 2014;16(3):247-56, 56 e2.

136. Lee DJ, Kessel E, Edinger D, He D, Klein PM, Voith von Voithenberg L, et al. Dual antitumoral potency of EG5 siRNA nanoplexes armed with cytotoxic bifunctional glutamyl-methotrexate targeting ligand. Biomaterials. 2016;77:98-110.

137. Dong D, Gao W, Liu Y, Qi XR. Therapeutic potential of targeted multifunctional nanocomplex co-delivery of siRNA and low-dose doxorubicin in breast cancer. Cancer Lett. 2015;359(2):178-86.

138. Waldmann T, Schneider R. Targeting histone modifications--epigenetics in cancer. Curr Opin Cell Biol. 2013;25(2):184-9.

139. Dawson MA, Kouzarides T. Cancer epigenetics: from mechanism to therapy. Cell. 2012;150(1):12-27.

140. Calcagno AM, Fostel JM, To KK, Salcido CD, Martin SE, Chewning KJ, et al. Single-step doxorubicin-selected cancer cells overexpress the ABCG2 drug transporter through epigenetic changes. Br J Cancer. 2008;98(9):1515-24.

141. Almeida LO, Abrahao AC, Rosselli-Murai LK, Giudice FS, Zagni C, Leopoldino AM, et al. NFκB mediates cisplatin resistance through histone modifications in head and neck squamous cell carcinoma (HNSCC)(). FEBS Open Bio. 2014;4:96-104.

142. Mungamuri SK, Murk W, Grumolato L, Bernstein E, Aaronson SA. Chromatin modifications sequentially enhance ErbB2 expression in ErbB2-positive breast cancers. Cell Rep. 2013;5(2):302-13.

143. Sandhu R, Rivenbark AG, Coleman WB. Enhancement of chemotherapeutic efficacy in hypermethylator breast cancer cells through targeted and pharmacologic inhibition of DNMT3b. Breast Cancer Res Treat. 2012;131(2):385-99.

144. Sowinska A, Jagodzinski PP. RNA interference-mediated knockdown of DNMT1 and DNMT3B induces CXCL12 expression in MCF-7 breast cancer and AsPC1 pancreatic carcinoma cell lines. Cancer Lett. 2007;255(1):153-9.

145. Suzuki M, Sunaga N, Shames DS, Toyooka S, Gazdar AF, Minna JD. RNA interference-mediated knockdown of DNA methyltransferase 1 leads to promoter demethylation and gene re-expression in human lung and breast cancer cells. Cancer Res. 2004;64(9):3137-43.

146. Jiang J, Yang SJ, Wang JC, Yang LJ, Xu ZZ, Yang T, et al. Sequential treatment of drug-resistant tumors with RGD-modified liposomes containing siRNA or doxorubicin. Eur J Pharm Biopharm. 2010;76(2):170-8.

147. Zhang XX, Eden HS, Chen X. Peptides in Cancer Nanomedicine: Drug Carriers, Targeting Ligands and Protease Substrates. J Control Release. 2012;159(1):2-13.

148. Zheng W, Yin T, Chen Q, Qin X, Huang X, Zhao S, et al. Co-delivery of Se nanoparticles and pooled SiRNAs for overcoming drug resistance mediated by P-glycoprotein and class III beta-tubulin in drug-resistant breast cancers. Acta Biomater. 2016;31:197-210.

149. Li YT, Chua MJ, Kunnath AP, Chowdhury EH. Reversing multidrug resistance in breast cancer cells by silencing ABC transporter genes with nanoparticle-facilitated delivery of target siRNAs. Int J Nanomedicine. 2012;7:2473-81.

150. Aliabadi HM, Maranchuk R, Kucharski C, Mahdipoor P, Hugh J, Uludag H. Effective response of doxorubicin-sensitive and -resistant breast cancer cells to combinational siRNA therapy. J Control Release. 2013;172(1):219-28.

151. Rajput S, Puvvada N, Kumar BN, Sarkar S, Konar S, Bharti R, et al. Overcoming Akt Induced Therapeutic Resistance in Breast Cancer through siRNA and Thymoquinone Encapsulated Multilamellar Gold Niosomes. Mol Pharm. 2015;12(12):4214-25.

152. Ran R, Liu Y, Gao H, Kuang Q, Zhang Q, Tang J, et al. PEGylated hyaluronic acid-modified liposomal delivery system with anti-gamma-glutamylcyclotransferase siRNA for drug-resistant MCF-7 breast cancer therapy. Journal of pharmaceutical sciences. 2015;104(2):476-84.

153. Blanchard Z, Paul BT, Craft B, ElShamy WM. BRCA1-IRIS inactivation overcomes paclitaxel resistance in triple negative breast cancers. Breast cancer research : BCR. 2015;17:5.

154. Seitz S, Rick FG, Schally AV, Treszl A, Hohla F, Szalontay L, et al. Combination of GHRH antagonists and docetaxel shows experimental effectiveness for the treatment of triple-negative breast cancers. Oncol Rep. 2013;30(1):413-8.

155. Ghebeh H, Lehe C, Barhoush E, Al-Romaih K, Tulbah A, Al-Alwan M, et al. Doxorubicin downregulates cell surface B7-H1 expression and upregulates its nuclear expression in breast cancer cells: role of B7-H1 as an anti-apoptotic molecule. Breast cancer research : BCR. 2010;12(4):R48.

156. Health USNIo. Safety Study of CALAA-01 to Treat Solid Tumor Cancers clinicaltrials.gov: Calando Pharmaceuticals; 2013 [Available from: https://clinicaltrials.gov/ct2/show/NCT00689065?term=CALAA-01&rank=1.

157. ClinicalTrials.gov. EphA2 Gene Targeting Using Neutral Liposomal Small Interfering RNA Delivery: M.D. Anderson Cancer Center, Cancer Prevention Research Institute of Texas; May 2012 [updated March 2016. Available from: https://clinicaltrials.gov/ct2/show/NCT01591356?term=siRNA&rank=1.

158. Wittrup A, Lieberman J. Knocking down disease: a progress report on siRNA therapeutics. Nature reviews Genetics. 2015;16(9):543-52.

159. Kanasty RL, Whitehead KA, Vegas AJ, Anderson DG. Action and reaction: the biological response to siRNA and its delivery vehicles. Molecular Therapy. 2012;20(3):513-24.

160. Fedorov Y, Anderson EM, Birmingham A, Reynolds A, Karpilow J, Robinson K, et al. Off-target effects by siRNA can induce toxic phenotype. Rna. 2006;12(7):1188-96.

161. Bahadar H, Maqbool F, Niaz K, Abdollahi M. Toxicity of Nanoparticles and an Overview of Current Experimental Models. Iranian Biomedical Journal. 2016;20(1):1-11.

162. Parker N, Turk MJ, Westrick E, Lewis JD, Low PS, Leamon CP. Folate receptor expression in carcinomas and normal tissues determined by a quantitative radioligand binding assay. Anal Biochem. 2005;338(2):284-93.

163. Ross JF, Chaudhuri PK, Ratnam M. Differential regulation of folate receptor isoforms in normal and malignant tissues in vivo and in established cell lines. Physiologic and clinical implications. Cancer. 1994;73(9):2432-43.

164. Institute NC. Recurrent or Persistent Ovarian Epithelial, Fallopian Tube, and Primary Peritoneal Cancer Treatment 2015 [

165. Prabhakar U, Maeda H, Jain RK, Sevick-Muraca EM, Zamboni W, Farokhzad OC, et al. Challenges and key considerations of the enhanced permeability and retention effect for nanomedicine drug delivery in oncology. Cancer Res. 2013;73(8):2412-7.

166. Peer D, Karp JM, Hong S, Farokhzad OC, Margalit R, Langer R. Nanocarriers as an emerging platform for cancer therapy. Nat Nanotechnol. 2007;2(12):751-60.

167. Benoit DS, Srinivasan S, Shubin AD, Stayton PS. Synthesis of folate-functionalized RAFT polymers for targeted siRNA delivery. Biomacromolecules. 2011;12(7):2708-14.

168. Liu Y, Li K, Pan J, Liu B, Feng SS. Folic acid conjugated nanoparticles of mixed lipid monolayer shell and biodegradable polymer core for targeted delivery of Docetaxel. Biomaterials. 2010;31(2):330-8.

169. Morris RT, Joyrich RN, Naumann RW, Shah NP, Maurer AH, Strauss HW, et al. Phase II study of treatment of advanced ovarian cancer with folate-receptor-targeted therapeutic (vintafolide) and companion SPECT-based imaging agent (99mTc-etarfolatide). Ann Oncol. 2014;25(4):852-8.

170. Vlahov IR, Leamon CP. Engineering folate-drug conjugates to target cancer: from chemistry to clinic. Bioconjugate chemistry. 2012;23(7):1357-69.

171. Wang X, Li S, Shi Y, Chuan X, Li J, Zhong T, et al. The development of site-specific drug delivery nanocarriers based on receptor mediation. J Control Release. 2014;193:139-53.

172. Y. Lu PSL. Folate-mediated delivery of macromolecular anticancer

therapeutic agents. Advanced Drug Delivery Reviews. 2002;54:675-93.

173. Huang YH, Bao Y, Peng W, Goldberg M, Love K, Bumcrot DA, et al. Claudin-3 gene silencing with siRNA suppresses ovarian tumor growth and metastasis. Proc Natl Acad Sci U S A. 2009;106(9):3426-30.

174. Shahzad MM, Lu C, Lee JW, Stone RL, Mitra R, Mangala LS, et al. Dual targeting of EphA2 and FAK in ovarian carcinoma. Cancer Biol Ther. 2009;8(11):1027-34.

175. Li L, Gu W, Chen J, Chen W, Xu ZP. Co-delivery of siRNAs and anti-cancer drugs using layered double hydroxide nanoparticles. Biomaterials. 2014;35(10):3331-9.

176. Shen J, Yin Q, Chen L, Zhang Z, Li Y. Co-delivery of paclitaxel and survivin shRNA by pluronic P85-PEI/TPGS complex nanoparticles to overcome drug resistance in lung cancer. Biomaterials. 2012;33(33):8613-24.

177. Ghosh SK, Yigit MV, Uchida M, Ross AW, Barteneva N, Moore A, et al. Sequence-dependent combination therapy with doxorubicin and a survivin-specific small interfering RNA nanodrug demonstrates efficacy in models of adenocarcinoma. Int J Cancer. 2014;134(7):1758-66.

178. Goldberg MS, Xing D, Ren Y, Orsulic S, Bhatia SN, Sharp PA. Nanoparticle-mediated delivery of siRNA targeting Parp1 extends survival of mice bearing tumors derived from Brca1-deficient ovarian cancer cells. Proc Natl Acad Sci U S A. 2011;108(2):745-50.

179. Yin Q, Shen J, Chen L, Zhang Z, Gu W, Li Y. Overcoming multidrug resistance by co-delivery of Mdr-1 and survivin-targeting RNA with reduction-responsible cationic poly(beta-amino esters). Biomaterials. 2012;33(27):6495-506.

180. Endres T, Zheng M, Kilic A, Turowska A, Beck-Broichsitter M, Renz H, et al. Amphiphilic biodegradable PEG-PCL-PEI triblock copolymers for FRET-capable in vitro and in vivo delivery of siRNA and quantum dots. Mol Pharm. 2014;11(4):1273-81.

181. Zheng M, Liu Y, Samsonova O, Endres T, Merkel O, Kissel T. Amphiphilic and biodegradable hy-PEI-g-PCL-b-PEG copolymers efficiently mediate transgene expression depending on their graft density. International journal of pharmaceutics. 2012;427(1):80-7.

182. Yu Liu JN, Terry Steele, Olivia Merkel, Thomas Kissel. A new synthesis method and degradation of hyper-branched polyethylenimine grafted polycaprolactone block mono-methoxyl poly (ethylene glycol) copolymers (hy-PEI-g-PCL-b-mPEG) as potential DNA delivery vectors. Polymer. 2009;50(16):3895-904.

183. Zheng M, Librizzi D, Kilic A, Liu Y, Renz H, Merkel OM, et al. Enhancing in vivo circulation and siRNA delivery with biodegradable polyethylenimine-graft-polycaprolactone-block-poly(ethylene glycol) copolymers. Biomaterials. 2012;33(27):6551-8.

184. Akhtar S. Non-viral cancer gene therapy: beyond delivery. Gene Ther. 2006;13(9):739-40.

185. Bertrand N, Wu J, Xu X, Kamaly N, Farokhzad OC. Cancer nanotechnology: the impact of passive and active targeting in the era of modern cancer biology. Adv Drug Deliv Rev. 2014;66:2-25.

186. Merkel OM, Kissel T. Nonviral pulmonary delivery of siRNA. Acc Chem Res. 2012;45(7):961-70.

187. Liu L, Zheng, M., Renette, T., Kissel, T. Modular Synthesis of Folate Conjugated Ternary Copolymers: Polyethylenimine-*graft*-Polycaprolactone-*block*-Poly(ethylene glycol)-Folae for Targeted Gene Delivery. Bioconjugate Chemistry. 2012;23:1211-20.

188. Merkel OM, Beyerle A, Beckmann BM, Zheng M, Hartmann RK, Stoger T, et al. Polymer-related off-target effects in non-viral siRNA delivery. Biomaterials. 2011;32(9):2388-98.

189. Storey RF, Sherman, J.W. Kinetics and Mechanism of the Stannous Octoate-Catalyzed Bulk Polymerization of e-Caprolactone. Macromolecules. 2002(35):1504-12.

190. Hans M, Gasteier, P., Keus, H., Moeller, M. Ring-Opening Polymerization of e-Caprolactone by Means of Mono-and Multifunctional Initiators: Comparison of Chemical and Enzymatic Catalysis. Macromolecules. 2002;39:3184-93.

191. Merkel OM, Beyerle A, Librizzi D, Pfestroff A, Behr TM, Sproat B, et al. Nonviral siRNA delivery to the lung: investigation of PEG-PEI polyplexes and their in vivo performance. Mol Pharm. 2009;6(4):1246-60.

192. Elsayed M, Corrand V, Kolhatkar V, Xie Y, Kim NH, Kolhatkar R, et al. Influence of oligospermines architecture on their suitability for siRNA delivery. Biomacromolecules. 2014;15(4):1299-310.

193. Merkel OM, Librizzi D, Pfestroff A, Schurrat T, Buyens K, Sanders NN, et al. Stability of siRNA polyplexes from poly(ethylenimine) and poly(ethylenimine)-g-poly(ethylene glycol) under in vivo conditions: effects on pharmacokinetics and biodistribution measured by Fluorescence Fluctuation Spectroscopy and Single Photon Emission Computed Tomography (SPECT) imaging. J Control Release. 2009;138(2):148-59.

194. He C, Hu, Y., Yin, L., Tang, C., Yin, C. Effects of particle size and surface charge on cellular uptake and biodistribution of polymeric nanoparticles. Biomaterials. 2010;31(13):3657–66.

195. G. Storm SOB, T. Daemen, D. D. Lasic. Surface modification of nanoparticles to oppose uptake by the mononuclear phagocyte system. Adv Drug Deliv Rev. 1995;17(31).

196. Sons JW. Antibody-Mediated Drug Delivery Systems: Concepts, Technology, and Applications. Pathak Y, Benita, S., editor. Hoboken, New Jersey: John Wiley & Sons, Inc.; 2012.

197. Jiang WK, B. Y. S.; Rutka, J. T.; Chan, W. C. W. Nanoparticle-mediated cellular response is size-dependent. Nature Nanotechnology. 2008;3:145-50.

198. Lauweryns JM, Baert, J.H. Alveolar clearance and the role of the pulmonary lymphatics. Am Rev Respir Dis. 1977;115(4):625-83.

199. Li JM, Wang YY, Zhang W, Su H, Ji LN, Mao ZW. Low-weight polyethylenimine cross-linked 2-hydroxypopyl-beta-cyclodextrin and folic acid as an efficient and nontoxic siRNA carrier for gene silencing and tumor inhibition by VEGF siRNA. Int J Nanomedicine. 2013;8:2101-17.

200. Teow Y, Valiyaveettil S. Active targeting of cancer cells using folic acid-conjugated platinum nanoparticles. Nanoscale. 2010;2(12):2607-13.

201. Yu B, Tang C, Yin C. Enhanced antitumor efficacy of folate modified amphiphilic nanoparticles through co-delivery of chemotherapeutic drugs and genes. Biomaterials. 2014;35(24):6369-78.

202. Paulos CM, Reddy JA, Leamon CP, Turk MJ, Low PS. Ligand binding and kinetics of folate receptor recycling in vivo: impact on receptor-mediated drug delivery. Molecular pharmacology. 2004;66(6):1406-14.

203. Arima H, Yoshimatsu A, Ikeda H, Ohyama A, Motoyama K, Higashi T, et al. Folate-PEG-appended dendrimer conjugate with alpha-cyclodextrin as a novel cancer cell-selective siRNA delivery carrier. Mol Pharm. 2012;9(9):2591-604.

204. Fernandes JC, Qiu X, Winnik FM, Benderdour M, Zhang X, Dai K, et al. Low molecular weight chitosan conjugated with folate for siRNA delivery in vitro: optimization studies. Int J Nanomedicine. 2012;7:5833-45.

205. Van Rompaey E, Engelborghs Y, Sanders N, De Smedt SC, Demeester J. Interactions between oligonucleotides and cationic polymers investigated by fluorescence correlation spectroscopy. Pharm Res. 2001;18(7):928-36.

206. Xu S, Olenyuk BZ, Okamoto CT, Hamm-Alvarez SF. Targeting receptor-mediated endocytotic pathways with nanoparticles: rationale and advances. Adv Drug Deliv Rev. 2013;65(1):121-38.

207. Bazak R, Houri M, Achy SE, Kamel S, Refaat T. Cancer active targeting by nanoparticles: a comprehensive review of literature. Journal of cancer research and clinical oncology. 2015;141(5):769-84.

208. Bandara NA, Hansen MJ, Low PS. Effect of receptor occupancy on folate receptor internalization. Mol Pharm. 2014;11(3):1007-13.

209. Leamon CP, Low PS. Delivery of macromolecules into living cells: a method that exploits folate receptor endocytosis. Proc Natl Acad Sci U S A. 1991;88(13):5572-6.

210. Vergote I, Leamon CP. Vintafolide: a novel targeted therapy for the treatment of folate receptor expressing tumors. Therapeutic advances in medical oncology. 2015;7(4):206-18.

211. Lorusso PM, Edelman MJ, Bever SL, Forman KM, Pilat M, Quinn MF, et al. Phase I study of folate conjugate EC145 (Vintafolide) in patients with refractory solid tumors. Journal of clinical oncology : official journal of the American Society of Clinical Oncology. 2012;30(32):4011-6.

212. Reddy JA, Dorton R, Bloomfield A, Nelson M, Vetzel M, Guan J, et al. Rational combination therapy of vintafolide (EC145) with commonly used chemotherapeutic drugs. Clinical cancer research : an official journal of the American Association for Cancer Research. 2014;20(8):2104-14.

213. Dhawan D, Ramos-Vara JA, Naughton JF, Cheng L, Low PS, Rothenbuhler R, et al. Targeting folate receptors to treat invasive urinary bladder cancer. Cancer Res. 2013;73(2):875-84.

214. Silpe JE, Sumit M, Thomas TP, Huang B, Kotlyar A, van Dongen MA, et al. Avidity Modulation of Folate-Targeted Multivalent Dendrimers for Evaluating Biophysical Models of Cancer Targeting Nanoparticles. ACS chemical biology. 2013;8(9):2063-71.

215. Hong S, Leroueil PR, Majoros IJ, Orr BG, Baker JR, Jr., Banaszak Holl MM. The binding avidity of a nanoparticle-based multivalent targeted drug delivery platform. Chemistry & biology. 2007;14(1):107-15.

216. Kamen BA, Smith AK. A review of folate receptor alpha cycling and 5-methyltetrahydrofolate accumulation with an emphasis on cell models in vitro. Adv Drug Deliv Rev. 2004;56(8):1085-97.

217. Liu Y, Samsonova O, Sproat B, Merkel O, Kissel T. Biophysical characterization of hyper-branched polyethylenimine-graft-polycaprolactone-block-mono-methoxyl-poly(ethylene glycol) copolymers (hy-PEI-PCL-mPEG) for siRNA delivery. J Control Release. 2011;153(3):262-8.

218. Corona G, Giannini F, Fabris M, Toffoli G, Boiocchi M. Role of folate receptor and reduced folate carrier in the transport of 5-methyltetrahydrofolic acid in human ovarian carcinoma cells. International journal of cancer. 1998;75(1):125-33.

219. Bhattacharya D, Das M, Mishra D, Banerjee I, Sahu SK, Maiti TK, et al. Folate receptor targeted, carboxymethyl chitosan functionalized iron oxide nanoparticles: a novel ultradispersed nanoconjugates for bimodal imaging. Nanoscale. 2011;3(4):1653-62.

220. Li TS, Yawata T, Honke K. Efficient siRNA delivery and tumor accumulation mediated by ionically cross-linked folic acid-poly(ethylene glycol)-chitosan oligosaccharide lactate nanoparticles: for the potential targeted ovarian cancer gene therapy. European journal of pharmaceutical sciences : official journal of the European Federation for Pharmaceutical Sciences. 2014;52:48-61.

221. Esmaeili F, Ghahremani MH, Ostad SN, Atyabi F, Seyedabadi M, Malekshahi MR, et al. Folate-receptor-targeted delivery of docetaxel nanoparticles prepared by PLGA-PEG-folate conjugate. Journal of drug targeting. 2008;16(5):415-23.

222. Su C, Li H, Shi Y, Wang G, Liu L, Zhao L, et al. Carboxymethyl-beta-cyclodextrin conjugated nanoparticles facilitate therapy for folate receptor-positive tumor with the mediation of folic acid. International journal of pharmaceutics. 2014;474(1-2):202-11.

223. Elias DR, Poloukhtine A, Popik V, Tsourkas A. Effect of ligand density, receptor density, and nanoparticle size on cell targeting. Nanomedicine : nanotechnology, biology, and medicine. 2013;9(2):194-201.

224. Cruz LJ, Tacken PJ, Pots JM, Torensma R, Buschow SI, Figdor CG. Comparison of antibodies and carbohydrates to target vaccines to human dendritic cells via DC-SIGN. Biomaterials. 2012;33(16):4229-39.

225. Reddy JA, Abburi C, Hofland H, Howard SJ, Vlahov I, Wils P, et al. Folate-targeted, cationic liposome-mediated gene transfer into disseminated peritoneal tumors. Gene Ther. 2002;9(22):1542-50.

226. Ciuchi F, Di Nicola G, Franz H, Gottarelli G, Mariani P, Ponzi Bossi MG, et al. Self-Recognition and Self-Assembly of Folic Acid Salts: Columnar Liquid Crystalline Polymorphism and the Column Growth Process. Journal of the American Chemical Society. 1994;116(16):7064-71.

227. Matsue H, Rothberg KG, Takashima A, Kamen BA, Anderson RG, Lacey SW. Folate receptor allows cells to grow in low concentrations of 5-methyltetrahydrofolate. Proceedings of the National Academy of Sciences. 1992;89(13):6006-9.

228. Sadat SM, Saeidnia S, Nazarali AJ, Haddadi A. Nano-pharmaceutical formulations for targeted drug delivery against HER2 in breast cancer. Current cancer drug targets. 2015;15(1):71-86.

229. Gaumet M, Vargas A, Gurny R, Delie F. Nanoparticles for drug delivery: The need for precision in reporting particle size parameters. European Journal of Pharmaceutics and Biopharmaceutics. 2008;69(1):1-9.

230. Patil YB, Swaminathan SK, Sadhukha T, Ma L, Panyam J. The use of nanoparticle-mediated targeted gene silencing and drug delivery to overcome tumor drug resistance. Biomaterials. 2010;31(2):358-65.

231. Davis ME, Zuckerman JE, Choi CHJ, Seligson D, Tolcher A, Alabi CA, et al. Evidence of RNAi in humans from systemically administered siRNA via targeted nanoparticles. Nature. 2010;464(7291):1067-70.

232. Park TG, Jeong JH, Kim SW. Current status of polymeric gene delivery systems. Advanced Drug Delivery Reviews. 2006;58(4):467-86.

233. Breunig M, Hozsa C, Lungwitz U, Watanabe K, Umeda I, Kato H, et al. Mechanistic investigation of poly(ethylene imine)-based siRNA delivery: Disulfide bonds boost intracellular release of the cargo. Journal of Controlled Release. 2008;130(1):57-63.

234. Soppimath KS, Aminabhavi TM, Kulkarni AR, Rudzinski WE. Biodegradable polymeric nanoparticles as drug delivery devices. Journal of Controlled Release. 2001;70(1–2):1-20.

235. Parveen S, Sahoo SK. Nanomedicine: clinical applications of polyethylene glycol conjugated proteins and drugs. Clinical pharmacokinetics. 2006;45(10):965-88.

236. Parveen S, Sahoo SK. Polymeric nanoparticles for cancer therapy. Journal of drug targeting. 2008;16(2):108-23.

237. Ferrara N, Hillan KJ, Novotny W. Bevacizumab (Avastin), a humanized anti-VEGF monoclonal antibody for cancer therapy. Biochemical and Biophysical Research Communications. 2005;333(2):328-35.

238. Lucas B, Remaut K, Sanders NN, Braeckmans K, De Smedt SC, Demeester J. Towards a better understanding of the dissociation behavior of liposome-oligonucleotide complexes in the cytosol of cells. J Control Release. 2005;103(2):435-50.

239. Zheng M, Kissel, T. Biodegradable Multifunctional Nanocarriers for PDNA and SiRNA Delivery. 2012.

240. Griffin WC. Classification of Surface-Active Agents by 'HLB'. Journal of the Society of Cosmetic Chemists. 1949;1(5):311-26.

241. Mohammadi M, Li Y, Abebe DG, Xie Y, Kandil R, Kraus T, et al. Folate receptor targeted three-layered micelles and hydrogels for gene delivery to activated macrophages. Journal of Controlled Release. 2016;244, Part B:269-79.

242. O'Mahony AM, Cronin MF, McMahon A, Evans JC, Daly K, Darcy R, et al. Biophysical and structural characterisation of nucleic acid complexes with modified cyclodextrins using circular dichroism. Journal of pharmaceutical sciences. 2014;103(5):1346-55.

243. Jones M-C, Leroux J-C. Polymeric micelles – a new generation of colloidal drug carriers. European Journal of Pharmaceutics and Biopharmaceutics. 1999;48(2):101-11.

244. Wei H, Zhang X-Z, Zhou Y, Cheng S-X, Zhuo R-X. Self-assembled thermoresponsive micelles of poly(N-isopropylacrylamide-b-methyl methacrylate). Biomaterials. 2006;27(9):2028-34.

245. Steven K. Jones AS, Daniel Feldmann, Peter Hoffmann,and Olivia Merkel. Revisiting the Value of Competition Assays in Folate Receptor-Mediated Drug Delivery Submitted.

246. Meyer M, Philipp A, Oskuee R, Schmidt C, Wagner E. Breathing Life into Polycations: Functionalization with pH-Responsive Endosomolytic Peptides and Polyethylene Glycol Enables siRNA Delivery. Journal of the American Chemical Society. 2008;130(11):3272-3.

247. Li J, Wang Y, Liang R, An X, Wang K, Shen G, et al. Recent advances in targeted nanoparticles drug delivery to melanoma. Nanomedicine: Nanotechnology, Biology and Medicine. 2015;11(3):769-94.

248. Choi HS, Liu W, Liu F, Nasr K, Misra P, Bawendi MG, et al. Design considerations for tumour-targeted nanoparticles. Nat Nano. 2010;5(1):42-7.

249. Yin Win K, Feng S-S. Effects of particle size and surface coating on cellular uptake of polymeric nanoparticles for oral delivery of anticancer drugs. Biomaterials. 2005;26(15):2713-22.

250. Geng Y, Dalhaimer P, Cai S, Tsai R, Tewari M, Minko T, et al. Shape effects of filaments versus spherical particles in flow and drug delivery. Nat Nano. 2007;2(4):249-55.

251. Veiseh O, Gunn JW, Zhang M. Design and fabrication of magnetic nanoparticles for targeted drug delivery and imaging. Advanced Drug Delivery Reviews. 2010;62(3):284-304.

252. Champion JA, Katare YK, Mitragotri S. Particle shape: A new design parameter for micro- and nanoscale drug delivery carriers. Journal of Controlled Release. 2007;121(1–2):3-9.

253. Yuan YY, Mao CQ, Du XJ, Du JZ, Wang F, Wang J. Surface charge switchable nanoparticles based on zwitterionic polymer for enhanced drug delivery to tumor. Advanced Materials. 2012;24(40):5476-80.

254. Patil S, Sandberg A, Heckert E, Self W, Seal S. Protein adsorption and cellular uptake of cerium oxide nanoparticles as a function of zeta potential. Biomaterials. 2007;28(31):4600-7.

255. Dickerson EB, Blackburn WH, Smith MH, Kapa LB, Lyon LA, McDonald JF. Chemosensitization of cancer cells by siRNA using targeted nanogel delivery. BMC cancer. 2010;10:10.

256. Watts JK, Corey DR. Clinical status of duplex RNA. Bioorganic & medicinal chemistry letters. 2010;20(11):3203-7.

257. Durcan N, Murphy C, Cryan SA. Inhalable siRNA: potential as a therapeutic agent in the lungs. Mol Pharm. 2008;5(4):559-66.

258. Davies LA, Seguela C, Varathalingam A, Cheng SH, Hyde SC, Gill DR. Identification of transfected cell types following non-viral gene transfer to the murine lung. The journal of gene medicine. 2007;9(3):184-96.

259. Renette T, Librizzi D, Endres T, Merkel O, Beck-Broichsitter M, Bege N, et al. Poly(ethylene carbonate) nanoparticles as carrier system for chemotherapy showing prolonged in vivo circulation and anti-tumor efficacy. Macromolecular bioscience. 2012;12(7):970-8.

260. Pippin CG, Parker TA, McMurry TJ, Brechbiel MW. Spectrophotometric method for the determination of a bifunctional DTPA ligand in DTPA-monoclonal antibody conjugates. Bioconjugate chemistry. 1992;3(4):342-5.

261. Merkel OM, Librizzi D, Pfestroff A, Schurrat T, Behe M, Kissel T. In vivo SPECT and real-time gamma camera imaging of biodistribution and pharmacokinetics of siRNA delivery using an optimized radiolabeling and purification procedure. Bioconjugate chemistry. 2009;20(1):174-82.

262. Rose SD, Kim DH, Amarzguioui M, Heidel JD, Collingwood MA, Davis ME, et al. Functional polarity is introduced by Dicer processing of short substrate RNAs. Nucleic acids research. 2005;33(13):4140-56.

263. Landen C, Birrer M, Sood A. Early events in the pathogenesis of epithelial ovarian cancer. Journal of clinical oncology : official journal of the American Society of Clinical Oncology. 2008;26.

264. Scully RE. Pathology of ovarian cancer precursors. J Cell Biochem. 1995;23.

265. Neesham D. Ovarian cancer screening. Aust Fam Physician. 2007;36.

266. Zhao LJ, Xu H, Qu JW, Zhao WZ, Zhao YB, Wang JH. Modulation of drug resistance in ovarian cancer cells by inhibition of protein kinase C-alpha (PKC-alpha) with small interference RNA (siRNA) agents. Asian Pac J Cancer Prev. 2012;13(8):3631-6.

267. Jones SK, Merkel OM. Tackling breast cancer chemoresistance with nano-formulated siRNA. Gene Ther. 2016;23(12):821-8.

268. Chen Y, Bathula SR, Li J, Huang L. Multifunctional Nanoparticles Delivering Small Interfering RNA and Doxorubicin Overcome Drug Resistance in Cancer. J Biol Chem. 2010;285(29):22639-50.

269. Trinh P, Atzet S, Curtain S, Ratner BD. Characterization of poly (2-hydroxyethyl methacrylate) scaffolds for tissue engineering. J Undergraduate Res Bioeng. 2008;2010(8):98-104.

270. Jones S, Merkel O. Indium-Labeling of siRNA for Small Animal SPECT Imaging. Methods in molecular biology (Clifton, NJ). 2016;1372:79-88.

271. Mathias CJ, Wang S, Lee RJ, Waters DJ, Low PS, Green MA. Tumor-selective radiopharmaceutical targeting via receptor-mediated endocytosis of gallium-67-deferoxamine-folate. Journal of nuclear medicine : official publication, Society of Nuclear Medicine. 1996;37(6):1003-8.

272. Vanderhyden BC, Shaw TJ, Ethier J. Animal models of ovarian cancer. Reproductive biology and endocrinology : RB&E. 2003;1:67.

273. Fong MY, Kakar SS. Ovarian cancer mouse models: a summary of current models and their limitations. Journal of Ovarian Research. 2009;2(1):12.

274. Shaw TJ, Senterman MK, Dawson K, Crane CA, Vanderhyden BC. Characterization of intraperitoneal, orthotopic, and metastatic xenograft models of human ovarian cancer. Molecular Therapy. 2004;10(6):1032-42.

275. Mao S, Neu M, Germershaus O, Merkel O, Sitterberg J, Bakowsky U, et al. Influence of polyethylene glycol chain length on the physicochemical and biological properties of poly(ethylene imine)-graft-poly(ethylene glycol) block copolymer/SiRNA polyplexes. Bioconjugate chemistry. 2006;17(5):1209-18.

276. Zini R, Barre J, Bree F, Tillement JP, Sebille B. Evidence for a concentration-dependent polymerization of a commercial human serum albumin. Journal of chromatography. 1981;216:191-8.

277. Lu W, Zhang G, Zhang R, Flores LG, Huang Q, Gelovani JG, et al. Tumor Site–Specific Silencing of NF-κB p65 by Targeted Hollow Gold Nanosphere–Mediated Photothermal Transfection. Cancer Research. 2010;70(8):3177-88.

278. Oyewumi MO, Yokel RA, Jay M, Coakley T, Mumper RJ. Comparison of cell uptake, biodistribution and tumor retention of folate-coated and PEG-coated gadolinium nanoparticles in tumor-bearing mice. Journal of Controlled Release. 2004;95(3):613-26.

279. van de Water FM, Boerman OC, Wouterse AC, Peters JGP, Russel FGM, Masereeuw R. INTRAVENOUSLY ADMINISTERED SHORT INTERFERING RNA ACCUMULATES IN THE KIDNEY AND SELECTIVELY SUPPRESSES GENE FUNCTION IN RENAL PROXIMAL TUBULES. Drug Metabolism and Disposition. 2006;34(8):1393-7.

280. Hansen AE, Petersen AL, Henriksen JR, Boerresen B, Rasmussen P, Elema DR, et al. Positron Emission Tomography Based Elucidation of the Enhanced Permeability and Retention Effect in Dogs with Cancer Using Copper-64 Liposomes. ACS Nano. 2015;9(7):6985-95.

281. Wang AZ. EPR or no EPR? The billion-dollar question. Science Translational Medicine. 2015;7(294):294ec112-294ec112.

282. Bartlett DW, Su H, Hildebrandt IJ, Weber WA, Davis ME. Impact of tumor-specific targeting on the biodistribution and efficacy of siRNA nanoparticles measured by multimodality in vivo imaging. Proc Natl Acad Sci U S A. 2007;104(39):15549-54.

283. Gutbier B, Kube SM, Reppe K, Santel A, Lange C, Kaufmann J, et al. RNAi-mediated suppression of constitutive pulmonary gene expression by small interfering RNA in mice. Pulmonary Pharmacology & Therapeutics. 2010;23(4):334-44.

284. Urban-Klein B, Werth S, Abuharbeid S, Czubayko F, Aigner A. RNAi-mediated gene-targeting through systemic application of polyethylenimine (PEI)-complexed siRNA in vivo. Gene Ther. 2004;12(5):461-6.

285. Hobel S, Koburger I, John M, Czubayko F, Hadwiger P, Vornlocher HP, et al. Polyethylenimine/small interfering RNA-mediated knockdown of vascular endothelial growth factor in

vivo exerts anti-tumor effects synergistically with Bevacizumab. The journal of gene medicine. 2010;12(3):287-300.

ABSTRACT

FOLATE RECEPTOR ALPHA TARGETED DELIVERY AND CHARACTERIZATION OF POLYETHYLENEIMINE-GRAFT-POLYCAPROLACTONE-BLOCK-POLY(ETHYLENE GLYCOL) CONTAINING SIRNA MICELLEPLEXES

by

STEVEN K. JONES

August 2017

Advisor: Dr. Olivia M. Merkel

Major: Cancer Biology

Degree: Doctor of Philosophy

This dissertation focuses on the ability of polyethyleneimine-graft-polycaprolactone-block-poly(ethylene glycol) (PEI-g-PCL-b-PEG-Fol) folate-decorated tri-block copolymers ability to deliver a targeted dose of siRNA. The micelleplexes that are formed upon electrostatic interaction with siRNA are used to deliver siRNA in a targeted manner to ovarian cancer cells that over-express Folate Receptor-α (FRα). Each conjugate showed suitable sizes below 200 nm with full siRNA condensation ability. Furthermore, flow cytometry and western blot analysis demonstrated that the best FRα-targeted polymer could effectively deliver siRNA which resulted in protein knockdown of Toll-like receptor 4 (TLR4). Consequently, TLR4 knock down within SKOV-3 cells re-sensitized them toward paclitaxel (PTX) treatment, and apoptotic events increased. This study demonstrates that PEI-g-PCL-b-PEG-Fol conjugates are a reliable siRNA delivery system and can mediate therapeutic TLR4 knockdown within ovarian cancer cells.

Subsequently, folate receptor binding studies were performed using Atomic Force Microscopy (AFM) to assess the binding force and probability between folic acid decorated micelleplexes and free folic acid. AFM cantilevers were decorated with active FRα and our studies

demonstrate that our micelleplexes have a stronger binding force and binding probability than free folic acid. Both results show that the folate-decorated micelleplexes out-compete for the binding of folic acid due to their multivalent nature and therefore stronger binding avidity. Uptake studies with low concentrations of folic acid only show a slight inhibition of folic acid micelleplex uptake, while not affecting the non-targeted micelleplexes. However, increasing concentrations of folic acid seen within literature, inhibited the uptake of targeted and non-targeted micelleplexes. These data suggest that excess folic does not block the micelleplexes from binding to the receptor, but perhaps affecting all nanoparticle uptake due to a cellular event, a physical destabilization of the cationic condensation of the nucleic acids, or causing an aggregation of the micelles therefore affecting its uptake.

In vivo studies were performed with an orthotopic SKOV-3/luc xenograft model to assess the conjugate's effectiveness at targeted siRNA delivery and knockdown capabilities. A Bruker In-Vivo Xtreme imaging system was utilized to monitor tumor growth and luciferase knockdown while Indium-111 labeled siRNA was designed to monitor siRNA whole body distribution, tumor targeting, and pharmacokinetic parameters by SPECT/CT and gamma scintillation counting. Upon I.P. injection, both the targeted and non-targeted siRNA containing micelleplexes showed 5-6% tumor uptake. However, when compared to scrambled siRNA, the targeted micelleplexes could achieve a 62% luciferase knockdown. Overall, this platform for *in vivo* siRNA delivery with amphiphilic tri-block copolymers provides a promising option for gene knockdown for ovarian cancers.

AUTOBIOGRAPHICAL STATEMENT

EDUCATION

Doctor of Philosophy in Cancer Biology
Wayne State University (2012-2017)
Department of Oncology, Detroit, Michigan, USA
Advisor: Dr. Olivia Merkel
Bachelor of Science in Biochemistry
University of Detroit Mercy (2008-2012)

GRANTS

- Pre-doctoral Fellowship in Cancer Research from the DeRoy Testamentary Foundation (2015-2016)
- Society of Nuclear Medicine and Molecular Imaging Bradley-Alavi Student Fellowship (2015)
- Ruth L. Kirschstein National Research Award T-32 Training Grant- National Institute of Health (NIH) (2014-2015)

SELECTED PUBLICATIONS

- **S. Jones**, K. Douglas, A. Shields, and OM. Merkel. "SPECT/CT and Bioluminescence Imaging of Folate Receptor Alpha Tumor Targeting within an Orthotopic Ovarian Cancer Model". *Manuscript in progress* 2017.
- **S. Jones**, *A. Kusowski, A. Mukhopadhyay, T. Stemmler, and* OM. Merkel. "An Insight into the Biophysical Characteristics of Folate Receptor targeted siRNA micelleplexes". *Manuscript in progress* 2017.
- **S. Jones**, A. Sarkar, Feldmann, D.P., P. Hoffmann, OM. Merkel. " Revisiting the Value of Competition Assays in Folate Receptor-Mediated Drug Delivery " *Submitted.* ACS Nano, nn-2017-01843h
- **S. Jones**, OM. Merkel. "siRNA Utilization in Breast Cancer Resistance Treatment" Nature Gene Therapy. 2016;23(12):821-8.
- McHugh CI, Lawhorn-Crews J, Modi D, Douglas, K., **Jones SK**, Mangner TJ, Collins JM, Shields AF: "Effects of capecitabine treatment on the uptake of thymidine analogs using exploratory PET imaging agents: 18F-FAU, 18F-FMAU, and 18F-FLT". Cancer Imaging 2016.
- **S. Jones**, OM. Merkel. "Indium-labeling of siRNA for small animal SPECT imaging". *Methods in Molecular Biology (Springer **2016**), RNA lmaging: Methods and protocols, 1372, 79-88.*
- **S. Jones**, V. Lizzio, OM. Merkel. "Folate Receptor Targeted Delivery of siRNA and Paclitaxel to Ovarian Cancer Cells via Folate Conjugated Triblock Co-polymer to Overcome Chemotherapy Resistance". Biomacromolecules **2015**, doi: 10.1021/acs.biomac.5b01189.